ΑΡΙΣΤΟΤΕΛΕΙΟ ΠΑΝΕΠΙΣΤΗΜΙΟ ΘΕΣΣΑΛΟΝΙΚΗΣ

ΠΟΛΥΤΕΧΝΙΚΗ ΣΧΟΛΗ

ΤΜΗΜΑ ΧΗΜΙΚΩΝ ΜΗΧΑΝΙΚΩΝ

ΓΕΩΡΓΙΟΥ Ν. ΝΙΚΟΛΑΪΔΗ

ΔΙΠΛΩΜΑΤΟΥΧΟΥ ΧΗΜΙΚΟΥ ΜΗΧΑΝΙΚΟΥ, M.Sc.

ΜΟΝΤΕΛΟΠΟΙΗΣΗ, ΠΡΟΣΟΜΟΙΩΣΗ ΚΑΙ ΒΕΛΤΙΣΤΟΠΟΙΗΣΗ ΔΙΕΡΓΑΣΙΩΝ ΔΙΑΧΩΡΙΣΜΟΥ ΑΕΡΙΩΝ ΜΕ ΜΕΘΟΔΟΥΣ ΠΡΟΣΡΟΦΗΣΗΣ ΓΙΑ ΤΗ ΜΕΓΙΣΤΗ ΔΕΣΜΕΥΣΗ ΔΙΟΞΕΙΔΙΟΥ ΤΟΥ ΑΝΘΡΑΚΑ

ΔΙΔΑΚΤΟΡΙΚΗ ΔΙΑΤΡΙΒΗ

ΘΕΣΣΑΛΟΝΙΚΗ 2017

ΓΕΩΡΓΙΟΥ Ν. ΝΙΚΟΛΑΪΔΗ

ΔΙΠΛΩΜΑΤΟΥΧΟΥ ΧΗΜΙΚΟΥ ΜΗΧΑΝΙΚΟΥ, M.Sc.

ΜΟΝΤΕΛΟΠΟΙΗΣΗ, ΠΡΟΣΟΜΟΙΩΣΗ ΚΑΙ ΒΕΛΤΙΣΤΟΠΟΙΗΣΗ ΔΙΕΡΓΑΣΙΩΝ ΔΙΑΧΩΡΙΣΜΟΥ ΑΕΡΙΩΝ ΜΕ ΜΕΘΟΔΟΥΣ ΠΡΟΣΡΟΦΗΣΗΣ ΓΙΑ ΤΗ ΜΕΓΙΣΤΗ ΔΕΣΜΕΥΣΗ ΔΙΟΞΕΙΔΙΟΥ ΤΟΥ ΑΝΘΡΑΚΑ

ΔΙΔΑΚΤΟΡΙΚΗ ΔΙΑΤΡΙΒΗ

Υποβλήθηκε στο τμήμα Χημικών Μηχανικών Α.Π.Θ.,

Τομέας Ανάλυσης, Σχεδιασμού και Ρύθμισης Χημικών Διεργασιών και Εγκαταστάσεων

Ημερομηνία Προφορικής Εξέτασης: Τετάρτη 14/6/2017

Εξεταστική επιτροπή

Καθηγητής Μ.Χ. Γεωργιάδης, Επιβλέπων

Καθηγητής Ε.Σ. Κικκινίδης, Μέλος Τριμελούς Συμβουλευτικής Επιτροπής

Αν. Καθηγητής Μ. Κώστογλου, Μέλος Τριμελούς Συμβουλευτικής Επιτροπής

Καθηγήτρια Α.Α. Λεμονίδου, Εξετάστρια

Λέκτορας Ι. Τσιβιντζέλης, Εξεταστής

Διευθυντής Ερευνών ΙΔΕΠ/ΕΚΕΤΑ, Σ. Σ. Βουτετάκης, Εξεταστής

Διευθυντής Ερευνών ΙΔΕΠ/ΕΚΕΤΑ, Α. Λάππας, Εξεταστής

ΜΟΝΤΕΛΟΠΟΙΗΣΗ, ΠΡΟΣΟΜΟΙΩΣΗ ΚΑΙ ΒΕΛΤΙΣΤΟΠΟΙΗΣΗ ΔΙΕΡΓΑΣΙΩΝ ΔΙΑΧΩΡΙΣΜΟΥ ΑΕΡΙΩΝ ΜΕ ΜΕΘΟΔΟΥΣ ΠΡΟΣΡΟΦΗΣΗΣ ΓΙΑ ΤΗ ΜΕΓΙΣΤΗ ΔΕΣΜΕΥΣΗ ΔΙΟΞΕΙΔΙΟΥ ΤΟΥ ΑΝΘΡΑΚΑ

ISBN

ARISTOTLE UNIVERSITY OF THESSALONIKI

SCHOOL OF ENGINEERING

DEPARTMENT OF CHEMICAL ENGINEERING

GEORGE N. NIKOLAIDIS

DIPLOMA IN CHEMICAL ENGINEERING, M.Sc.

MODELLING, SIMULATION AND OPTIMISATION OF GAS SEPARATION PROCESSES USING PRESSURE/VACUUM SWING ADSORPTION (P/VSA) FOR EFFICIENT POST-COMBUSTION CARBON DIOXIDE CAPTURE

A Thesis
Submitted in Fulfillment of the Requirements

for the Degree of Doctor of Philosophy

THESSALONIKI 2017

GEORGE N. NIKOLAIDIS

DIPLOMA IN CHEMICAL ENGINEERING, M.Sc.

MODELLING, SIMULATION AND OPTIMISATION OF GAS SEPARATION PROCESSES USING PRESSURE/VACUUM SWING ADSORPTION (P/VSA) FOR EFFICIENT POST-COMBUSTION CARBON DIOXIDE CAPTURE

A Thesis

Submitted in Fulfillment of the Requirements

for the Degree of Doctor of Philosophy

Examination Committee Members

Professor M. C. Georgiadis, Supervisor

Professor E. S. Kikkinides, Member of Advisory Committee

Associate Professor M. V. Kostoglou, Member of Advisory Committee

Professor A. A. Lemonidou, Examiner

Lecturer I. Tsivintzelis, Examiner

Research Director CPERI /CERTH, S. S. Voutetakis, Examiner

Research Director CPERI /CERTH, A. Lappas, Examiner

MODELLING, SIMULATION AND OPTIMISATION OF GAS SEPARATION PROCESSES USING PRESSURE/VACUUM SWING ADSORPTION (P/VSA) FOR EFFICIENT POST-COMBUSTION CARBON DIOXIDE CAPTURE

ISBN

TABLE OF CONTENTS

LIST OF FIGURES

LIST OF TABLES

ACKNOWLEDGMENTS

The work in this thesis has been carried out in the Department of Chemical Engineering at Aristotle University of Thessaloniki (Greece) from April 2013 to May 2017.

Undoubtedly, I am truly indebted to my thesis supervisor, Professor Michael C. Georgiadis, for his mentorship, motivation and encouragement along these last four years, since he has supported me with his patience and knowledge whilst allowing me the room to work in my own way. I am really grateful for his invaluable guidance, support, advice and help, which made this research work meaningful and fruitful. I would also like to express my thankfulness to him for all the opportunities that he has provided to me throughout the course of this study. Without his continual support it would have been impossible for me to complete this thesis. I was delighted to have Professor Eustathios S. Kikkinides as my co-advisor because he directed me to focus my research on industrial post-combustion CO_2 capture problems. His ability to answer every question aspect of any idea I had was of the utmost importance making me think of new ways of approaching a problem. His guidance and advice throughout the project have been very indispensable for completion of this thesis.

I would like to gratefully acknowledge the financial support received from the European Union with EFENIS (Efficient Energy Integrated Solutions for Manufacturing Industries) - FP7 project (Contract No. ENER/FP7/296003) to carry out this thesis. I also gratefully acknowledge the financial support received from the European Union and the Greek State with MOFCCS (Post-Combustion Carbon Capture Using MOFs: Materials and Process Development) - FENCO-NET project (Contract No.13 FENCO-13-940). I would also like to take this opportunity to express my thankfullness for the financial support received from the European Union with two additional mobility projects: DISKNET (DIStributed Knowledge - Based Energy Saving NETworks) - IRSES FP7 project (Contract No. FP7-PEOPLE-2011-IRSES-294933) and ESE (Energy Systems Engineering) - IRSES FP7 project (Contract No. PIRSES-GA-2011-294987) which allowing me to realize part of my studies in foreign universities.

I would also like to express my gratitude to Professor Petro Kapustenko (National Technical University - Kharkiv Politechnical Institute, Kharkiv Ukraine), to Professor Yassine Zarhloule (High Institute of Technology University Mohammed I, Oujda Morocco), and to Associate Professor Liu Pei, (Tsinghua University, Beijing China) for their hospitality, help and support as well as the fruitful discussions and collaborations made during my secondments to their research groups.

Also, I do owe my deepest gratitude to my friends and colleagues at the Department of Chemical Engineering researcher Dr Nikolaos Koltsaklis, and PhD candidates Panagiotis Karakostas and Romuald Győrgy who helped me throughout this period of time, as well as to all the staff of the Department of Chemical Engineering of Aristotle University of Thessaloniki and especially my friend researcher Dr Kostas Tsioptsias, for their encouragement and friendship.

I would like also to take this oppurtunity to express my thankfullness to the directors of my new professional environment at the company Pagouni S.A. namely, Zisis Pagounis, Eugenia Pagouni and Katerina Pagouni for the many facilities they have provided to me during the final stage of this thesis, as well as for the absolute confidence they have showed to me.

Last, but foremost, I offer my sincerest gratitude to my loving family, my wife Athina, and my children Helena and Platon, who have fully supported me throughout my research project. There is no reasonable way I can describe how they have helped me over the last few years. They have been a great source of love, understanding, patience, motivation and encouragement, and I will be forever grateful for their help. Without their continual support it would have been impossible for me to finish this work.

Last, but not least, I would like to thank my parents, for their immeasurable help, love, support and belief. I would like to dedicate this thesis to my late father who never lived long enough to see me through to the end of this study. You will always be the source of my inspiration and a part of me. May your soul rest in peace and I will always love you.

ABSTRACT in Greek (Περίληψη)

Στην παρούσα διδακτορική διατριβή γίνεται ανάπτυξη και εφαρμογή του μαθηματικού πλαισίου προσομοίωσης και βελτιστοποίησης με χρήση του περιβάλλοντος gPROMS™ για τη δέσμευση του διοξειδίου του άνθρακα (CO_2) από απαέρια καύσης χρησιμοποιώντας διεργασία προσρόφησης με βαθμιδωτή μεταβολή πίεσης/κενού P/VSA (Pressure/Vacuum Swing Adsorption). Το προτεινόμενο μαθηματικό πλαίσιο αξιολογείται με σύγκριση με πειραματικά και θεωρητικά δεδομένα από την διεθνή βιβλιογραφία και παρουσιάζει καλή συμφωνία σε όρους διαφόρων δεικτών απόδοσης της διεργασίας. Γίνεται συστηματική εξέταση διαφόρων τύπων προσροφητικών υλικών (ζεόλιθος 13X, ενεργός άνθρακας, οργανομεταλλικές πορώδεις δομές MOFs) σε διεργασία P/VSA ενός σταδίου, καθώς επίσης και συνδυασμών προσροφητικών υλικών (ζεόλιθος 13X, οργανομεταλλικές πορώδεις δομές MOFs) σε διεργασία P/VSA δύο σταδίων με σκοπό τη σύγκριση της συμπεριφοράς τους σε σχέση με την ποιότητα διαχωρισμού για ένα εύρος λειτουργικών συνθηκών. Επιπλέον γίνεται συστηματική εξέταση νέων προσροφητικών υλικών που προκύπτουν από μεταβολή της ισοθέρμου ισορροπίας του 13X ζεολίθου σε διεργασία P/VSA ενός σταδίου και μελετάται η επίδραση του βέλτιστου σχεδιασμού του προσροφητικού υλικού των κλινών στην απόδοση λειτουργίας της διεργασίας και εξετάζονται πιθανά συνδυαστικά οφέλη μεταξύ προσροφητικού υλικού και διεργασίας P/VSA. Επίσης διεξάγονται μελέτες δυναμικής βελτιστοποίησης τόσο της διεργασίας P/VSA ενός σταδίου όσο και της διεργασίας P/VSA δύο σταδίων, κάτω από ρεαλιστικούς σχεδιαστικούς και λειτουργικούς περιορισμούς της διεργασίας με σκοπό την ελαχιστοποίηση της καταναλισκόμενης ενέργειας για προκαθορισμένες ελάχιστες απαιτήσεις στην καθαρότητα του CO_2 και στην ανάκτηση του CO_2.

Από τις μελέτες δυναμικής βελτιστοποίησης προκύπτει ότι υπάρχει μια πολύπλοκη συσχέτιση μεταξύ των βέλτιστων δεικτών απόδοσης της διεργασίας P/VSA και των συνθηκών λειτουργίας που ποικίλει μεταξύ των διαφόρων προσροφητικών υλικών και δεν μπορεί να ποσοτικοποιηθεί με απλή σύγκριση των ισόθερμων προσρόφησης CO_2/N_2 και των διαφόρων φυσικοχημικών δεδομένων όπως π.χ. της εκλεκτικότητας ισορροπίας και της δυναμικότητας προσρόφησης-εκρόφησης

ισορροπίας. Έχει έτσι δειχθεί ότι οι στρατηγικές μοντελοποίησης, προσομοίωσης και βελτιστοποίησης της διεργασίας P/VSA, παρέχουν τον πιο αξιόπιστο τρόπο για να αξιολογηθούν τόσο ποιοτικά, όσο και ποσοτικά διάφορα προσροφητικά υλικά καθώς επίσης και συνδιασμοί προσροφητικών υλικών για τη μέγιστη δέσμευση του CO_2.

Η διατριβή αυτή δείχνει ότι η διεργασία P/VSA δύο σταδίων είναι μια αποδοτική και υποσχόμενη βιομηχανική τεχνολογία δέσμευσης του CO_2 εξαιτίας της σχετικά χαμηλότερης κατανάλωσης ενέργειας σε σχέση με την ανταγωνιστική διεργασία χημικής απορρόφησης του CO_2 με χρήση μονοαιθανολαμίνης. Συμπερασματικά, για να γίνει πιο ανταγωνιστική η δέσμευση και η αποθήκευση του CO_2 σε μια μελλοντική βιώσιμη αγορά ενέργειας, νέες καινοτόμες διεργασίες δέσμευσης CO_2 απαιτούνται να αναπτυχθούν, οι οποίες να μπορούν να μειώσουν τόσο το κόστος δέσμευσης CO_2, όσο και το συνολικό κόστος της πάγιας επένδυσης της εγκατάστασης. Η παρούσα διδακτορική διατριβή κινήθηκε επιτυχώς προς αυτήν την κατεύθυνση, με την συστηματική μελέτη μιας νέας γενιάς καινοτόμων προσροφητικών υλικών των οργανομεταλλικών πορώδων δομών (MOFs) και των νέων προσροφητικών υλικών που προκύπτουν από μεταβολή της ισοθέρμου ισορροπίας του 13X ζεολίθου και την αξιολόγηση της επίδρασης του βέλτιστου σχεδιασμού του προσροφητικού υλικού των κλινών στην απόδοση λειτουργίας της διεργασίας P/VSA.

ABSTRACT

This thesis presents a mathematical modelling framework for the simulation and optimisation of P/VSA (Pressure/Vacuum Swing Adsorption) process for post-combustion CO_2 capture from dry flue gas. The core of the modelling framework represents a detailed adsorbent bed model relying on a coupled set of mixed partial differential and algebraic equations (PDAEs) for mass, heat and momentum balance at both bulk gas and particle level, equilibrium isotherm equations, transport and thermo-physical properties of the gas mixture and boundary conditions according to the operating steps. The proposed modelling framework has been implemented in the gPROMS™ modelling environment. The framework provides a comprehensive qualitative and quantitative insight into the key phenomena taking place in the process. A systematic parametric analysis provides significant insight into the most critical design and operating variables, and their effect on process performance indicators.

The modelling framework has been first validated against literature data, illustrating good agreement in terms of several process performance indicators. Accordingly, the model has been used to evaluate three available potential adsorbents for CO_2 capture, namely, zeolite 13X, activated carbon and metal organic framework (MOF), Mg-MOF-74. The results from systematic comparative simulations demonstrate that zeolite 13X has the best process performance among the three adsorbents, in terms of CO_2 purity and CO_2 recovery. On the other hand, Mg-MOF-74 appears to be a promising adsorbent for CO_2 capture, as it has considerably higher CO_2 productivity compared to the other two adsorbents. Furthermore, process optimisation studies using zeolite 13X and Mg-MOF-74, have been performed to minimize energy consumption for specified minimum requirements in CO_2 purity and CO_2 recovery at nearly atmospheric feed pressures. The optimisation results indicate that the minimum target of 90% in CO_2 purity and 90% in CO_2 recovery is met for the single-stage VSA process for both adsorbents under different adsorption and desorption pressures thus resulting in different energy requirements.

As a next step, an integrated two-stage P/VSA process for post-combustion CO_2 capture from dry flue gas has been simulated and optimised. In the first stage CO_2 is

concentrated to 40-60% at almost atmospheric pressure and in the second stage it is further concentrated to 95%. All possible combinations of two different types of adsorbents (zeolite 13X and Mg-MOF-74) have been employed, to study the effect of adsorbent type on key process performance indicators. The results from systematic comparative simulations demonstrate that the combination of adsorbents zeolite 13X − Mg-MOF-74 illustrates the best process performance, in terms of CO_2 purity and CO_2 recovery, followed by the use of zeolite 13X at both stages of the process. Furthermore, process optimisation studies employing the above combinations of adsorbents have been performed to minimize energy consumption for specified minimum requirements in CO_2 purity and CO_2 recovery. The optimisation results indicate that the minimum target of 95% in CO_2 purity and 90% in CO_2 recovery is met for the integrated two-stage P/VSA process, for both combinations of adsorbents under different adsorption and desorption pressures thus resulting in different energy requirements and CO_2 productivities.

Furthermore, a single-stage P/VSA process for CO_2 capture from dry flue gas has been considered using new zeolite 13X-based adsorbents resulting from perturbation on the 13X zeolite isotherm. First zeolite 13X, the current benchmark commercial adsorbent for CO_2 capture, has been considered. The modelling framework has been used to study and evaluate new zeolite 13X-based adsorbents for more efficient CO_2 capture. The results from systematic comparative simulation studies demonstrate that a modified zeolite 13X-based adsorbent leads to a better process performance compared with the original zeolite 13X. Accordingly, process optimisation studies employing the above potential adsorbents are performed to minimize energy consumption for specified minimum requirements in CO_2 purity and CO_2 recovery. The optimisation results indicate that the minimum target of 95% in CO_2 purity and 90% in CO_2 recovery is easily met for the single-stage P/VSA process for both potential adsorbents under different adsorption and desorption pressures thus resulting in different energy requirements and CO_2 productivities.

LIST OF ABBREVIATIONS

CCS	Carbon Capture and Sequestration
CSS	Cyclic Steady State
CFDM	Centered Finite Difference Method
DAEs	Differential and Algebraic Equations
GHGs	Greenhouse Gases
LDF	Linear Driving Force
MOFs	Metal Organic Frameworks
MOL	Method Of Lines
PDAEs	Partial Differential and Algebraic Equations
PSA	Pressure Swing Adsorption
P/VSA	Pressure Vacuum Swing Adsorption
RPSA	Rapid Pressure Swing Adsorption
SLPM	Standard Liters per Minute
TSA	Temperature Swing Adsorption
VSA	Vacuum Swing Adsorption

CHAPTER 1
INTRODUCTION

1. Introduction

1.1. Anthropogenic greenhouse gases (GHGs)

The composition of the earth's atmosphere is roughly 78% nitrogen, 21% oxygen, and 1% other gases. Water vapor, carbon dioxide (CO_2) and some other minor gases present in the atmosphere absorb some of the solar thermal radiation keeping an energetic balance that allows earth to be warmer than it should be. These gases are known as greenhouse gases (GHGs) because they act as a partial blanket for thermal radiation. This blanketing is a natural greenhouse effect. A higher concentration of any anthropogenic GHGs due to human activities, implies that the greenhouse effect will increase changing this energetic balance with still unknown consequences in global weather (Grande *et al.,* 2005).

It was observed that in the last century the ocean level has increased in a direct relationship with an increase in average ground temperature. To avoid serious catastrophes, many countries agreed in some commitments (e.g. Kyoto protocol) to stabilize the GHGs concentration in the atmosphere, for CO_2, CH_4, NO_x, SO_x, etc. As the country emissions of GHGs are not uniform and as local economic factors also have to be taken into account, the commitments are not equal to all countries (Grande *et al.,* 2005).

CO_2 emissions are quite high in the entire European continent with many countries being in the top 20 larger polluting countries of the world. The CO_2 emissions per capita of European countries are illustrated in Figure 1.1. Co-generation of electricity and heat has proved to be one of the most efficient and less polluting technologies for power generation. Even though, these units are still based on the combustion of fossil fuels, requiring additional processes for CO_2 sequestration and concentration for further uses.

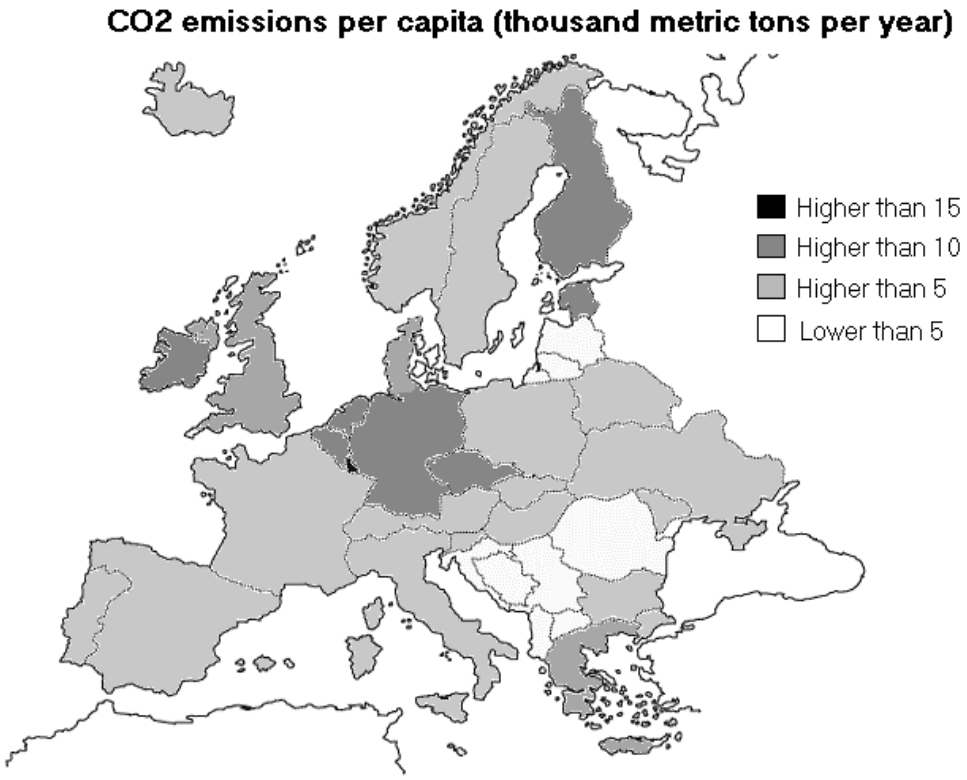

Figure 1.1. CO_2 emissions per capita of European countries (Grande *et al.,* 2005).

Anthropogenic CO_2 emissions are considered a great threat to the environment because of their contribution to the greenhouse effect and global warming. CO_2 is considered to be responsible for 60% of the global warming caused by GHGs (Houghton *et al.,* 2001). There are three ways to reduce CO_2 in the atmosphere: 1) more efficient use of energy, 2) use of alternative fuels and alternative energy sources, and 3) carbon capture and sequestration (CCS). The CCS process involves CO_2 separation followed by pressurization, transportation, and sequestration. According to the International Energy Agency's roadmap, 20% of the total CO_2 emissions should be removed by CCS by the year 2050 (IEA, 2008). A majority of current research efforts are devoted to the CO_2 removal from stationary power production sources. These sources are by far the most dominant contributors of the CO_2 emission, accounting for roughly 47% of the total anthropogenic CO_2 emissions (IPCC, 2005). Finally, due to the economies of scale, it is economically more attractive to implement CCS technologies on large-scale power plants. CO_2 capture is the most expensive part of CCS, accounting for more than 75% of the estimated

overall CCS cost (Feron and Hendriks, 2005). The National Energy Technology Laboratory, under the U.S. Department of Energy, has specified 95% CO_2 purity and 90% CO_2 recovery target levels for the CO_2 capture processes (NETL, 2012).

One of the main sources of anthropogenic GHGs is CO_2 from fossil fuel power stations. Today, fossil fuels provide about 85% of the global energy demand and the outlook is that they will remain the dominant source of energy for the next decades. Consequently, global energy-related CO_2 emissions, especially from power plants that burn fossil fuels, have increased, thereby increasing CO_2 concentration levels in the atmosphere (IEA/WEO, 2006). To avoid disruption in energy supply or economic instabilities until less contaminant energy production processes are implemented, the capture of CO_2 and its storage is presented as a temporary solution. One option to mitigate the emission of CO_2 is to capture it from emission sources, store it in the ocean or underground in geologic formations as it is illustrated in Figure 1.2. Thus it is important to develop energy-efficient industrial technologies for CO_2 capture.

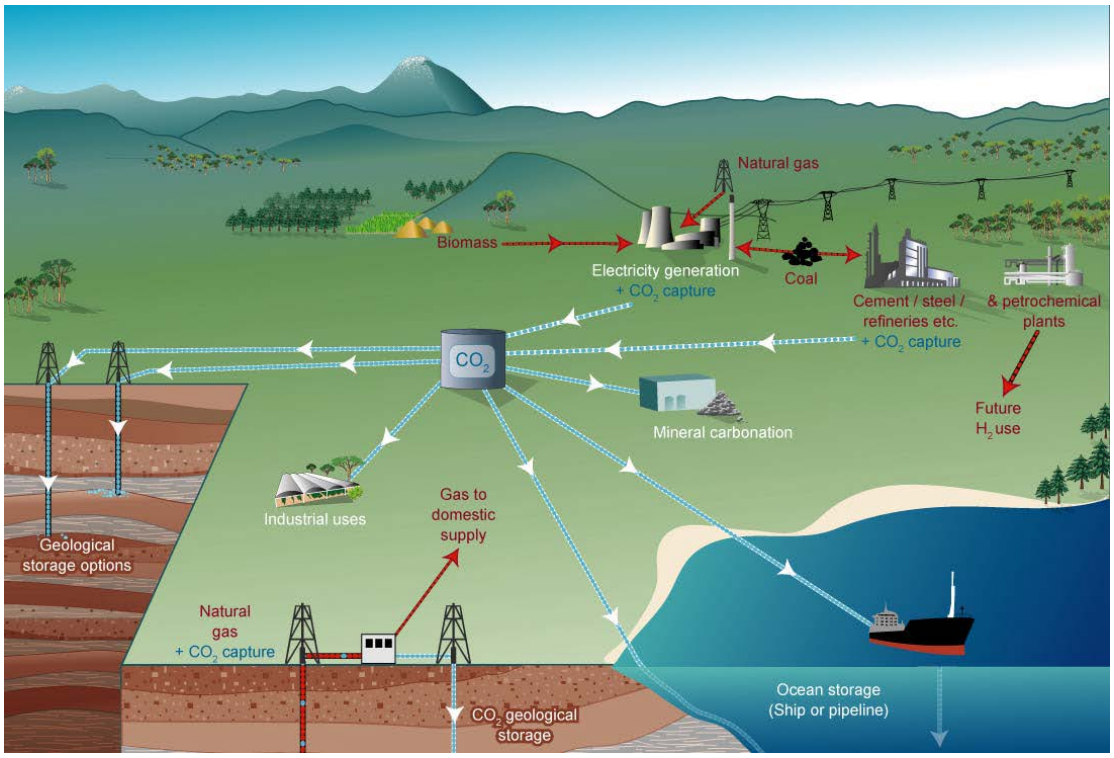

Figure 1.2. Schematic diagram of possible CCS systems showing the sources for which CCS might be relevant, transport of CO_2 and storage options (IPCC, 2005).

1.2. Overview of CO_2 capture technologies

Currently, there are three main available approaches to capture CO_2 from large scale industrial facilities or power plants: (i) pre-combustion capture, (ii) oxy-fuel combustion capture, and (iii) post-combustion capture (Abanades *et al.*, 2015). Pre-combustion capture involves first the gasification or reforming of solid, liquid or gaseous fuel into syngas, which is a combustible fluid mixture containing CO_2. CO_2 is separated from syngas before combustion. The syngas is then burned in a conventional combined-cycle arrangement integrated to the gasification unit (Integrated Gasification Combined Cycle, IGCC) to generate electric power. In oxy-fuel combustion the fuel is burned with oxygen instead of air, to produce a flue gas that consists of primarily CO_2. Post-combustion CO_2 capture involves the separation and capture of CO_2 from large exhaust sources including coal-fired power plants, cement industries, iron and steel mills and other industrial sectors. There are several commercial technologies available for post-combustion CO_2 capture: absorption, membranes separation, cryogenic separation process and adsorption (Aaron and Tsouris, 2005). An overview of CO_2 capture technologies is illustrated in Figure 1.3.

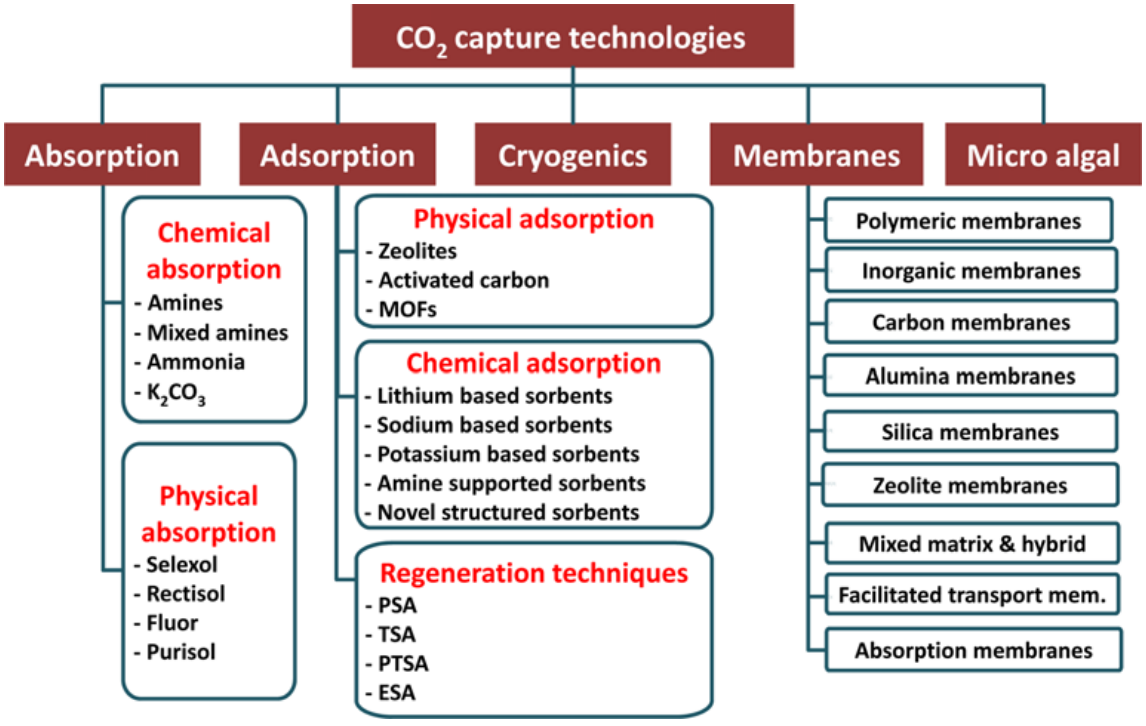

Figure 1.3. Overview of CO_2 capture technologies (Zaman and Lee, 2013).

Chemical absorption using a liquid solvent is a commercial technology available for post-combustion CO_2 capture. An appropriate solvent must dissolve CO_2, but not O_2, N_2 and other impurities. The solvent needs to be stable to the contact with fly ashes, SO_x and NO_x present in the flue gas. The more the solvent is attracted to CO_2, the higher the loading, but the higher the cost for the regeneration of the solvent as well. One of the most common solvents used for this operation is mono-ethanol-amine (MEA) aqueous solution, effective at low partial pressure of CO_2, while at high partial pressure of CO_2 solid solvents such as lithium hydroxide and lithium zirconate are preferable. The capture of CO_2 in industrial streams is actually performed mainly by chemical absorption in MEA and solvent extraction. One of the advantages of chemical absorption is that it is a well known process, both in terms of the mechanisms involved and the thermodynamics of the operation. Extending this technology to CO_2 sequestration from flue gases has several drawbacks: the global economics of the process (absorption technology is not very suitable for low molar fractions of CO_2), the extensive corrosion rate of the steel equipment due to high O_2 content in the flue gas, the high energy requirements for the regeneration of the solvent, the need of a frequent addition of new solvent and other operating and maintenance costs. Main improvements needed in this area are the development of new solvents and the optimisation of the regeneration step to increase the energy efficiency of the process (Aaron and Tsouris, 2005; Rao and Rubin, 2002).

In membranes separation the CO_2 selectively passes through the membrane and an enriched gas phase is obtained. The main advantage of membranes is the simplicity of the equipment needed. However, the efficiency of the separation is often not satisfactory due to poor selectivity or permeability of the membrane towards CO_2. Another drawback is that membranes do not usually perform well at high temperatures, which are common for flue gases coming from a stack. As in the case of the chemical absorption, also membranes can be degraded by the impurities of the flue gas. Mechanical and chemical stability are both a crucial issue. The results achieved by the current research in the direction of more stable membranes (new metallic, ceramic and alumina membranes) will determine whether this technology can stand alone or can be used within a hybrid separation system (Aaron and Tsouris, 2005). Furthermore, while membrane technology has a smaller

environmental footprint, most membranes are incapable of extracting CO_2 with high purity and recovery from flue gases (Hasan *et al.,* 2013).

The first step of the cryogenic separation process is the removal of all the components of the flue gas, except of N_2 and CO_2. Then, the binary mixture of N_2 and CO_2 is sent to a cryogenic chamber where the CO_2 is liquefied by appropriate manipulation of temperature and pressure. When the triple point of the CO_2 is reached (-56.6 C and 7.4 atm), CO_2 condenses while N_2 remains in gas phase. The main advantages of the cryogenic separation method are that it provides liquid CO_2, ready for the transport in pipelines, and the high purity which can be reached (even over 99.95%). On the other hand, the process is highly energy demanding both because of the effort needed to keep the system refrigerated, and because of the auxiliary step for the separation of the other components prior the refrigeration stage (Aaron and Tsouris, 2005).

While chemical absorption involves the dissolution of the CO_2 in the solvent, adsorption is a heterogeneous process. The adsorption of CO_2 to the adsorbent particles can be manipulated by varying the conditions of pressure, because higher pressure promote adsorption of the most attracted species to the adsorbent particle. This observation lead to the spread of Pressure Swing Adsorption (PSA) process. PSA is a promising technology for CO_2 capture due to its relatively better separation performance, higher productivity, lower energy consumption and lower capital investment cost in comparison to the traditional separation processes, such as cryogenic processes (Ruthven, 1984; Yang, 1987). Adsorption processes have the potential to deliver significant improvements over amine absorption capture processes due to their increased flexibility to adapt to different feed stream specifications and operating conditions, the possibility of developing novel tailor-made materials engineered for this purpose and the more efficient regeneration. PSA processes have been widely applied for the removal of CO_2 from various feed mixtures, such as CO_2 in the steam methane reformer off gas, natural gas, and flue gas (Sircar and Kratz, 1988). Cyclic adsorption processes such as PSA/VSA are some of several separation methods being investigated to remove CO_2 from flue gas and natural gas so that it can be compressed and stored underground in geologic formations (D'Alessandro *et al.,* 2010; IPCC, 2005).

1.3. Fundamentals of a PSA/VSA process

Separation of gases accounts for a major fraction of the production cost in chemical and petrochemical industry. There has been a growing demand for economical and energy efficient gas separation processes. The new generation of more selective adsorbents developed in recent years has enabled adsorption-based technologies to compete successfully with traditional gas separation techniques, such as cryogenic distillation and chemical absorption. A considerable increase in the applications of adsorptive gas separation technologies, such as PSA, have been reported during the last few decades. A PSA process is a widely used industrial unit operation process for separating gas mixtures where one or more gases are preferentially adsorbed at high pressure and then desorbed at a lower pressure and has become the state-of-the-art separation technology. PSA like all adsorption separation processes requires the use of a fixed adsorbent bed packed with a microporous-mesoporous adsorbent material that selectively adsorbs one component (or a group of related components) from a gas mixture. This selectivity can be either thermodynamic or kinetic in nature, based on differences in adsorption equilibrium or in adsorption kinetics (diffusion rates), respectively, between the components to be separated. Evidently the adsorbent, and hence the adsorbent bed, will be saturated after a period of time. For this reason the adsorption step must be accompanied by a regeneration or desorption step, where the preferentially adsorbed species are removed from the adsorbent that can be further used in the next cycle. The adsorption step is terminated well before the strongly adsorbed species breaks through the adsorbent bed, while the desorption step is generally terminated before complete regeneration of the adsorbent bed. The effluent during the adsorption step that no-longer contains the preferentially adsorbed species is called the light product or “raffinate”, while the effluent during the desorption step that contains the strongly adsorbed species in larger proportions compared to the feed stream, is often called the heavy product or “extract” (Ruthven, 1984; Ruthven *et al.,* 1994; Yang, 1987). The main purpose of a PSA process is to purify the weakly adsorbed gas (light product or “raffinate”), or alternatively to concentrate the strongly adsorbed gas (heavy product or “extract”). A simple flow chart of a two-bed Skarstrom cycle is shown in Figure 1.4.

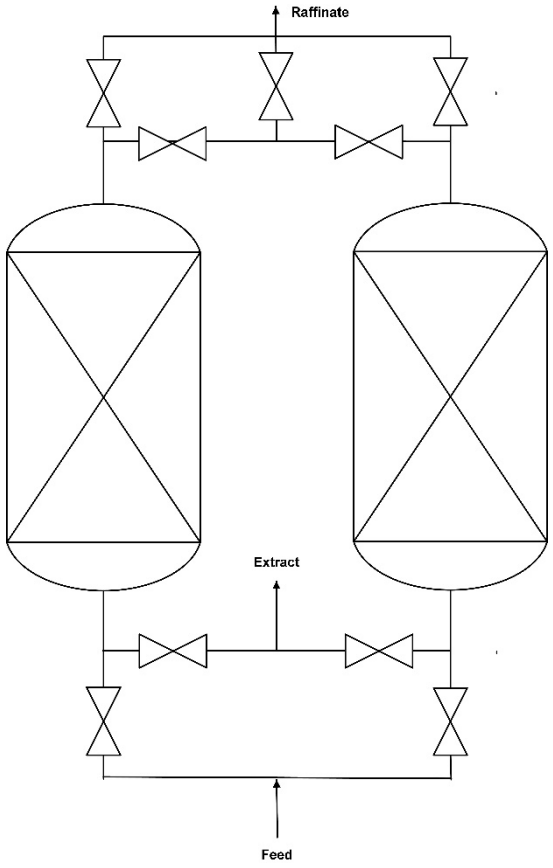

Figure 1.4. A simple flow chart of a two-bed Skarstrom cycle (Kikkinides *et al.,* 2011).

PSA processes involve the preferential adsorption of certain components of a gas mixture on a microporous-mesoporous solid adsorbent at a relatively high pressure, via gas-solid contact in a packed adsorbent bed, in order to produce a gas stream enriched in weakly adsorbed components of the feed gas. The adsorbed components are then desorbed from the solid adsorbent by lowering their gas-phase partial pressures inside the adsorbent bed to enable adsorbent re-usability. The desorbed gases are enriched in the strongly adsorbed components of the feed gas. No external heat is generally used for desorption. While a PSA process carries out adsorption at super-ambient pressure and desorption at near-ambient pressure level, a Vacuum Swing Adsorption (VSA) process undergoes adsorption at near-ambient pressure, while desorption is achieved under vacuum and a Pressure Vacuum Swing Adsorption (P/VSA) process refers to cycling between adsorption step at pressures above atmospheric and desorption step under vacuum. When the total cycle time is

smaller than 30 seconds, the process is normally called Rapid Pressure Swing Adsorption (RPSA).

Since the adsorption equilibrium depends on specific operating conditions (composition, temperature and pressure), by changing one of these process parameters it is possible to regenerate the adsorbent. When the regeneration of the adsorbent is performed by reducing the total pressure of the system, the process is termed PSA, the total pressure of the system changes (swings) between high pressure in feed and low pressure in regeneration. When the regeneration of the adsorbent is performed by increasing the temperature of the system, the process is termed Temperature Swing Adsorption (TSA), the temperature of the system changes (swings) between high temperature in regeneration and low temperature in feed.

A major advantage of PSA over TSA process, is that, in PSA process, pressure can be changed (swing) much more rapidly than temperature, resulting in much faster cycle operations and thus higher product productivity. The thermodynamic principle of PSA and TSA processes is illustrated in Figure 1.5.

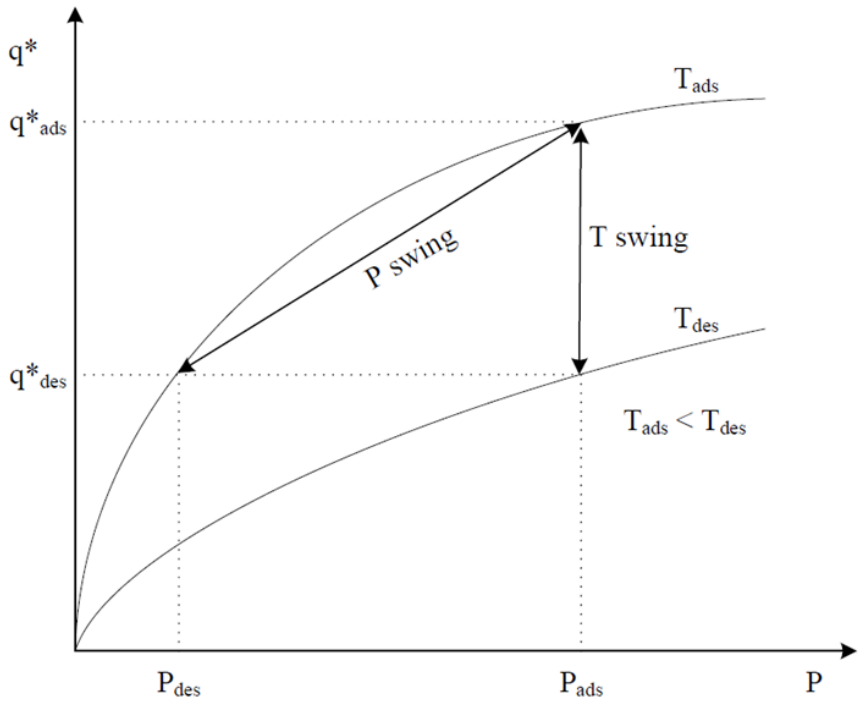

Figure 1.5. Gas-solid adsorption equilibrium isotherms and change in equilibrium solid loading with pressure and temperature (Agarwal, 2010).

The relation between the equilibrium amount adsorbed and the total pressure of the fluid phase at a particular temperature is called an adsorption isotherm. Figure 1.5 also shows how adsorption/desorption is facilitated by changing total pressure or temperature of the system. It must be noted that an adsorption process is always exothermic while desorption is always endothermic. Since the overall change in system's entropy is negative during adsorption, enthalpy change must be negative to ensure a net negative change in the Gibbs free energy (vice-versa for desorption). Consequently, adsorption is favored at a lower temperature, while desorption at a higher one. Similarly, at a high pressure, more adsorbate molecules interact with the molecules at the adsorbent surface leading to a higher adsorbent surface coverage and higher equilibrium solid loading. Hence, adsorption is favored at a higher pressure while lowering the pressure facilitates desorption.

The main advantages of PSA processes are (Agarwal, 2010):

- PSA processes operate at ambient temperatures and do not require any solvent for product recovery or adsorbent regeneration. As a result, their capital investment cost is quite less compared to cryogenic distillation technologies. Operating cost for these processes comes from the energy requirements for compression and vacuum generation.
- Pressure manipulation serves as an extra degree of thermodynamic freedom, thus introducing significant flexibility in process design as compared with conventional technologies such as cryogenic distillation, extraction or chemical absorption.
- Numerous microporous-mesoporous adsorbents are available which are specifically tailored and engineered for a particular application, thus exhibiting high selectivity and adsorption capacity which leads to extremely high purity and recovery separation performance.
- Optimum combination between adsorbent materials and a PSA process while synthesizing the separation scheme drives innovation and leads to highly efficient designs for PSA processes.

1.4. Adsorbent properties

Porous materials with large internal surface areas serve as a host for different applications, for example gas storage, mixture separation and catalysis. Porous materials are classified by their pore size according to the International Union of Pure and Applied Chemistry (IUPAC):

- Microporous materials have pore diameters of less than 20 Å
- Mesoporous materials have pore diameters between 20 Å and 500 Å
- Macroporous materials have pore diameters greater than 500 Å

The pore size can play a crucial role in the adsorption and diffusion of adsorbates and consequently on their final separation performance. In micropores, where the adsorbate size and pore size is comparable, Van der Waals and electrostatic interactions of guest molecules and pore walls as well as guest-guest interactions become significant making them good candidates for gas storage and separation applications. In these conditions, preferential adsorption, steric hindrance and molecular sieving effects can all contribute to the separation of different adsorbate molecules. In mesopores, interactions between adsorbates occur more frequently compared to weaker interactions between adsorbates and the framework walls but high adsorption capacity is still achievable. In macropores, the specific surface area is very small and they hardly play a role in adsorption (Ruthven, 1984; Ruthven *et al.,* 1994).

Adsorbents are characterized by surface properties such as specific surface area. The role of an adsorbent is to provide surface for selective adsorption of certain components from the fluid phase. The creation of a large internal surface area in a limited volume is commercially achieved by casting adsorbents from microporous materials. In addition to micropores, some adsorbents have larger pores called macropores which result from aggregation of fine powders into particle-pellets.

Two classes of adsorbents can be considered: homogeneous and composites adsorbents (Ruthven, 1984; Ruthven *et al.,* 1994). Homogeneous adsorbents are those whose pore structure persists throughout the entire solid. Since the size of the pores is determined by the chemical structure of the adsorbent, in homogeneous

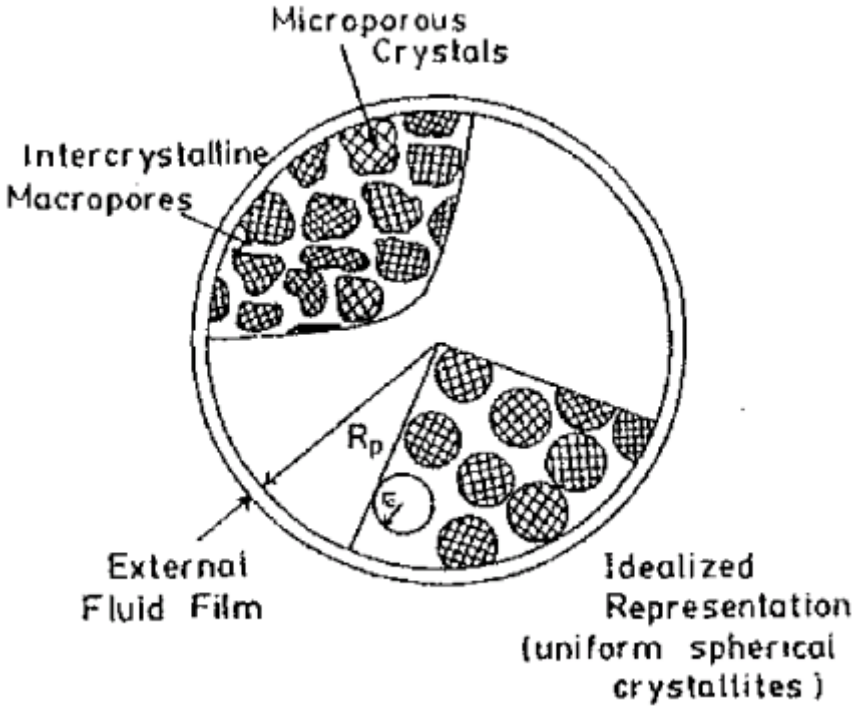

Figure 1.6. A composite adsorbent particle-pellet with different mass transfer resistances (Ruthven *et al.,* 1994).

adsorbents the pore size distribution is unimodal. Examples of homogeneous adsorbents are silica gel, activated alumina, activated carbon and homogeneous ion exchange resins. Composite adsorbents are obtained by the aggregation of small microporous microparticles, bound together with a clay binder to form a pellet, which is a composite structure that contains both macropores and micropores. The structure of a composite adsorbent particle-pellet is illustrated in Figure 1.6, showing the three main mass transfer resistances: external film resistance, microporous or intracrystalline resistance (within the microporous crystals) and macroporous or intercrystalline resistance (within the paths described by the binder). Examples of composite adsorbents are carbon molecular sieves, pelletized zeolites and macroreticular ion exchange resins. Macropores function as diffusion paths of adsorbate molecules from outside the particle-pellet to the micropores. As a result of such porous network, adsorption/desorption kinetics is controlled by intra-particle diffusion.

Hence, the desirable properties which an adsorbent should have are as follows (Nilchan, 1997):

- Capacity: An adsorbent is desired to provide a large specific surface area for a large adsorption capacity. A low capacity adsorbent leads to longer and expensive adsorbent beds.
- Selectivity: An adsorbent must selectively retain one or more adsorbates from the fluid phase. This can be achieved either by equilibrium selectivity, in which species adsorb differently as a consequence of different equilibrium affinities, or by kinetic selectivity, in which relative adsorption depends on the difference of intra-particle diffusion rates among different adsorbate species.

Adsorption capacity, which is the amount of gas adsorbed at the feed condition, is the most common measurement that material developers use to demonstrate the potential of new materials. For the special case of CO_2 capture while the adsorbent must adsorb a significant amount of CO_2 in order to be useful in a capture process, it is more important that it can be regenerated. To account for this, the concept of working capacity has been developed, which is the difference between the amount of gas adsorbed at the adsorption and desorption pressures. Furthermore, because desorption is endothermic, the adsorbent bed temperature decreases as the pressure decreases, shifting the adsorption isotherm and decreasing the working capacity. Because CO_2 typically has a large heat of adsorption it is especially critical to consider thermal effects when analyzing CO_2 capture. Figure 1.7 demonstrates the adsorption capacity and working capacity for a pressure swing between a CO_2 partial pressure of 0.15 bar (typical feed conditions) and 0.01 bar (typical conditions at the end of regeneration step). The starting temperature is 320 K and the final temperature is 300 K (assuming 20 K temperature swing during blowdown step). It is clear that the actual working capacity obtained in practice (A = adiabatic working capacity) is lower than the apparent isothermal working capacity (A + B) and significantly lower than the absolute capacity (A + B + C).

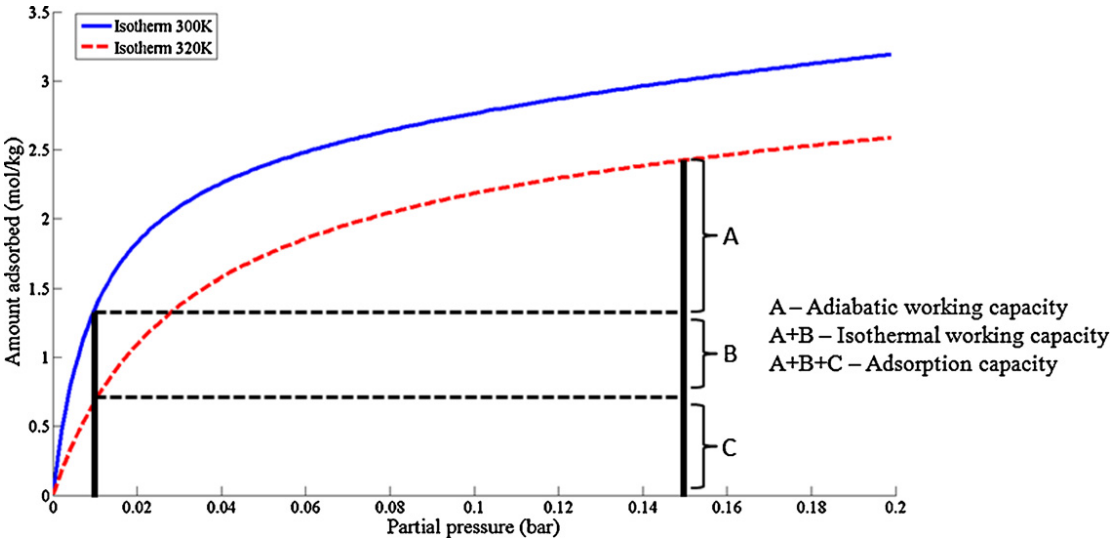

Figure 1.7. Demonstration of adsorption capacity and working capacity for pressure swing on a typical adsorbent (Maring and Webley, 2013).

1.5. Typical operating steps of a PSA/VSA process

Practical PSA/VSA processes are substantially sophisticated with multi-beds executing a wide variety of non-steady-state operating steps in a non-trivial sequence. Besides adsorption and desorption, such a sequence also involves a big variety of operating steps essential to control product gas purity and recovery, and optimise overall separation efficiency of the process. Each adsorbent bed undergoes this sequence of operating steps repeatedly, and thus the entire PSA/VSA system operates in a cyclic manner. The scheduling of PSA/VSA units is carried out in different operating steps which normally involve some changes in the operating conditions of the adsorbent bed. The typical operating steps of a PSA/VSA process are (Nikolic *et al.,* 2008):

- Pressurization (FP, LPP, HPP): the adsorbent bed pressure is increased to the feed pressure. This step can be done with the feed stream co-currently (FP), or with the light product counter-currently to feed stream (LPP), or with the heavy product co-currently to feed stream (HPP). The correct selection of the pressurization step can be very important in some cases.
- Feed or Adsorption (F, Ads): step where high pressure feed is admitted to the adsorbent bed and where the strongly adsorbed component (heavy product or extract) is preferentially adsorbed. In this step, the stream with the weakly adsorbed components (light product or raffinate) is withdrawn by the other adsorbent bed end.
- Co-current depressurization (CoD): before the strongly adsorbed component breakthrough, feed is stopped and the pressure of the adsorbent bed is reduced normally, co-currently to feed stream.
- Counter-current depressurization or Blowdown (CnD): in this step, the strongly adsorbed components are partially removed from the adsorbent. The blowdown is carried out at the lowest pressure of the system and normally counter-current to feed direction.
- Light reflux or purge (LR): in order to remove the strongly adsorbed component from the gas phase, a counter-current purge with the weakly adsorbed components is carried out. This step is also carried out at the

lowest pressure of the system, although some intermediate pressures can be employed.

- Heavy reflux or rinse (HR): in P/VSA processes where the strongly adsorbed component should be recovered with high purity, it is advisable to use a co-current stream with the strongly adsorbed component before blowdown in order to displace the weakly adsorbed components from gas phase.
- Pressure equalization (PE): this step is carried out by putting in contact two adsorbent beds at different pressure levels where the streams taken from one adsorbent bed from the depressurization steps are recycled to other adsorbent bed and can be repeated several times in order to save compression energy.

1.6. Cyclic Steady State (CSS)

PSA/VSA processes have an important functional difference compared to other separation processes including absorption, distillation and membrane processes: The process operates under transient conditions, while the above mentioned processes operate at steady state (Ruthven, 1984; Ruthven *et al.,* 1994; Yang, 1987). Hence, from an operational point of view, PSA/VSA is an intrinsic dynamic process operating in a cyclic manner with a fixed cycle time and each adsorbent bed undergoing the same sequence of steps. After a number of cycles, the adsorbent bed approaches a "cyclic steady state" (CSS) in which the conditions at the end of each cycle are identical to those at the start of the same cycle. Starting from a given initial condition, a PSA/VSA process takes a number of cycles to reach a state in time, called CSS, where the values of all variables of the system at the end of a cycle are same as at the start of the same cycle.

1.7. Process performance indicators

The design of a cost-competitive and highly productive PSA/VSA process requires the optimisation of the process conditions with respect to the usually conflicting objectives process performance indicators. A challenging task in comparing various process alternatives and design options for PSA/VSA processes is the quantification of their performance with measuring some important performance indicators such as product purity, product recovery, product productivity and energy consumption defined in equations 1.1, 1.2, 1.3 and 1.4, respectively. These process performance indicators have been extensively used to benchmark different PSA/VSA processes.

$$\text{product purity} = \frac{\text{moles of component in the product stream}}{\text{total moles of product stream}} \tag{1.1}$$

$$\text{product recovery} = \frac{\text{moles of component in the product stream}}{\text{moles of component in the feed stream}} \tag{1.2}$$

$$\text{product productivity} = \frac{\text{moles of component in the product stream}}{(\text{amount of adsorbent used})\ (\text{cycle time})} \tag{1.3}$$

$$\text{energy consumption} = \text{sum of all compression and vacuum sources used} \tag{1.4}$$

Product purity and product recovery are related to the separation efficiency of the PSA/VSA process. Most works on PSA/VSA processes have shown that normally the product purity and product recovery present a trade-off for the design. In the case of recovering the weakly adsorbed gas, if more purge (light reflux) is used, more of the contaminants can be desorbed from the adsorbent bed and light product purity increases, but since more amount of light product is exiting from the bottom end of the adsorbent bed, light product recovery is smaller. A similar effect is observed in the case of concentrating the strongly adsorbed gas. If more rinse (heavy reflux) is used, more of the contaminants can be desorbed from the adsorbent bed and heavy product purity increases, but since more amount of heavy product is exiting from the top end of the adsorbent bed, heavy product recovery decreases.

Product purity is usually set by the customer requirements while product recovery is to be maximized at the specified purity levels. In most of the PSA/VSA processes, this leads towards a trade-off situation as design changes to improve product recovery adversely affects the product purity. Product recovery and product purity have a

strong effect on operating costs related to the production, as their definitions incorporates the information of both feed and the product streams. On the other hand, capital cost due to the use of expensive adsorbents can also be quite significant.

Finally it is important to note that all process performance indicators are calculated once the system reaches CSS. Furthermore, in the present study, the term product refers to the heavy product (extract), which is CO_2 in the specific PSA/VSA process.

1.8. Commercial PSA/VSA processes

While initial commercial PSA/VSA applications (based on the patents of Skarstrom) included gas drying and purification of dilute mixtures, current industrial applications include solvent vapor recovery, air fractionation, simultaneous production of hydrogen and carbon dioxide from steam methane reformer off gas (SMROG), separation of hydrocarbons such as carbon monoxide-hydrogen, carbon dioxide-methane, n-parafins separation, alcohol dehydration and carbon dioxide capture from flue gas. The production of pure hydrogen from various gas mixtures by using PSA/VSA processes has become the state-of-the-art industrial technology. In most commercial PSA/VSA cycles, the weakly adsorbed component (light product or raffinate) in the mixture is the desired product and enriching the strongly adsorbed component (heavy product or extract) is not a concern. On the other hand, for CO_2 sequestration, it is necessary to concentrate CO_2 to a high purity in order to reduce the compression and the transportation cost. Moreover, safety and environmental issues are the additional reasons for concentrating CO_2 to a high purity. Typically adsorbents preferentially adsorb CO_2 from a flue gas mixture, consequently making it a heavy product. The conventional PSA/VSA cycles are inappropriate for concentrating heavy product because the light reflux step in these cycles uses a portion of the light product gas, which necessarily dilutes the heavy component in the heavy product stream. As a result, a pure light product is easy to attain from such cycles, but not a pure heavy product. Thus, it is necessary to develop PSA/VSA processes specifically targeted to obtain pure strongly adsorbed component (CO_2 in this case). Because the product purity of the heavy product is limited by the gas mixture occupying the void spaces in the adsorbent bed, its purity can be increased by displacing the gas mixture in the void spaces with a pure heavy product gas. For instance, for the separation of CO_2 from a flue gas mixture (CO_2/N_2), the displacement can be accomplished by purging the adsorbent bed with CO_2 after the adsorption step in the PSA/VSA cycle. Hence, in order to obtain a pure heavy product gas, a heavy product pressurization step or a heavy reflux step is necessary in the cycle, similar to a light product pressurization step or a light reflux step in the conventional PSA/VSA cycles (IEA/WEO, 2006).

Several challenges exist in designing an adsorption-based process for CO_2 capture. First of all, the high CO_2 purity and CO_2 recovery (both >= 90%) required from a feed with low concentration of CO_2 makes the capture process challenging. Second, all existing adsorbents preferentially adsorb CO_2 than N_2 from a flue gas mixture due to its higher polarity. Thus, enriched CO_2 is recovered as the extract product. Designing PSA/VSA cycles for heavy product (extract) purification has not received much attention in the literature as most cycles focus on purifying the light product (raffinate). Third, the flue gas emissions from existing power plants are significantly larger than what existing gas separation plants can handle. For example, a 500 MW post-combustion coal-fired power plant produces approximately 10,000 tones CO_2 per day, which makes CO_2 productivity and equipment size (such as adsorbent beds, vacuum pumps, and compressors) critical factors. To increase the CO_2 productivity and reduce plant size, shorter cycle times are needed. Finally, the presence of moisture poses a significant challenge as most commercial adsorbents with high selectivity of CO_2 over N_2 also adsorb water strongly. This reduces the effective adsorbent capacity of CO_2 and lowers process performance (Haghpanah *et al.,* 2013b).

A variety of PSA/VSA cycles have been developed for the capture and concentration of CO_2 from flue gas. To design an appropriate cycle, it is essential to understand the nature of the separation problem. A typical dry flue gas from a post-combustion power plant is at 25-50 C, 1 bar, and consists of 15% CO_2 and 85% N_2.

The National Energy Technology Laboratory, under the U.S. Department of Energy (DOE), has specified 95% CO_2 purity and 90% CO_2 recovery targets for the CO_2 capture processes (NETL, 2012). Considering the low concentration of CO_2 in the flue gas, it is important to realize that pressurizing the entire flue gas stream can be expensive (Haghpanah *et al.,* 2013a).

As it has been already noted there is a trade-off among CO_2 purity in product gas, CO_2 recovery and energy consumption to capture 1kg CO_2 by the adsorption technology. When the flow rate of flue gas increases, a greater amount of CO_2 is adsorbed in the packed adsorbent bed during the same feed time, that results in the increase of CO_2 purity in product gas and the reduce of the energy consumption, but the CO_2 recovery is decreased.

The most important design decision when developing a PSA/VSA cycle is the choice of adsorbent (Kumar *et al.,* 1994; Ruthven *et al.,* 1994). However, it is still unclear how adsorbent properties such as adsorbent capacity, adsorbent selectivity and heat of adsorption correspond to process performance which is measured by product purity, product recovery, product productivity and energy requirements (Maring and Webley, 2013).

1.9. Review of state-of-the-art

1.9.1. Review of single-stage PSA/VSA processes for CO_2 capture

A fairly comprehensive review of the previous studies suggested in the literature on PSA/VSA cycle configurations for post-combustion CO_2 capture from flue gas is presented in this section. This literature review highlights the difficulties associated with choosing one PSA/VSA cycle configuration over another for a given application. Single-stage PSA/VSA cycle configurations suggested in the literature for post-combustion CO_2 capture are summarized in Table 1.1.

Kikkinides *et al.,* (1993) studied a cycle configuration (four-bed four-step) of single-stage VSA process and improved CO_2 purity and CO_2 recovery incorporating a heavy reflux step and recycling the effluent stream from the light product (raffinate) end of the adsorbent bed back to the adsorbent bed with the feed stream. With activated carbon as adsorbent for a flue gas containing 17% CO_2 this cycle configuration was able to achieve CO_2 purity of 99.997% and CO_2 recovery of 68.4%. With carbon molecular sieve (CMS) as adsorbent for a flue gas containing 17% CO_2 this cycle configuration was able to achieve CO_2 purity of 91.5% and CO_2 recovery of 68.4%.

Chue *et al.,* (1995) compared activated carbon and zeolite 13X using a cycle configuration (three-bed eight-step) of single-stage VSA process. They studied a VSA process from a feed containing 16% CO_2 with a heavy reflux step. With zeolite 13X as adsorbent CO_2 purity of 99% and CO_2 recovery of 45% were achieved and with activated carbon as adsorbent CO_2 purity of 98% and CO_2 recovery of 42% were reported. They suggested that despite a high heat of adsorption of CO_2, zeolite 13X is a better adsorbent than activated carbon because of its higher working capacity, lower purge requirement, and higher equilibrium selectivity.

Takamura *et al.,* (2001) studied a cycle configuration (four-bed eight-step) of single-stage VSA process for a flue gas containing 13% CO_2 with both heavy reflux and light reflux steps (dual reflux) and light-end pressure equalization steps. With a mixture of zeolites NaX, NaA as adsorbent this cycle configuration gave an enriched stream containing 91.6% CO_2 with a CO_2 recovery of 58.8%.

Table 1.1. Single-stage PSA/VSA cycle configurations suggested in the literature for post-combustion CO_2 capture.

PSA/VSA cycle configuration	operating step sequence	adsorbent	P_H, bar	P_L, bar	CO_2 Purity, %	CO_2 Recovery, %	Reference
4-bed 4-step	LPP,F+R,HR,CnD	AC	1.20	0.10	100	68.4	(Kikkinides *et al.,* 1993)
4-bed 4-step	LPP,F+R,HR,CnD	CMS	1.20	0.10	91.5	68.4	(Kikkinides *et al.,* 1993)
3-bed 8-step	FP,F,CoD,R,N,HR,CnD,N	13X	1.10	0.07	99.0	45.0	(Chue *et al.,* 1995)
3-bed 8-step	FP,F,CoD,R,N,HR,CnD,N	AC	1.10	0.07	98.0	42.0	(Chue *et al.,* 1995)
4-bed 8-step	FP,F,HR,PE,CnD,LR,PE,N	NaX, NaA	1.10	0.10	91.6	58.8	(Takamura *et al.,* 2001)
3-bed 8-step	FP,F,CoD,PE,HPP,HR,CnD,PE	AC	1.50	0.10	99.8	34.0	(Na *et al.,* 2001)
3-bed 7-step	FP,F,PE,HR,N,CnD,PE	AC	2.00	0.10	99.0	55.0	(Na *et al.,* 2002)
2-bed 4-step	FP,F,CnD,LR	13X	1.14	0.04	70.0	68.0	(Na *et al.,* 2002)
2-bed 6-step	PE,FP,F,PE,CnD,LR	13X	1.14	0.07	82.0	57.0	(Na *et al.,* 2002)
3-bed 5-step	FP,F,HR,CnD,LR	13X	1.14	0.07	83.0	54.0	(Na *et al.,* 2002)
2-bed 4-step	FP,F,CnD,LR	13X	3.00	1.00	78.0	50.0	(Gomes and Yee, 2002)
3-bed 8-step	FP,F,CoD,PE,HPP,HR,CnD,PE	13X	1.50	0.05	99.5	69.0	(Choi *et al.,* 2003)
2-bed 4-step	HPP,FP,CoD,CnD	13X	1.50	0.05	48.0	94.0	(Chou and Chen, 2004)
2-bed 5-step	HPP,FP,F,CoD,CnD	13X	1.50	0.05	43.0	88.0	(Chou and Chen, 2004)
3-bed 4-step	LPP,F,CnD,LR	13X	1.50	0.05	58.0	75.0	(Chou and Chen, 2004)
3-bed 6-step	LPP,FP,F,HR,CoD,CnD	13X	1.50	0.05	63.0	70.0	(Chou and Chen, 2004)
2-bed 4-step	FP,F,CnD,LR	13X	14.3	0.90	56.4	97.5	(Ko *et al.,* 2005)
2-bed 4-step	FP,F,CnD,LR	13X	13.5	0.90	71.9	94.4	(Ko *et al.,* 2005)
1-bed 4-step	FP,F,CoD,CnD	13X	6.82	0.15	90.0	93.8	(Ko *et al.,* 2005)
2-bed 4-step	LPP,F,CnD,LR	13X	1.30	0.10	51.5	66.0	(Grande *et al.,* 2005)
3-bed 5-step	LPP,F,HR,CnD,LR	13X	1.30	0.10	83.1	65.7	(Grande *et al.,* 2005)
5-bed 5-step	F,HR,CnD,LR,LPP	HTlc	1.39	0.11	72.2	82.2	(Reynolds *et al.,* 2006)
5-bed 5-step	F,HR,CnD,LR,LPP	HTlc	1.39	0.11	75.5	48.8	(Reynolds *et al.,* 2006)
4-bed 4-step	F,HR,CnD,LPP	HTlc	1.39	0.11	82.7	17.4	(Reynolds *et al.,* 2006)
5-bed 5-step	F,HR,CnD,LR,LPP	HTlc	1.39	0.11	98.7	98.7	(Reynolds *et al.,* 2008)
5-bed 5-step	F+R,HR,CnD,LR,LPP	HTlc	1.39	0.11	98.6	91.8	(Reynolds *et al.,* 2008)
4-bed 4-step	F,HR,CnD,LPP	HTlc	1.39	0.11	99.2	15.2	(Reynolds *et al.,* 2008)

PSA/VSA cycle configuration	operating step sequence	adsorbent	P_H, bar	P_L, bar	CO_2 Purity, %	CO_2 Recovery, %	Reference
5 bed 5-step	F,HR,CnD,LR,LPP	HTlc	1.39	0.11	96.6	71.1	(Reynolds *et al.,* 2008)
6 bed 6-step	F,R,HR,CnD,LR,LPP	HTlc	1.39	0.11	96.5	71.1	(Reynolds *et al.,* 2008)
5 bed 5-step	F+R,HR,CnD,LR,LPP	HTlc	1.39	0.11	96.5	71.0	(Reynolds *et al.,* 2008)
3-bed 6-step	F,PE,PE,CnD,PE,PE	13X	1.20	0.05	83.0	83.0	(Zhang *et al.,* 2008)
3-bed 9-step	F,F,F,PE,HR,CnD,PE,LPP,LPP	13X	1.20	0.05	95.0	70.0	(Zhang *et al.,* 2008)
3-bed 5-step	F,PE,CnD,PE,LPP	13X	1.20	0.05	85.7	77.6	(Zhang and Webley, 2008)
3-bed 6-step	F,PE,HR,CnD,PE,LPP	13X	1.20	0.05	95.2	66.9	(Zhang and Webley, 2008)
2-bed 6-step	F+R,FP+F,HR,CnD,CnD,LR	13X	6.00	0.50	95.0	80.1	(Agarwal *et al.,* 2010)
2-bed 8-step	F+R,FP+F,HR,PE,CnD,CnD,LR ,PE	13X	1.83	0.50	90.0	85.0	(Agarwal *et al.*, 2010)
1-bed 4-step	FP,F,CnD,LR	AC	3.24	0.10	63.0	96.0	(Shen *et al.,* 2011)
3-bed 7-step	F,CoD,HR,PE,CnD,LR,PE	5A	1.17	0.06	85.0	79.0	(Liu *et al.,* 2012)
3-bed 8-step	FP,F,CoD,HR,PE,CnD,LR,PE	13XAPG	1.17	0.08	82.3	84.7	(Wang *et al.,* 2013b)
3-bed 8-step	FP,F,CoD,HR,PE,CnD,LR,PE	5A	1.17	0.08	85.0	79.0	(Wang *et al.,* 2013b)
2-bed 4-step	FP,F,CoD,CnD	13X	1.00	0.10	88.7	35.8	(Haghpanah *et al.,* 2013a)
2-bed 4-step	F,CoD,CnD,LPP	13X	1.00	0.03	90.0	96.5	(Haghpanah *et al.,* 2013a)
2-bed 4-step	F,CoD,CnD,LPP	13X	1.00	0.03	95.0	92.5	(Haghpanah *et al.,* 2013a)
2-bed 6-step	F,CoD,HR,CnD,LR,LPP	13X	1.00	0.03	98.5	99.4	(Haghpanah *et al.,* 2013b)
2-bed 4-step	LPP,F,CoD,CnD	13X	1.50	0.02	94.8	89.7	(Krishnamurthy *et al.,* 2014)

Operating step legend: (F) feed or adsorption, (FP) feed pressurization, (HPP) heavy product pressurization, (LPP) light product pressurization, (CnD) counter-current depressurization, (CoD) co-current depressurization, (PE) light-end pressure equalization, (HR) heavy reflux, (LR) light reflux, (R) recycle, (N) null

Pressure level legend: (P_H) high pressure, (P_L) low pressure

Adsorbent type legend: (HTlc) K-promoted Hydrotalcite, (NaX, 13X, NaA, 13XAPG) molecular sieve zeolites, (AC, ACBs) activated carbon, (CMS) carbon molecular sieve

Na *et al.,* (2001; 2002) studied two different cycle configurations (three-bed eight-step and three-bed seven-step) of single-stage VSA process. Light reflux step was not used for any of these cycle configurations, whereas heavy reflux step and light-end pressure equalization steps were used in all of them. With activated carbon as adsorbent for both cycle configurations for a flue gas containing 17% CO_2 the three-bed eight-step cycle configuration gave 99.8% CO_2 purity and 34% CO_2 recovery and for a flue gas containing 13% CO_2 the three-bed seven-step cycle configuration gave 99% CO_2 purity and 55% CO_2 recovery.

Park *et al.,* (2002) analyzed three different cycle configurations (two-bed four-step, two-bed six-step, three-bed five-step) of single-stage VSA process. Heavy reflux step was used only for the third cycle configuration, whereas light reflux step was used in all cycle configurations. They studied a feed containing 10% CO_2 with zeolite 13X as adsorbent in all cycle configurations. The first cycle configuration (two-bed four-step) with light reflux step was able to achieve CO_2 purity of 70% and CO_2 recovery of 68%. Then the second cycle configuration (two-bed six-step) with light reflux step and light-end pressure equalization steps was able to achieve CO_2 purity of 82% and CO_2 recovery of 57%. Finally the third cycle configuration (three-bed five-step) with both light reflux step and heavy reflux step (dual reflux) was able to achieve CO_2 purity of 83% and CO_2 recovery of 54% which was a significant improvement in CO_2 purity in comparison with first cycle configuration, although in the meantime CO_2 recovery was decreased (trade-off).

Gomes and Yee (2002) studied a cycle configuration (two-bed four-step) of single-stage PSA process in which they didn't apply vacuum in order to recover CO_2. For a flue gas containing 8.3% CO_2 with zeolite 13X as adsorbent and with light reflux step CO_2 purity of 78% and CO_2 recovery of 50% were achieved. They showed that the light reflux step itself is not sufficient to obtain pure heavy product (extract).

Choi *et al.,* (2003) studied a cycle configuration (three-bed eight-step) of single-stage VSA process for a flue gas containing 13% CO_2 with zeolite 13X as adsorbent incorporating both heavy reflux step and light-end pressure equalization steps. With this cycle configuration, 69% of the CO_2 was captured with 99.5% purity.

Chou and Chen (2004) analyzed four different cycle configurations (two-bed four-step, two-bed five-step, three-bed four-step, three-bed six-step) of single-stage VSA

process from a feed containing 20% CO_2 with zeolite 13X as adsorbent. The first cycle configuration (two-bed four-step) without any kind of reflux steps was able to achieve CO_2 purity of 48% and CO_2 recovery of 94% while the second cycle configuration (two-bed five-step) without any kind of reflux steps was able to achieve CO_2 purity of 43% and CO_2 recovery of 88%. The third cycle configuration (three-bed four-step) with light reflux step was able to achieve CO_2 purity of 58% and CO_2 recovery of 75% while the fourth cycle configuration (three-bed six-step) with heavy reflux step was able to achieve CO_2 purity of 63% and CO_2 recovery of 70%.

Ko *et al.,* (2005) optimised a cycle configuration (two-bed four-step) of PSA process to minimize energy consumption both at normal and high temperatures. They studied a feed containing 15% CO_2 with light reflux step with zeolite 13X as adsorbent. The optimum results were CO_2 purity of 56.4% and CO_2 recovery of 97.5% at normal temperature and CO_2 purity of 71.94% and CO_2 recovery of 94.43% at high temperature. Ko *et al.,* (2005) optimised also a cycle configuration (one-bed four-step) of fractionated P/VSA process at high temperature from a feed containing 15% CO_2 with zeolite 13X as adsorbent to increase CO_2 purity to 90% and CO_2 recovery to 93.81%.

Grande *et al.,* (2005) studied two different cycle configurations (two-bed four-step, three-bed five-step) of single-stage VSA process from a feed containing 15% CO_2 with zeolite 13X as adsorbent with light product pressurization. The first cycle configuration (two-bed four-step) with light reflux step was able to achieve CO_2 purity of 51.54% and CO_2 recovery of 66% while the second cycle configuration (three-bed five-step) with both light reflux step and heavy reflux step (dual reflux) was able to achieve CO_2 purity of 83.1% and CO_2 recovery of 65.7%.

Reynolds *et al.,* (2006; 2008) have studied complex cycle configurations involving heavy reflux step and light reflux step using K-promoted Hydrotalcite (HTlc) as adsorbent for CO_2 capture from flue gas containing 15% CO_2, 75% N_2 and 10% H_2O at high temperature. They have emphasized the importance of including heavy reflux step to obtain heavy product (extract) at a high purity. They considered different cycle configurations (four-bed four-step, five-bed five-step, six-bed six-step) of single-stage VSA process. The best process performance achieved from a cycle

configuration (five-bed five-step) with both heavy reflux step and light reflux step (dual reflux) resulting in CO_2 purity of 98.7% and CO_2 recovery of 98.7% although, at an extremely small feed throughput.

Webley and co-workers have done an extensive research in the field of carbon dioxide separation by adsorption (Xiao *et al.,* 2008; Zhang and Webley, 2008; Zhang *et al.,* 2008). They compared several cycle configurations of single-stage VSA process and they showed that CO_2 purity can be increased by particularly incorporating heavy reflux step and light-end pressure equalization steps, although in the meantime CO_2 recovery can be decreased (trade-off). However, a deep vacuum pressure (0.05 bar) was required. From their experiments, it was clear that CO_2 purity, CO_2 recovery and energy consumption considerably varied as the operating conditions were altered and as expected, enhanced performance in VSA process can be obtained when the feed gas contains higher CO_2 concentration.

Zhang *et al.,* (2008) performed VSA experiments using two different cycle configurations (three-bed six-step, three-bed nine-step) of single-stage VSA process. For both cycle configurations, they used zeolite 13X and dry flue gas containing 12% CO_2. With the first cycle configuration (three-bed six-step) without heavy reflux step and with two light-end pressure equalization steps CO_2 purity of 83% and CO_2 recovery of 83% were achieved while with the second cycle configuration (three-bed nine-step) with heavy reflux step and with one light-end pressure equalization step CO_2 purity of 95% and CO_2 recovery of 70% were achieved.

Xiao *et al.,* (2008) simulated a cycle configuration (three-bed nine-step) of single-stage VSA process for a flue gas containing 12% CO_2 with zeolite 13X as adsorbent incorporating two light-end pressure equalization steps without heavy reflux step. With this cycle configuration CO_2 purity of 92.5% and CO_2 recovery of 75% were reported.

In another study, Zhang and Webley (2008) reported two different cycle configurations (three-bed five-step, three-bed six-step) of single-stage VSA process. For both cycle configurations, they used zeolite 13X and dry flue gas containing 12% CO_2. With the first cycle configuration (three-bed five-step) without heavy reflux step and with light-end pressure equalization step CO_2 purity of 85.7% and CO_2 recovery of 77.6% were obtained while with the second cycle configuration (three-

bed six-step) with heavy reflux step and with light-end pressure equalization step CO_2 purity of 95.2% and CO_2 recovery of 66.9% were obtained.

Agarwal *et al.,* (2010) proposed two different cycle configurations (two-bed six-step, two-bed eight-step) of single-stage VSA process with both heavy reflux step and light reflux step (dual reflux) for a dry flue gas containing 15% CO_2 with zeolite 13X as adsorbent. They optimised the first cycle configuration (two-bed six-step) in order to maximize CO_2 recovery using a superstructure-based approach. The optimum cycle resulted in a CO_2 purity of 95% and a CO_2 recovery of 80.09% with an energy consumption of 637 kWh/tone CO_2 captured. In the second cycle configuration (two-bed eight-step) they have incorporated light-end pressure equalization step, both heavy reflux step and light reflux step (dual reflux) and they optimised this cycle configuration in order to minimize energy consumption. The optimum cycle gave the minimum energy consumption of 465 kWh/tone CO_2 captured at 90% CO_2 purity and 85% CO_2 recovery.

Shen *et al.,* (2011) studied a cycle configuration (one-bed four-step) of single-stage VSA process for a flue gas containing 15% CO_2 with activated carbon as adsorbent incorporating light reflux step. With this cycle configuration CO_2 purity of 63% and CO_2 recovery of 96% were reported.

Liu *et al.,* (2012) studied a cycle configuration (three-bed seven-step) of single-stage P/VSA process for a flue gas containing 15% CO_2 with zeolite 5A as adsorbent incorporating light-end pressure equalization step with both heavy reflux step and light reflux step (dual reflux). With this cycle configuration CO_2 purity of 85% and CO_2 recovery of 79% were achieved.

Wang *et al.,* (2013b) studied a cycle configuration (three-bed eight-step) of single-stage P/VSA process for a flue gas containing 16.4% CO_2 with zeolite 13XAPG as adsorbent incorporating light-end pressure equalization step with both heavy reflux step and light reflux step (dual reflux). With this cycle configuration CO_2 purity of 82.3% and CO_2 recovery of 84.7% were obtained. With the same cycle configuration (three-bed eight-step) of single-stage P/VSA process for a flue gas containing 16% CO_2 with zeolite 5A as adsorbent CO_2 purity of 85% and CO_2 recovery of 79% were obtained.

Haghpanah *et al.,* (2013a) optimised a cycle configuration (two-bed four-step) of single-stage VSA process for a flue gas containing 15% CO_2 with zeolite 13X as adsorbent. With this cycle configuration CO_2 purity of 88.7% and CO_2 recovery of 35.8% were reported.

In another study, Haghpanah *et al.,* (2013b) systematically developed and evaluated a variety of cycle configurations of single-stage VSA process using Zeochem 13X zeolite as adsorbent to capture CO_2 from a dry flue gas containing 15% CO_2. A multi-objective optimisation algorithm has been used to generate full purity-recovery and energy-productivity Pareto fronts of the analyzed cycle configurations of single-stage VSA process. The first cycle configuration (two-bed four-step) with light product pressurization step was able to achieve CO_2 purity of 90% and CO_2 recovery of 96.5% with a minimum energy consumption of 131 kWh/tone CO_2 captured. This requires an evacuation pressure of 0.03 bar. This energy consumption increases to 153.8 kWh/tone CO_2 captured for CO_2 purity of 95% and CO_2 recovery of 92.5% at the same evacuation pressure. In addition to the first cycle configuration (two-bed four-step) with light product pressurization step, other cycle configurations such as (two-bed five-step) with light product pressurization step and light reflux step, (two-bed six-step) with light product pressurization step and both light reflux step and heavy reflux step (dual reflux) and (two-bed six-step) with light product pressurization step, light-end pressure equalization step and heavy reflux step were also able to meet 90% CO_2 purity and 90% CO_2 recovery requirements. The best performance based on CO_2 purity and CO_2 recovery gave the cycle configuration (two-bed six-step) with light product pressurization step and both light reflux step and heavy reflux step (dual reflux). With this cycle configuration CO_2 purity of 98.5% and CO_2 recovery of 99.4% were reported at the evacuation pressure of 0.03 bar. It is important to note that it is difficult to achieve both high CO_2 purity and high CO_2 recovery by a single-stage VSA process without employing deep vacuum desorption.

Krishnamurthy *et al.,* (2014) used a P/VSA pilot plant to obtain 94.8 ± 1% CO_2 purity and 89.7 ± 7% CO_2 recovery for CO_2 capture from dry flue gas containing 15% CO_2 at a deep vacuum pressure of 0.02 bar using 13X zeolite as adsorbent with a cycle configuration (two-bed four-step) of single-stage P/VSA process which includes a light product pressurization step. This was the first pilot plant study in which nearly

95% CO_2 purity and 90% CO_2 recovery were achieved in a single-stage P/VSA process by employing deep vacuum desorption.

Most of the previous mentioned studies demonstrate that deep vacuum levels (<0.05 bar) are essential to capture CO_2 in a VSA process in order to achieve CO_2 purity of over 90% with CO_2 recovery ranging from 70% to 90%. However deep vacuum levels are not indicative of industry practice. The deeper vacuum requires multistage pump units which would increase the capital cost and the operating cost of the process as well. In addition, the operating valves which can withstand low pressure are very expensive especially for the rapid VSA cycles as well as one must take into consideration the requirement of very large pipe sizes to limit extreme velocities at low vacuum pressures (Liu *et al.*, 2012).

Most of these studies are bench-scale and deal with extremely small feed throughput. From these studies, it is not clear why a particular cycle configuration was chosen or one cycle configuration had a better performance than other cycle configurations. The literature review shows that so far there has not been developed a systematic algorithm or method to design and evaluate a PSA/VSA cycle configuration in order to obtain a pure light product (raffinate) or a pure heavy product (extract) or both of them simultaneously. Although this literature review offers some trends and guidelines, a fully systematic methodology is still required to design PSA/VSA cycle configurations (Agarwal *et al.,* 2010).

This literature review provide physical insight on the roles of different steps such as light product pressurization step, light reflux step, heavy reflux step and light-end pressure equalization step in the context of a cycle configuration. These studies showed that classical cycle configurations with light reflux step without heavy reflux step cannot produce heavy product (extract) at high purity since a light reflux step dilutes the heavy product and decreases its purity (Agarwal *et al.,* 2010; Gomes and Yee, 2002). The researchers have emphasized the importance of including heavy reflux step to obtain heavy product (extract) at a high purity (Reynolds *et al.,* 2006; Reynolds *et al.,* 2008). However, the heavy reflux step is energetically unfavorable and thus, not preferred by the optimiser when the minimization of the energy consumption is the priority (Haghpanah *et al.,* 2013b).

1.9.2. Review of integrated two-stage P/VSA processes for CO_2 capture

Most of the previous studies have demonstrated the difficulty to achieve the DOE target values for CO_2 purity and CO_2 recovery in a single-stage P/VSA process at nearly atmospheric feed pressure when the CO_2 concentration in the flue gas is low (15% or less), without employing deep vacuum levels (<0.05 bar). However such deep vacuum levels are not practically applied in industrial scale. In order to achieve the requested performance in terms of CO_2 purity and CO_2 recovery, the flue gas resulting from the combustion of coal needs to undergo a two-stage P/VSA process. In this direction, two successive P/VSA units have been reported in the literature in order to capture and concentrate CO_2 from flue gas obtaining CO_2 purity ≥ 95% with CO_2 recovery ≥ 90% without employing deep vacuum desorption (Haghpanah *et al.,* 2014; Leperi *et al.,* 2016; Liu *et al.,* 2011; Riboldi and Bolland, 2015; Shen *et al.,* 2012; Wang *et al.,* 2012; Wang *et al.,* 2013a). All these studies provide physical insight on the role of different steps such as light reflux step, heavy reflux step and light-end pressure equalization step in the context of a cycle configuration. The performances of two successive P/VSA units reported in the literature for post-combustion CO_2 capture are summarized in Table 1.2. However, it must be noted that such a cycle configuration leads to an increase in capital and operating cost due to the additional P/VSA unit.

Liu *et al.,* (2011) simulated a two-stage P/VSA process using zeolite 5A as adsorbent at both stages for CO_2 capture from dry flue gas with 15% CO_2 and 85% N_2. A three-bed five-step cycle configuration was considered for the first stage, with both heavy reflux step and light reflux step (dual reflux), at a desorption pressure of 0.10 bar, while a two-bed six-step cycle configuration was considered for the second stage, with light reflux step and light-end pressure equalization step, at a desorption pressure of 0.15 bar. The first stage produced an enriched stream containing 69.15% CO_2 with a CO_2 recovery of 98.92% while the second stage produced an enriched stream containing 96.05% CO_2 with a CO_2 recovery of 91.97%. The overall process performance of a two-stage P/VSA process was 96.05% CO_2 purity, 91.05% CO_2 recovery and 0.33 mol CO_2/Kg·h CO_2 productivity with total energy consumption of

Table 1.2. Performance comparison of two successive P/VSA units reported in the literature for post-combustion CO_2 capture.

two-stage P/VSA configuration	adsorbents	cycle time, s	P_{feed}, bar	P_{blow}, bar	CO_2 Purity, %	CO_2 Recovery, %	CO_2 Productivity, (mol CO_2/Kg·h)	Energy, (MJ/Kg CO_2)	Reference
3-bed 5-step/ 2-bed 6-step	5A-5A	900-860	1.50-1.50	0.10-0.15	96.05	91.05	0.33	0.65	(Liu *et al.,* 2011)
3-bed 5-step/ 2-bed 6-step	13XAPG-13XAPG	900-860	1.50-1.50	0.10-0.10	96.54	93.35	0.71	0.53	(Wang *et al.,* 2012)
2-bed 4-step/ 2-bed 5-step	AC-AC	560-620	1.30-3.45	0.10-0.10	95.29	74.36	0.85	0.72	(Shen *et al.,* 2012)
3-bed 8-step/ 2-bed 6-step	13X-AC	780-560	1.16-1.23	0.08-0.20	95.60	90.20	-	2.44	(Wang *et al.,* 2013a)
3-bed 5-step/ 2-bed 5-step	5A-5A	2106-1760	1.00-2.00	0.10-0.10	95.10	90.14	-	-	(Riboldi and Bolland, 2015)
1-bed 4-step/ 1-bed 4-step	CMS-CMS	443-412	1.00-1.00	0.04-0.07	90.00	89.94	-	0.96	(Haghpanah *et al.,* 2014)
1-bed 4-step/ 1-bed 4-step	13X-13X	1113-806	1.49-2.76	0.10-0.13	95.00	90.00	0.49	1.13	(Leperi *et al.,* 2016)

0.65 MJ/Kg CO_2.

Shen *et al.,* (2012) studied a two-stage P/VSA process using activated carbon as adsorbent at both stages for CO_2 separation from dry flue gas with 15% CO_2 and 85% N_2. They considered a cycle configuration (two-bed four-step) with light reflux step for the first stage and a cycle configuration (two-bed five-step) with light-end pressure equalization step for the second stage in this simulation study. The first stage gave a concentrated stream containing 43.86% CO_2 with a CO_2 recovery of 90.94% while the second stage gave a concentrated stream containing 95.29% CO_2 with a CO_2 recovery of 81.78%. The overall process performance of a two-stage P/VSA process resulted in a CO_2 purity of 95.29%, a CO_2 recovery of 74.36% and a CO_2 productivity of 0.85 mol CO_2/Kg·h at a desorption pressure of 0.10 bar at both stages, with total energy requirements 0.72 MJ/Kg CO_2.

Wang *et al.,* (2012) simulated a two-stage P/VSA process using zeolite 13XAPG as adsorbent at both stages for CO_2 capture from dry flue gas with 15% CO_2 and 85% N_2. A three-bed five-step cycle configuration was considered for the first stage, with both heavy reflux step and light reflux step (dual reflux), while a two-bed six-step cycle configuration was considered for the second stage, with light-end pressure equalization step and light reflux step. The first stage resulted in 65.38% CO_2 purity and 98.92% CO_2 recovery, while the second stage produced 96.54% CO_2 purity and

94.37% CO_2 recovery. The overall process performance of a two-stage P/VSA process was 96.54% CO_2 purity, 93.35% CO_2 recovery and 0.71 mol CO_2/Kg·h CO_2 productivity at a desorption pressure of 0.10 bar at both stages, with total energy consumption 0.53 MJ/Kg CO_2.

Wang *et al.,* (2013a) studied a two-stage P/VSA process using zeolite 13XAPG at the first stage and pitch based activated carbon beads ACBs at the second stage as adsorbents for CO_2 separation from a dry flue gas with 16.5% CO_2 and 83.5% N_2. They studied a cycle configuration (three-bed eight-step) with both heavy reflux step and light reflux step (dual reflux) for the first stage and a cycle configuration (two-bed six-step) with light-end pressure equalization step and heavy reflux step for the second stage in an existing coal-fired power plant. The first stage resulted in a CO_2 purity of 74.5% at a desorption pressure of 0.08 bar while the second stage resulted in a CO_2 purity of 95.6% at a desorption pressure of 0.20 bar. The overall process performance of a two-stage P/VSA process resulted in a CO_2 purity of 95.6% and a CO_2 recovery of 90.2%, with total energy requirements 2.44 MJ/Kg CO_2.

Riboldi and Bolland (2015) simulated a two-stage P/VSA process using zeolite 5A as adsorbent at both stages for post-combustion CO_2 capture from dry flue gas. They considered a cycle configuration (three-bed five-step) with both heavy reflux step and light reflux step (dual reflux) for the first stage and a cycle configuration (two-bed five-step) with light-end pressure equalization step for the second stage. The first stage resulted in a CO_2 purity of 49.7% with a CO_2 recovery of 93.8% while the second stage gave a CO_2 purity of 95.1% with a CO_2 recovery of 96.1%. The overall process performance of a two-stage P/VSA process was 95.1% CO_2 purity and 90.14% CO_2 recovery at a desorption pressure of 0.10 bar at both stages.

Haghpanah *et al.,* (2014) optimised a two-stage P/VSA process using carbon molecular sieve (CMS) as adsorbent at both stages for post-combustion CO_2 capture from a dry flue gas with 15% CO_2 and 85% N_2. A one-bed four-step cycle configuration was considered at both stages. In the first stage, CO_2 is enriched to 63.8% with 91.4% recovery at a desorption pressure of 0.04 bar. In the second stage, CO_2 purity and CO_2 recovery were 90% and 98.4%, respectively at a desorption pressure of 0.07 bar. The overall process performance of a two-stage P/VSA process

was 90% CO_2 purity and 89.94% CO_2 recovery, with energy requirements 0.96 MJ/Kg CO_2.

To investigate post-combustion capture of CO_2 in the presence of water, Leperi *et al.,* (2016) studied a two-stage P/VSA process. A one-bed four-step cycle configuration with light reflux step was considered at both stages. Four potential adsorbents, zeolites 13X and 5A and MOFs HKUST-1 and Ni-MOF-74, were investigated, evaluated, and compared. The results showed that under dry flue gas conditions, zeolite 13X was the best performing adsorbent to minimize the overall cost of capturing 90% of CO_2 from flue gas at a purity of 90% and compressing it for pipeline transportation at 110 bar. They also performed additional optimisation studies of a two-stage P/VSA process using zeolite 13X as adsorbent at both stages for CO_2 capture from dry flue gas to achieve 95% CO_2 purity, 90% CO_2 recovery and 0.49 mol CO_2/Kg·h CO_2 productivity with total energy consumption 1.13 MJ/Kg CO_2.

The above studies illustrate that an integrated two-stage P/VSA process is necessary to achieve satisfactory characteristics of the CO_2 rich stream to be transported and stored. The resulting CO_2 purity and CO_2 recovery must meet the target values set by DOE. The CO_2 purity in product gas should be more than 95% in order to reduce the costs of CO_2 compression, liquefaction, transportation and storage.

CHAPTER 2
MODELLING AND OPTIMISATION OF A PSA/VSA PROCESS FOR CO_2 CAPTURE

2. Modelling and optimisation of a PSA/VSA process for CO_2 capture

2.1. Fundamentals of PSA/VSA process modelling

Modelling of PSA/VSA processes has been extensively studied to gain a clear understanding of this rather complex process. The core of the modelling framework represents a detailed adsorbent bed model relying on a coupled set of mixed partial differential and algebraic equations (PDAEs) for mass, heat and momentum balance at both bulk gas and particle level, equilibrium isotherm equations, transport and thermo-physical properties of the gas mixture and boundary conditions according to the operating steps, which reflect the transient nature of the process and capture the underlying physics in details. With such models, it is now possible to accurately predict the dynamic behavior of a PSA/VSA process, and to adequately account for all the factors that affect the performance of any given PSA/VSA process (Kikkinides *et al.,* 2011; Nikolic *et al.,* 2008).

The development of PSA/VSA process models requires an accurate model representation of the adsorption-diffusion process at the micro-scale pore level, the mass transport characteristics at the particle-pellet level and a transport model, coupled with the conservation equations of mass, heat and momentum, at the adsorbent bed level. The behavior of each adsorbent bed is described by a set of PDAEs in space and time. Moreover, the flow pattern between the adsorbent beds is needed to describe the adsorbent bed interconnections (Kikkinides *et al.,* 2011).

Simulation of PSA/VSA processes is performed by solving the above system of PDAEs for each adsorbent bed repeatedly for many cycles until CSS conditions is achieved.

Then process performance is evaluated by calculating some important process performance indicators including product purity, product recovery, product productivity and energy consumption (Ruthven *et al.,* 1994). Such simulations can replace many expensive and time consuming laboratory and/or pilot scale experimental studies allowing innovative modifications of existing design cycle configurations without any actual cost (Biegler *et al.,* 2004; Kumar *et al.,* 1994).

Most of the PSA/VSA simulation models that exist in the literature solve the system of PDAEs for each adsorbent bed cycle after cycle using the profiles of all variables at the end of each cycle as initial conditions for the next cycle, until CSS is achieved, when the profiles of all variables within the adsorbent bed at the end of the each operating step remain unchanged (within a pre-defined tolerance) as the process goes from cycle number n to cycle number n+1. This is known as the successive substitution approach and it is a stable procedure since it simulates the actual PSA/VSA process. However it can be computationally expensive because it is often slow in convergence requiring hundreds or thousands of cycles to reach CSS. Over the last two decades a few commercial software programs have been developed to effectively simulate the various PSA/VSA processes. Nevertheless, the design and optimisation of PSA/VSA processes still remains a challenging problem due to the complexity of the process applications from an operational and computational point of view, particularly as multi-adsorbent, multi-bed configurations are required to face real industrial applications. In such cases, adsorbent bed interactions play an important role in the proper simulation of the relevant PSA/VSA process operation and performance. It has been shown that incorporating a gas valve equation into the PSA/VSA model to control flow rate is the best approach to realistically describe adsorbent bed interactions and this approach has been adopted in the current study of the dynamic behavior of multi-bed PSA/VSA process (Choi and Wen-Chung, 1994; Kikkinides *et al.,* 2011; Nikolic *et al.,* 2008).

One can develop various PSA/VSA models of different complexity to describe equilibrium and transport properties at adsorbent bed, particle and/or pore scale for binary or multi-component mixtures. Moreover process complexity increases as more adsorbent beds are employed in the process design and operation. A large number of studies have been reported in the literature describing multi-bed

PSA/VSA models (Agarwal *et al.,* 2010; Biegler *et al.,* 2004; Choi *et al.,* 2003; Chou and Chen, 2004; Chue *et al.,* 1995; Gomes and Yee, 2002; Grande *et al.,* 2005; Haghpanah *et al.,* 2013a; Haghpanah *et al.,* 2013b; Hasan *et al.,* 2013; Jiang *et al.,* 2003; Jiang *et al.,* 2004; Kikkinides *et al.,* 1993; Ko *et al.,* 2005; Kumar *et al.,* 1994; Lee and Park, 2015; Na *et al.,* 2001; Na *et al.,* 2002; Nikolic *et al.,* 2008; Nikolic *et al.,* 2009; Nilchan and Pantelides, 1998; Park *et al.,* 2002; Rajagopalan *et al.,* 2016; Reynolds *et al.,* 2006; Reynolds *et al.,* 2008; Shen *et al.,* 2011; Takamura *et al.,* 2001; Xiao *et al.,* 2008; Zhang and Webley, 2008; Zhang *et al.,* 2008).

To simulate the behavior of a multi-bed PSA/VSA configuration two different approaches are commonly employed: the “Unibed” and the “Multi-bed” (Jiang *et al.,* 2004). The “Unibed” approach assumes that all adsorbent beds undergo identical operating steps so only one adsorbent bed is needed to simulate the multi-bed cycle. Information about the effluent streams are stored in data buffers and linear interpolation is used to obtain information between two time points. The “Multi-bed” approach considers a multi-bed PSA/VSA process as a sequence of repetitive stages within the cycle (Kikkinides *et al.,* 2011). The “Unibed” approach, first mentioned in the work of Kumar *et al.,* (1994) attempts to reduce the size of equations in a PSA/VSA system by employing only one adsorbent bed for simulation purposes. It is important to note that the “Unibed” approach has been adopted in the current study in order to simulate the behavior of a PSA/VSA process.

The three key factors related to PSA/VSA operation are the following (Khajuria, 2011):

1. All adsorbent beds of a PSA/VSA system for a fixed PSA/VSA cycle undergoes identical sequence of operating steps but with a fixed time delay.
2. The duration of a particular operating step for any adsorbent bed is exactly the same.
3. During the operating steps where two adsorbent beds are interconnected to each other, any adsorbent bed will only require the process conditions information of the bed end (connecting end) of the other adsorbent bed while interacting.

Consequently, the temporal profiles of the effluent streams for the bed-interconnecting operating steps are stored separately in data buffers and are utilized

later in the cycle, thereby eliminating the need for extra adsorbent beds to perform the full operation. For example, for a four bed PSA/VSA system only a single adsorbent bed is actually simulated and during the operating steps such as co-current depressurization step where the adsorbent bed is connected to another adsorbent bed undergoing counter-current pressure equalization, the effluent temporal profiles of pressure, temperature, species gaseous concentration etc. are stored in data buffers to be later used as influent temporal profiles during the corresponding pressure-equalization step. One key assumption here is the independence of the final CSS conditions to the initial adsorbent bed conditions and the transient behavior of the operating steps, as a result of adsorbent bed interconnections.

In an industrial multi-bed PSA/VSA process, all adsorbent beds undergo identical sequence of operating steps. Hence, for cycles constituting uncoupled operating steps, simulating one adsorbent bed is adequate to fully capture the performance of a multi-bed PSA/VSA process. For cycles involving operating steps where two or more adsorbent beds are coupled, i.e., output from one adsorbent bed is the input for another, output stream data from the source adsorbent bed are stored in data buffers and used for feeding these streams to the receiving adsorbent bed via linear interpolation. As short time intervals are used for data collection, linear interpolation has been found to provide sufficient accuracy (Haghpanah *et al.,* 2013).

2.2. Modelling framework

2.2.1. Problem statement

The development of a modelling framework for efficient simulation and optimisation strategies for the design of PSA/VSA processes with detailed adsorption and transport models is presented (Kikkinides *et al.,* 2011; Nikolic *et al.,* 2008). Depending on the general assumptions describing the adsorbent (porous solid) – adsorbate (gas mixture) system one can employ a broad variety of mathematical models and equations to describe the PSA/VSA process (Ruthven, 1984; Ruthven *et al.,* 1994; Yang, 1987).

The following general assumptions have been considered in the derivation of the model equations:

- The axial dispersion model is used to describe bulk fluid transport in the adsorbent bed.
- A linear driving force (LDF) mechanism is employed to describe adsorption-desorption kinetics.
- Thermal equilibrium is established instantaneously between the gas and solid phase (adsorbent).
- The adsorbent is represented by uniform micro-porous spheres.
- The gas phase is described by the ideal gas law.
- There are not variations of any property along the radial direction in the adsorbent bed.
- The physical properties of the adsorbent and adsorbent bed void are constant.
- Competitive adsorption behaviors are described by the dual-site Langmuir isotherm equation.
- The pressure drop through the adsorbent bed is calculated by the Ergun equation in each operating step.
- There are not empty spaces at the top and the bottom of each adsorbent bed.

As a result one needs to consider the following model equations that describe each operating step in the PSA/VSA process (Kikkinides *et al.,* 2011; Nikolic *et al.,* 2008):

- A mass balance for each component in gas phase.
- An energy balance that includes gas, solid and adsorbed phase.
- A momentum balance that predicts the pressure drop along the adsorbent bed.
- A transport model describing non-selective mass transfer in the macropores of the adsorbent, and surface or activated diffusion of the adsorbate (gas mixture) in the micropores of the adsorbent.
- An equilibrium isotherm describing the thermodynamic relationship between the gas mixture and adsorbed phase.

Furthermore, gas valve equations are needed to describe adsorbent bed interactions, while several auxiliary equations are supplied to determine important process performance indicators.

2.2.2. Nomenclature

$b_{(1)}$	dual-site Langmuir isotherm parameter of first site, 1/Pa
$b_{(2)}$	dual-site Langmuir isotherm parameter of second site, 1/Pa
C	molar concentration of gas phase in bulk gas, mol/m^3
C^{in}	molar concentration of gas phase at the inlet of adsorbent bed, mol/m^3
c_p	specific heat capacity of bulk gas referring to constant pressure, J/(kg·K)
c_v	specific heat capacity of bulk gas referring to constant volume, J/(kg·K)
c_p^p	specific heat capacity of the particle, J/(kg·K)
C_{valve}	gas valve constant, -
D	adsorbent bed diameter, m
D_e	effective diffusivity, m^2/s
D_k	Knudsen diffusivity, m^2/s
D_m	molecular diffusivity, m^2/s
$\mathrm{D_v}$	molecular diffusion volume, cm^3/mol
D_z	mass axial dispersion coefficient, m^2/s

E	energy consumption of the compressor/vacuum pump, J
F	molar flow rate, mol/s
$k_{1(1)}$	dual-site Langmuir isotherm parameter of first site, mol/kg
$k_{2(1)}$	dual-site Langmuir isotherm parameter of first site, 1/K
$k_{3(1)}$	dual-site Langmuir isotherm parameter of first site, 1/Pa
$k_{4(1)}$	dual-site Langmuir isotherm parameter of first site, K
$k_{1(2)}$	dual-site Langmuir isotherm parameter of second site, mol/kg
$k_{2(2)}$	dual-site Langmuir isotherm parameter of second site, 1/K
$k_{3(2)}$	dual-site Langmuir isotherm parameter of second site, 1/Pa
$k_{4(2)}$	dual-site Langmuir isotherm parameter of second site, K
k_f	overall mass transfer coefficient, m/s
k_h	overall heat transfer coefficient, J/(m^2·K·s)
$k_{h,wall}$	heat transfer coefficient of the adsorbent bed wall, J/(m^2·K·s)
L	adsorbent bed length, m
MW	molecular weight, g/mol
N_{comp}	number of components, -
N_{in}	number of moles of the feed stream of the compressor/vacuum pump, mol
N_g	mass generation term, mass flux through the particle surface, mol/(m^3·s)
n_c	isentropic compression efficiency of the compressor, -
n_v	isentropic evacuation efficiency of the vacuum pump, -
Nu	Nusselt number, -
P	total pressure of the adsorbent bed, Pa
P_{atm}	atmospheric pressure, Pa
Pr	Prandtl number, -
P_{feed}	pressure of the feed stream, Pa
P_{in}	pressure at the inlet of the gas valve, Pa
P_{out}	pressure at the outlet of the gas valve, Pa
P_{vac}	pressure of the leaving stream of the vacuum pump, Pa
Q	adsorbed amount per unit mass of adsorbent, mol/kg

Q^*	adsorbed amount per unit mass of adsorbent in equilibrium state, mol/kg
$q_{m(1)}$	dual-site Langmuir isotherm parameter of first site, mol/kg
$q_{m(2)}$	dual-site Langmuir isotherm parameter of second site, mol/kg
q_g	heat generation term, heat flux through the particle surface, J/(m^3·s)
q_{wall}	heat generation term, heat flux through the wall surface, J/(m^3·s)
R	universal gas constant, J/(mol·K)
R_{bed}	adsorbent bed radius, m
Re	Reynolds number, -
R_p	particle radius, m
R_{pore}	pore radius, m
Sc	Schmidt number, -
Sh	Sherwood number, -
SP	stem position of the gas valve, -
t	time, s
t_{Ads}	time of adsorption step, s
t_{Blow}	time of blowdown step, s
t_{Evac}	time of evacuation step, s
t_{cycle}	total cycle time, s
t_{CC}	time of pressurization with light product step, s
t_{CoC}	time of pressurization with feed step, s
t_{PED}	time of pressure equalization (depressurization) step, s
t_{PER}	time of pressure equalization (repressurization) step, s
T	temperature of the bulk gas, K
T_{feed}	temperature of the feed stream, K
T^{in}	temperature of the fluid at the inlet of the adsorbent bed, K
T_{wall}	temperature of the adsorbent bed wall, K
u	interstitial velocity, m/s
u^{in}	interstitial velocity at the inlet of the adsorbent bed, m/s
y	molar fraction in gas phase, -
z	axial discretization domain, m

Greek letters

a_{ij}	selectivity of component *i* over component *j* of an adsorbent,-
γ	specific heat capacity ratio, -
ΔH_{ads}	isosteric heat of adsorption, J/mol
ΔQ^*	equilibrium working capacity, mol/kg
ε_{bed}	porosity of the adsorbent bed, -
ε_p	porosity of the particle, -
λ	thermal conductivity of bulk gas, J/(m·K·s)
λ_z	heat axial dispersion coefficient, J/(m·K·s)
μ	viscosity of bulk gas, Pa·s
ρ	density of bulk gas, kg/m^3
ρ^p	density of the particle, kg/m^3
τ_p	tortuosity factor of the particle, -

Subscripts

i	component

Superscripts

p	particle

2.2.3. Mathematical model formulation

The mathematical modelling of a fixed adsorbent bed must take into account the simultaneous mass, heat and momentum balances at both, bulk gas flow and adsorbent particle level, adsorption isotherm, transport and thermo-physical properties of the gas mixture and a set of boundary conditions for each operating step at the inlet and at the outlet of the adsorbent bed and at the interface between the bulk gas and particle surface as it is illustrated in Figure 2.1. Phenomena that occur within the particles could be described by using a specific transport mechanism. The mass and heat transfer rates through a particle surface to the bulk gas flow have to be calculated with mathematical models taking into account detailed mass and heat transfer mechanisms at the adsorbent particle level. The mass transfer in the adsorbent particles can be described by several diffusion

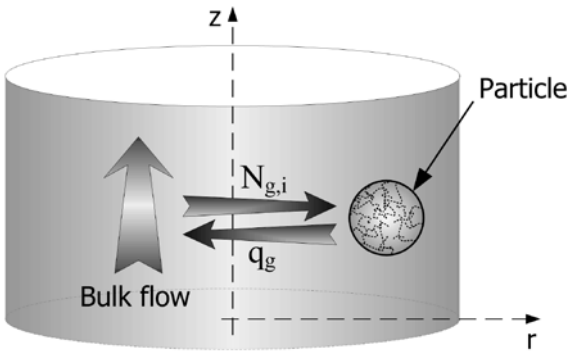

Figure 2.1. Interaction between bulk gas flow and adsorbent particle (Kikkinides *et al.,* 2011).

mechanisms. The most common diffusion mechanisms in the literature are: (i) local equilibrium (LEQ), (ii) linear driving force (LDF), (iii) surface diffusion (SD), (iv) pore diffusion (PD) (Ruthven, 1984; Ruthven *et al.,* 1994; Yang, 1987). The first two mechanisms (LEQ and LDF) simplify the solution of the model equations significantly by removing the need to solve the mass balance at the particle scale. The last two mechanisms (SD and PD) are more rigorous approaches that take into account mass balance at both scales (bulk fluid flow and adsorbent particle).

A single adsorbent bed is the main building block of a multi-bed PSA/VSA process. Each adsorbent bed is connected to several storage and sink tanks via gas valves. The adsorbent bed is properly connected to all other adsorbent beds of a multi-bed PSA/VSA process at both ends via gas valves. A single adsorbent bed contains one adsorbent layer and its main role is to describe the boundary conditions for the different operating steps.

Mass balance

The mass balance equation which describes the mass transfer in the bulk gas flow is provided by:

$$\varepsilon_{bed}\frac{\partial(uC_i)}{\partial z}+\varepsilon_{bed}\frac{\partial C_i}{\partial t}+(1-\varepsilon_{bed})N_{g,i}=\varepsilon_{bed}\frac{\partial}{\partial z}\left(D_{z,i}\frac{\partial C_i}{\partial z}\right),\quad \forall z\in(0,L), i=1,\dots,N_{comp} \tag{2.1}$$

where ε_{bed} is the porosity of the adsorbent bed, u is the interstitial velocity, C_i is the molar concentration of component *i* in bulk gas, $D_{z,i}$ is the mass axial dispersion

coefficient of component *i* and the term $N_{g,i}$ is the mass generation term given per unit volume of adsorbent which quantifies the mass transfer occurring between bulk flow and particles. The actual expression for $N_{g,i}$ depends on the nature of the resistances to the mass transfer and for linear drive force (LDF) mechanism is described by the following equation:

$$N_{g,i} = \rho^p \frac{\partial Q_i}{\partial t}, \qquad \forall z \in (0, L), i = 1, \dots, N_{comp} \tag{2.2}$$

where Q_i is the adsorbed amount of component *i* per unit mass of adsorbent and ρ^p is the density of the particle.

Heat balance

The heat balance equation which describes the heat transfer in the bulk gas flow is:

$$\varepsilon_{bed} \frac{\partial(\rho c_p T u)}{\partial z} + \varepsilon_{bed} \frac{\partial(\rho c_p T)}{\partial t} + (1 - \varepsilon_{bed}) q_g + q_{wall} = \varepsilon_{bed} \frac{\partial}{\partial z}\left(\lambda_z \frac{\partial T}{\partial z}\right), \quad \forall z \in (0, L) \tag{2.3}$$

where ρ is the density of bulk gas, c_p is the specific heat capacity of bulk gas, T is the temperature of the bulk gas, λ_z is the heat axial dispersion coefficient and q_g and q_{wall} are heat generation terms, again given per unit volume of adsorbent. The generation term q_g quantifies the heat transfer occurring between bulk flow and particles, while the generation term q_{wall} takes into account heat losses through the adsorbent bed wall. The actual expression for q_g depends on the nature of the resistances to the heat transfer and for linear drive force (LDF) mechanism is provided by the following equation:

$$q_g = \frac{\partial(\rho^p c_p^p T)}{\partial t} + \rho^p \sum_{i=1}^{N_{comp}} \Delta H_{ads,i} \frac{\partial Q_i}{\partial t}, \qquad \forall z \in (0, L) \tag{2.4}$$

where c_p^p is the specific heat capacity of the particle and $\Delta H_{ads,i}$ is the isosteric heat of adsorption of component *i.*

In general, three thermal operating modes exist in a PSA/VSA process: isothermal, non-isothermal and adiabatic.

In the case of isothermal mode, the heat balance becomes:

$$\frac{\partial T}{\partial z} = 0, \qquad \forall z \in (0, L) \tag{2.5}$$

In the case of non-isothermal mode the heat transfer through the adsorbent bed wall cannot be neglected and the following equation can be used:

$$q_{wall} = \frac{3k_{h,wall}}{R_{bed}}(T - T_{wall}), \ \ \forall z \in (0, L) \tag{2.6}$$

where $k_{h,wall}$ is the heat transfer coefficient of the adsorbent bed wall, T_{wall} is the temperature of the adsorbent bed wall and R_{bed} is the adsorbent bed radius.

In the case of adiabatic mode $\mathrm{q_{wall}} = 0$ and then equation (2.3) becomes:

$$\frac{\partial(\rho c_p T u)}{\partial z} + \frac{\partial(\rho c_p T)}{\partial t} + \frac{(1 - \varepsilon_{bed})}{\varepsilon_{bed}} q_g = \frac{\partial}{\partial z}\left(\lambda_z \frac{\partial T}{\partial z}\right), \ \ \forall z \in (0, L) \tag{2.7}$$

Momentum balance

The pressure drop is an important variable in modelling of fixed adsorbent beds having a high impact on the separation quality and operating cost. The hydrodynamics of flow through porous media is the most commonly described by using one of the following correlations for pressure drop:

Darcy equation (linear-laminar flow):

$$-\frac{\partial P}{\partial z} = 180\left(\frac{1 - \varepsilon_{bed}}{\varepsilon_{bed}}\right)^2 \frac{\mu u}{\left(2R_p\right)^2}, \qquad \forall z \in (0, L) \tag{2.8}$$

Ergun equation (non-linear, turbulent flow):

$$-\frac{\partial P}{\partial z} = 150\left(\frac{1 - \varepsilon_{bed}}{\varepsilon_{bed}}\right)^2 \frac{\mu u}{\left(2R_p\right)^2} + 1.75\left(\frac{1 - \varepsilon_{bed}}{\varepsilon_{bed}}\right)\frac{\rho u|u|}{2R_p}, \qquad \forall z \in (0, L) \tag{2.9}$$

where P is the total pressure of the adsorbent bed, μ is the viscosity of bulk gas and R_p is the particle radius.

Equation of state

An equation of state is necessary to link concentration with temperature and pressure in the gas mixture. The ideal gas law is provided by the following equation:

$$P = \sum_{i=1}^{N_{comp}} C_i RT\,, \qquad \forall z \in [0, L] \tag{2.10}$$

where R is the universal gas constant.

Thermo-physical properties

The physical properties (density, viscosity, thermal conductivity, specific heat capacity) of the gas mixture are functions of temperature, pressure and composition and can be assumed constant or calculated using some of the available correlations or thermo-physical packages.

Axial dispersion coefficients

Axial concentration and temperature gradients always exist in packed beds. Hence, a diffusive mass and heat transfer will always occur and tend to degrade the performance of the process. An accurate prediction of mass and heat axial dispersion coefficients is therefore very important for detailed modelling of the flow through the packed adsorbent bed. Several correlations for prediction of mass and heat axial dispersion coefficients exist in the literature. Wakao developed some of the most widely used. The mass axial dispersion coefficient $D_{z,i}$ and the heat axial dispersion coefficient λ_z can be calculated by using Wakao correlations (Wakao and Funazkri, 1978; Wakao *et al.,* 1979):

$$D_{z,i} = \frac{D_{m,i}}{\varepsilon_{bed}}(20 + 0.5ScRe), \qquad \forall z \in [0, L], i = 1, \dots, N_{comp} \tag{2.11}$$

$$\lambda_z = \lambda(7 + 0.5PrRe), \qquad \forall z \in [0, L] \tag{2.12}$$

where $D_{m,i}$ is the molecular diffusivity of component *i*, λ is the thermal conductivity of bulk gas, Sc is the Schmidt number, Re is the Reynolds number and Pr is the Prandtl number given by the following equations:

$$Sc = \frac{\mu}{\rho D_{m,i}}, \qquad \forall z \in [0, L], i = 1, \dots, N_{comp} \tag{2.13}$$

$$Re = \frac{u\varepsilon_{bed}(2R_p)\rho}{\mu}, \qquad \forall z \in [0, L] \tag{2.14}$$

$$Pr = \frac{c_p \mu}{\lambda}, \qquad \forall z \in [0, L] \tag{2.15}$$

The molecular diffusivity of component *i* $D_{m,i}$ is independent of the composition and for a binary mixture can be calculated by using Chapman-Enskog equation (Ruthven, 1984; Yang, 1987):

$$D_{m,i} = 1.8583 * 10^{-7} \frac{\sqrt{T^3 \left(\frac{1}{MW_1} + \frac{1}{MW_2}\right)}}{P\sigma_{12}^2 \Omega_{12}}, \qquad \forall r \in [0, R_p], i = 1,2 \tag{2.16}$$

where MW_i is the molecular weight of component *i*, σ_{12} is the collision diameter from the Lennard-Jones potential and Ω_{12} is the collision integral which is a function of $\frac{k_B T}{\varepsilon_{12}}$, where k_B is Boltzmann's constant and ε_{12} is the Lennard-Jones force constant given by the following equation:

$$\sigma_{12} = \frac{\sigma_1 + \sigma_2}{2}, \qquad \varepsilon_{12} = \sqrt{\varepsilon_1 \varepsilon_2} \tag{2.17}$$

The molecular diffusivity of component *i* $D_{m,i}$ for a binary mixture can be calculated alternatively from Fuller correlation:

$$D_{m,i} = 1.013 * 10^{-7} T^{1.75} \frac{\sqrt{\left(\frac{1}{MW_1} + \frac{1}{MW_2}\right)}}{P X_{12}^2}, \qquad \forall r \in [0, R_p], i = 1,2 \tag{2.18}$$

where X_{12} is a constant which is a function of molecular diffusion volumes of components $D_{v,i}$ given by the following equation:

$$X_{12} = D_{v,1}^{1/3} + D_{v,2}^{1/3} \tag{2.19}$$

Overall mass and heat transfer coefficients

An accurate prediction of overall mass and heat transfer coefficients is very important for detailed modelling of the flow through the packed adsorbent bed. Several correlations for prediction of overall mass and heat transfer coefficients exist in the literature. The overall mass transfer coefficient of component *i* $k_{f,i}$ and the overall heat transfer coefficient k_h can be calculated by using Wakao correlations (Wakao and Funazkri, 1978; Wakao *et al.,* 1979):

$$Sh = \frac{(2R_p)k_{f,i}}{D_{m,i}} = (2 + 1.1Sc^{0.33}Re^{0.6}), \qquad \forall z \in [0, L], i = 1, \dots, N_{comp} \tag{2.20}$$

$$Nu = \frac{(2R_p)k_h}{\lambda} = (2 + 1.1Pr^{0.33}Re^{0.6}), \qquad \forall z \in [0, L] \tag{2.21}$$

Linear driving force (LDF) mechanism

The overall uptake rate in a particle is expressed as a function of the bulk gas flow concentration through a linear driving force (LDF) mechanism:

$$\frac{\partial Q_i}{\partial t} = \frac{15D_{e,i}}{R_p^2}(Q_i^* - Q_i), \qquad \forall z \in [0, L], i = 1, \dots, N_{comp} \tag{2.22}$$

where Q_i^* is the adsorbed amount of component *i* per unit mass of adsorbent in equilibrium with the gas phase and $D_{e,i}$ is the effective diffusivity of component *i*. The effective diffusivity of component *i* $D_{e,i}$ (for macropore controlled transport mechanism) can be calculated by using Bosanquet equation (Ruthven, 1984; Yang, 1987):

$$D_{e,i} = \frac{\varepsilon_p}{\tau_p}\frac{D_{m,i}D_{k,i}}{D_{m,i} + D_{k,i}}, \qquad \forall r \in [0, R_p], i = 1, \dots, N_{comp} \tag{2.23}$$

where ε_p is the porosity of the particle, τ_p is the tortuosity factor of the particle and $D_{k,i}$ is the Knudsen diffusivity of component *i*. The Knudsen diffusivity of component *i* $D_{k,i}$ can be calculated by using Kauzmann correlation (Ruthven, 1984; Yang, 1987):

$$D_{k,i} = 97R_{pore}\sqrt{\frac{T}{MW_i}}, \qquad \forall r \in [0, R_p], i = 1, \dots, N_{comp} \tag{2.24}$$

where R_{pore} is the pore radius.

Gas-solid phase equilibrium isotherms

The quantitative description of gas-solid phase interactions at equilibrium conditions in the form of models or correlations is extremely important for the accurate design and simulation of PSA/VSA processes. At constant temperature the model that describes the concentration of a component in the adsorbed phase as a function of the gas composition and pressure, is called the adsorption isotherm. Adsorption isotherms are given in the form of algebraic or integral equations that are used to determine the amount of gas adsorbed within the adsorbent particles as a function of pressure, temperature and composition of the bulk gas. These equations contain several semi-empirical parameters that are determined by fitting experimental

isotherm data at different temperatures. In general there are three different categories of single component adsorption isotherms: single and dual-site Langmuir isotherms, isotherms based on the Gibbs approach and isotherms based on the Potential-theory approach. For the case of multi-component mixtures the more widely used models are: Linear isotherms, Extended Langmuir equations, Loading Ratio Correlations (LRC), and Adsorbed Solution Theory (AST) (Ruthven, 1984; Yang, 1987).

The following dual-site Langmuir isotherm describes the adsorption equilibrium:

$$Q_i^* = \frac{q_{mi(1)} b_{i(1)} P_i}{1 + \sum_{i=1}^{N_{comp}} b_{i(1)} P_i} + \frac{q_{mi(2)} b_{i(2)} P_i}{1 + \sum_{i=1}^{N_{comp}} b_{i(2)} P_i} \tag{2.25}$$

where $q_{mi(j)}$ and $b_{i(j)}$ are the dual-site Langmuir isotherm parameters of component *i* and of *j* site and P_i is the partial pressure of component *i* which is a function of the molar fraction of component *i* in gas phase y_i and the total pressure *P* given by the Dalton's law:

$$P_i = y_i \mathrm{P} \tag{2.26}$$

The dual-site Langmuir isotherm parameters $q_{mi(j)}$ and $b_{i(j)}$ are calculated by the following equations (2.27.a-2.27.d):

$$q_{mi(1)} = k_{1,i(1)} + k_{2,i(1)} T \tag{2.27.a}$$

$$b_{i(1)} = k_{3,i(1)} \exp\left(\frac{k_{4,i(1)}}{T}\right) \tag{2.27.b}$$

$$q_{mi(2)} = k_{1,i(2)} + k_{2,i(2)} T \tag{2.27.c}$$

$$b_{i(2)} = k_{3,i(2)} \exp\left(\frac{k_{4,i(2)}}{T}\right) \tag{2.27.d}$$

Boundary conditions

For the inlet stream of the adsorbent bed Danckwert's boundary conditions are applied:

$$u\left(C_i - C_i^{in}\right) = D_{z,i} \frac{\partial C_i}{\partial z}, \qquad z = 0\ (L), i = 1, \dots, N_{comp} \tag{2.28}$$

$$\rho c_p u\left(T - T^{in}\right) = \lambda_z \frac{\partial T}{\partial z}\,, \qquad z = 0\ (L) \tag{2.29}$$

$$u = u^{in}, \qquad z = 0\ (L) \tag{2.30}$$

For the outlet stream or for the closed end of the adsorbent bed Danckwert's boundary conditions are applied:

$$\frac{\partial C_i}{\partial z} = 0\,, \qquad z = L\ (0), i = 1, \dots, N_{comp} \tag{2.31}$$

$$\frac{\partial T}{\partial z} = 0, \qquad z = L\ (0) \tag{2.32}$$

$$\frac{\partial u}{\partial z} = 0\,, \qquad z = L\ (0) \tag{2.33}$$

where u^{in}, C_i^{in} and T^{in} are interstitial velocity, concentration and temperature of the inlet stream of the adsorbent bed, respectively.

Gas valve equation

The molar flow rate of the gas stream entering or leaving the adsorbent bed is calculated by a gas valve equation recommended by the Fluids Control Institute Inc. provided by the following equations (Choi and Wen-Chung, 1994):

$$F = C_{valve}\, SP P_{in} \sqrt{\left| \frac{1 - (\frac{P_{out}}{P_{in}})^2}{\sum_{i=1}^{N_{comp}} y_i M W_i T} \right|}, \qquad if\ P_{out} > (\frac{1}{P_{crit}}) P_{in} \tag{2.34}$$

$$F = C_{valve}\, SP P_{in} \sqrt{\left| \frac{1 - (\frac{1}{P_{crit}})^2}{\sum_{i=1}^{N_{comp}} y_i M W_i T} \right|}, \qquad if\ P_{out} \leq (\frac{1}{P_{crit}}) P_{in} \tag{2.35}$$

where F is the molar flow rate, C_{valve} is the gas valve constant, SP is the stem position of the gas valve, P_{in} is the pressure at the inlet of the gas valve and P_{out} is the pressure at the outlet of the gas valve. The gas valve equation describes a one-way valve. The purpose of the one-way valve is to solely force the flow to the desired directions and avoid any non-permitted flows. It should be emphasized that the gas valve equation results in non-linear pressure history profiles during the pressure changing steps. In a typical pressurization step, P_{in} is equal to the pressure of source

tank (P_{feed}), while P_{out} is related to the corresponding pressure of the adsorbent bed being pressurized and it is increased, as it is proportional to the number of moles entering the adsorbent bed. On the other hand, in a typical depressurization step (e.g. blowdown, evacuation) P_{in} is related to the corresponding pressure of the adsorbent bed being depressurized and it is decreased, as it is proportional to the number of moles exiting the adsorbent bed, while P_{out} is equal to the pressure of sink tank (P_{blow}, P_{evac}).

The critical pressure P_{crit} is provided by the following equation:

$$P_{crit} = (\frac{2}{1+\gamma})^{\frac{\gamma}{1-\gamma}} \tag{2.36}$$

where the specific heat capacity ratio γ is provided by the following equation:

$$\gamma = \frac{c_p}{c_v} \tag{2.37}$$

where c_p is the specific heat capacity of bulk gas referring to constant pressure and c_v is specific heat capacity of bulk gas referring to constant volume.

Energy consumption

The energy consumption for compression of a real gas in a single-stage compressor is provided by the following equation:

$$E = \frac{1}{n_c}(\frac{\gamma}{\gamma-1})RT_{in}\left[\left(\frac{P_{out}}{P_{atm}}\right)^{\frac{\gamma-1}{\gamma}} - 1\right]N_{in} \tag{2.38}$$

where E is the energy consumption of the compressor, T_{in} is the temperature of the feed stream of the compressor, P_{atm} is the atmospheric pressure, P_{out} is the pressure of the leaving stream of the compressor, N_{in} is the number of moles of the feed stream of the compressor and n_c is the isentropic compression efficiency of the compressor.

The energy consumption for evacuation of a real gas in a single-stage vacuum pump is provided by the following equation:

$$E = \frac{1}{n_v}\left(\frac{\gamma}{\gamma-1}\right)RT_{in}\left[\left(\frac{P_{atm}}{P_{vac}}\right)^{\frac{\gamma-1}{\gamma}} - 1\right]N_{in} \tag{2.39}$$

where E is the energy consumption of the vacuum pump, T_{in} is the temperature of the feed stream of the vacuum pump, P_{vac} is the pressure of the leaving stream of

the vacuum pump, N_{in} is the number of moles of the feed stream of the vacuum pump, n_v is the isentropic evacuation efficiency of the vacuum pump. It is important to note that in this study n_c=0.72, n_v=0.72 and γ =1.4 have been considered in all energy calculations. The energy values have been reported in electrical equivalents.

Selectivity and working capacity

The selectivity of component *i* over component *j* of an adsorbent a_{ij} *(*for a gas mixture with two components where *i* is the strongly adsorbed component and *j* is the weakly adsorbed component) is provided by the following equation:

$$a_{ij} = \left(\frac{Q_i}{Q_j}\right)\left(\frac{y_j}{y_i}\right) \tag{2.40}$$

where y_i and y_j represent the molar fractions of component *i* and component *j* in the gas phase, respectively and Q_i and Q_j represent the corresponding adsorbed amounts (solid loadings) of component *i* and component *j* per unit mass of adsorbent, respectively.

The equilibrium working capacity of component *i* for a given adsorbent is defined as the difference between the equilibrium adsorption capacities under adsorption and desorption conditions:

$$\Delta Q_i^* = Q_{i\,(Pads)}^* - Q_{i\,(Pdes)}^*, \qquad \forall z \in (0, L), i = 1, \dots, N_{comp} \tag{2.41}$$

where ΔQ_i^* is the equilibrium working capacity of component *i* and $Q_{i\,(Pads)}^*$ and $Q_{i\,(Pdes)}^*$ represent the adsorbed amount (equilibrium adsorption capacity) of component *i* per unit mass of adsorbent in equilibrium with the gas phase under adsorption and desorption pressure, respectively.

2.3. State Transition Network (STN) approach

Nikolic *et al.,* (2009) developed a novel robust method to control the execution of a PSA/VSA process which relies on a state transition network (STN) representation of the process. States are represented by operating steps (that is an adsorbent bed can be in one of the operating states such as pressurization, adsorption, purge etc.), inputs are the time elapsed in the process, the time within the current cycle and several input parameters known a priory at the time of execution. Each state (the operating step) includes a set of boundary conditions and gas valves states (open/closed). A deterministic Finite State Machine (FSM) is implemented where the next possible state is uniquely determined for a given (current) state and input values. State transitions are decisions when the state change should occur (based on the input values). The start state is commonly co- or counter-current pressurization or pressure equalization (re-pressurization) step. This way, it is possible to control the execution of the process by specifying a few parameters such as the number of beds, the sequence of operating steps in one bed, the number of pressure equalization steps, and the start time and duration of each operating step.

An STN graph with all possible state transitions is presented in Figure 2.2. The overall idea is to identify which state transitions are feasible and the conditions under which a particular state change occurs under a given current state. In general, the cycle time and the time elapsed in the process are used to identify the position within the cycle. More specifically, by defining certain process parameters (such as the number of pressure equalization steps), and for a given sequence of operating steps in one bed and duration of certain operating steps in the cycle it is possible to distinguish between allowed and forbidden operating steps and make the decision about the transition.

In the current study the STN approach has been implemented for modelling of operating procedures in complex multi-bed PSA/VSA processes.

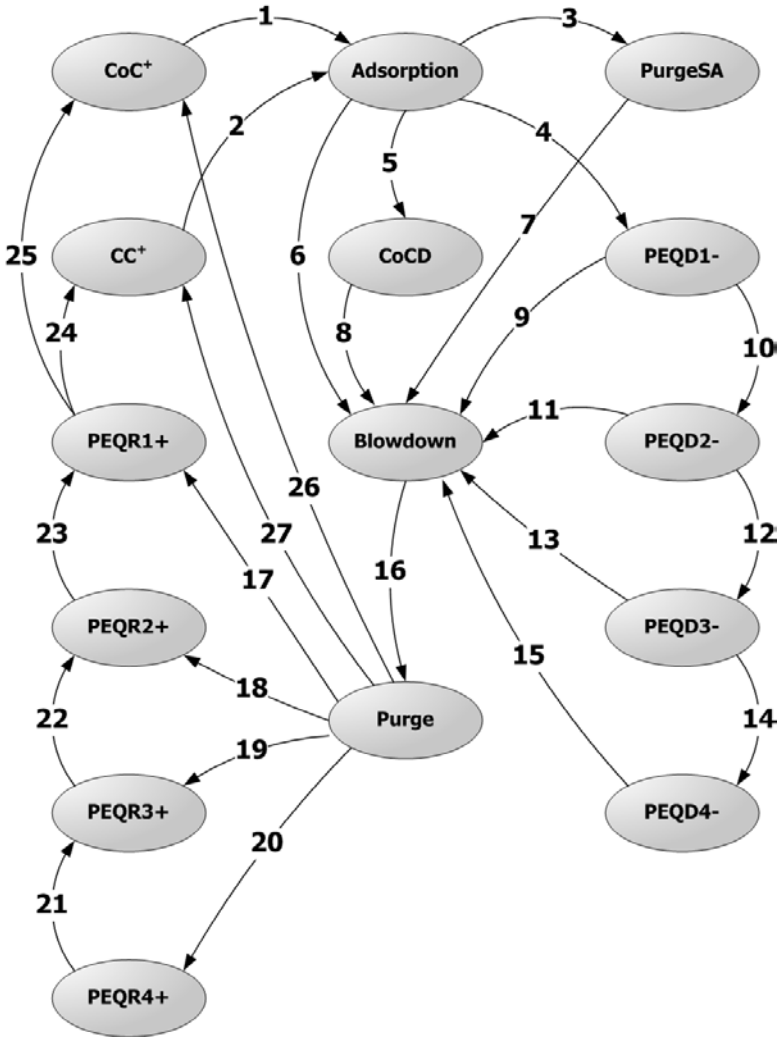

Figure 2.2. State transition network (STN) with all possible state transitions (Nikolic *et al.,* 2009).

2.4. Fundamentals of PSA/VSA process optimisation

The governing equations describing PSA/VSA processes are a system of coupled PDAEs which often involve sharp fronts moving in space. The nonlinearities and ill-conditioned matrices due to multiple adsorbent layers, non-isothermal effects and stringent product specifications may lead to the failure of numerical solvers. In addition, the transient operation yields dense constrained Jacobians, which pose heavy computational burden on gradient based optimisation techniques (Haghpanah *et al.,* 2013).

The selection of optimal design and operating parameters is a difficult task due to several reasons: highly complex mathematical models (large number of PDAEs necessary to describe the multi-scale transport phenomena in adsorbent bed and adsorbent particles), a large number of trade-offs between the key variables, and excessive computational requirements to reach the cyclic steady state. In addition, calculation of the optimal number of adsorbent beds and optimal schedule coupled with the optimisation of design and operating variables makes the problem of intractable size (Nikolic *et al.,* 2009).

The optimisation studies available in the literature mostly consider single objective optimisation problem. Two different scenarios have been proposed in the literature to reduce the computational requirements for the solution of the problem:

a) fixed number of adsorbent beds, fixed schedule and complex PSA/VSA model employed, and a subset of operating and design variables optimised (Biegler *et al.,* 2004; Cruz *et al.,* 2005; Cruz *et al.,* 2003; Hasan *et al.,* 2012; Hasan *et al.,* 2013; Jiang *et al.,* 2003; Jiang *et al.,* 2004; Khurana and Farooq, 2016; Ko *et al.,* 2005; Nikolic *et al.,* 2009; Nilchan and Pantelides, 1998; Sankararao and Gupta, 2007).

b) very simple PSA/VSA model employed, and number of adsorbent beds, schedule and a subset of operating and design variables optimised (Smith and Westerberg, 1991). The effect of number of adsorbent beds and different cycle configurations (sequence and duration of operating steps) has been systematically analyzed only by Smith and Westerberg. However, very simple PSA/VSA model has been used which rather roughly predict PSA/VSA process performance indicators therefore making it practically insensitive on many design and operating variables.

2.5. Numerical solution of the optimisation problem

Theoretical modelling of PSA/VSA processes have also been extensively studied to gain a clear understanding of this rather complex process. In general, PSA/VSA adsorbent bed model is a set of fairly complex PDAEs which reflect the transient nature of the process. The modelling framework provides a comprehensive qualitative and quantitative insight into the key phenomena taking place in a PSA/VSA process. With such models, it is now possible to accurately predict the dynamic behavior of a PSA/VSA process, and to adequately account for all the factors that affect the performance of any given PSA/VSA process.

The modelling equations have been implemented in the gPROMS™ modelling environment (PSE, 2011). The modelling equations are solved in sequence, cycle by cycle until CSS is achieved. The spatial domains are discretized using several options from finite difference and finite element schemes. The modelling equations comprise a system of non-linear PDAEs which is numerically solved using the method of lines (MOL). This method is based on the discretization of the distributed equations with respect to all spatial domains, which results in a mixed set of time-dependent ordinary differential and algebraic equations (DAEs). Then the resulting DAEs system is integrated over time by employing the integration code DASOLV which is based on the backward differentiation formula (BDF), and automatically adjusts the time step size as well as the integration order to maintain the error of integration within the tolerance defined by the user. In the present study the discretization algorithm applied for the numerical solution of the model is the centered finite difference method (CFDM) of second order with 50 discretization intervals for the discretization of axial domain showing nearly identical results with other discretization schemes which have been tested. The solvers employed in the simulations used a value of $1x10^{-5}$ for absolute tolerance. All computations reported have been carried out on a desktop workstation with Intel Core i5 3.10 GHz processor and 8.0 GB RAM.

The dynamic optimisation problem is solved using gPROMS™/gOPT tool, an implementation of the control vector parameterization approach in the gPROMS™ modelling system (PSE, 2011; Vassiliadis *et al.,* 1994). The axial domain is discretized

using centered finite difference method (CFDM) of second order with 50 discretization intervals. The equations that describe the model are generated by gPROMS™ as residuals with symbolically generated partial derivatives and used as inputs to gPROMS™/gOPT tool. The latter employs:

- A sophisticated integrator based on backward differentiation formulae methods for integrating differential and algebraic equations (DAEs).
- The SRQPD non-linear programming solver implementing a reduced sequential quadratic programming algorithm. The non-linear programming algorithm required the gradients of the constraint and the objective function with respect to the optimisation decision variables. These can be computed from the "sensitivities" with respect to the optimisation variables.

The solution of the optimisation problem is a two-stage iterative procedure in gPROMS™/gOPT tool. The first stage is the integration of the discretized model to obtain constraints residuals and/or gradients, and the second stage is the input of the SRQPD non-linear programming solver as described above.

Given the initial estimates for the optimisation variable *p,*

Repeat

1. Integrate DAEs to determine the objective function and constraints and if required their gradients with respect to *p*;
2. Call SRQPD to determine the new estimates for *p*

Until converge (e.g. optimisation tolerance 10^{-5}).

2.6. Concluding remarks

A mathematical modelling framework for the simulation and optimisation of PSA/VSA processes for post-combustion CO_2 capture from dry flue gas has been developed in this chapter. The core of the modelling framework represents a detailed adsorbent bed model relying on a coupled set of mixed partial differential and algebraic equations (PDAEs) for mass, heat and momentum balance at both bulk gas and particle level, equilibrium isotherm equations, transport and thermo-physical properties of the gas mixture and boundary conditions according to the operating steps. The proposed modelling equations have been implemented in the gPROMS™ modelling environment. The dynamic optimisation problem has been formulated and solved using gPROMS™/gOPT tool.

CHAPTER 3
SIMULATION AND OPTIMISATION OF A SINGLE-STAGE PSA/VSA PROCESS

3. Simulation and optimisation of a single-stage PSA/VSA process

3.1. Model validation

The modelling framework presented in chapter 2 has been validated against previously reported PSA/VSA models as well as experiments. The developed framework has been applied in a PSA/VSA process concerning the separation of CO_2 from dry flue gas (15% CO_2, 85% N_2) using zeolite 13X as adsorbent. The parameters of adsorbent bed model and the parameters of the dual-site Langmuir adsorption isotherm of CO_2 and N_2 on zeolite 13X have been adopted from the works of Ko *et al.,* (2004; 2005) and are summarized in the Table 3.1 and Table 3.2, respectively. The adsorption isotherms of CO_2 and N_2 on zeolite 13X in a temperature range from 298 K to 393 K are represented in Figure 3.1 and Figure 3.2, respectively. For the whole temperature range, the selectivity of CO_2/N_2 is very high, as it is illustrated in Figure 3.1 and Figure 3.2.

The sequence of the operating steps for one-bed four-step PSA/VSA cycle configuration is illustrated in Figure 3.3 and consist of: pressurization with the feed stream co-currently (CoC), adsorption (Ads), co-current depressurization or blowdown (CoD) to intermediate pressure and counter-current depressurization or evacuation (CnD) to lowest pressure. The simulation results of this study in terms of process performance indicators (CO_2 purity and CO_2 recovery) are in good agreement with the results of Ko *et al.,* (2004; 2005) and are summarized in Table 3.3.

It is illustrated that the proposed modelling framework predicts satisfactorily the behavior of the process. The small differences with the results of Ko *et al.,* (2004; 2005) can be mainly attributed to the use of a gas valve equation employed to calculate the flow rate and pressure at the end of the adsorbent bed during pressure changing steps, as opposed to linear change of velocity at the feed end used in the original works of Ko *et al.,* (2004; 2005). It should be emphasized that the gas valve equation results in exponential pressure histories during the pressure changing steps. Moreover, a different discretization method, and a different package for the thermo-physical properties calculations have been used compared to the works of Ko *et al.,* (2004; 2005).

Table 3.1. Parameters of adsorbent bed model.

parameter	value
adsorbent bed radius (R_{bed})	1.1×10^{-2} m
adsorbent bed length (L_{bed})	25×10^{-2} m
pore radius (R_{pore})	0.5×10^{-9} m
particle radius (R_p)	1.0×10^{-3} m
particle tortuosity (τ_p)	4.5
particle porosity (ε_p)	0.38
diffusion volume (D_v)	26.9 (CO_2); 18.5 (N_2)
adsorbent bed void (ε_{bed})	0.348
particle density (ρ_p)	1159.4 kg/m^3
universal gas constant (R)	8.314 J/(mol·K)
heat capacity of particles (C_p^p)	504 J/(kg·K)
heat transfer coefficient of the wall ($k_{h,wall}$)	60 J/(m^2·K·s)
heat of adsorption (ΔH_{ads})	23011.14 J/mol (CO_2)
heat of adsorption (ΔH_{ads})	14452.72 J/mol (N_2)

Table 3.2. Parameters of the dual-site Langmuir adsorption isotherm.

	zeolite 13X (Ko *et al*., 2005)		
	CO_2 (i = 1)	**N_2 (i = 2)**	**units**
$k_{1,i(1)}$	2.82	1.89	mol/Kg
$k_{2,i(1)}$	-3.50×10^{-4}	-2.25×10^{-4}	1/K
$k_{3,i(1)}$	2.83×10^{-9}	1.16×10^{-9}	1/Pa
$k_{4,i(1)}$	2598.20	1944.61	K
$k_{1,i(2)}$	3.97	1.89	mol/Kg
$k_{2,i(2)}$	-4.95×10^{-3}	-2.25×10^{-4}	1/K
$k_{3,i(2)}$	4.41×10^{-9}	1.16×10^{-9}	1/Pa
$k_{4,i(2)}$	3594.07	1944.61	K

Table 3.3. Process performance indicators simulation results with absolute deviations from the results of works of Ko *et al.,* (2004; 2005).

				Ko *et al.*	Ko *et al.*	this study	this study		
Reference	**P_{feed} (bar)**	**T_{feed} (K)**	**L/D**	**CO_2 Purity**	**CO_2 Recovery**	**CO_2 Purity**	**CO_2 Recovery**	**deviation CO_2 Purity**	**deviation CO_2 Recovery**
(Ko *et al.,* 2005)	6.52	370	11.36	88.94	96.90	84.82	97.93	-4.63	1.06
(Ko *et al.,* 2004)	6.94	365	11.36	95.46	15.00	92.12	14.35	-3.50	-4.33
(Ko *et al.,* 2004)	8.69	364	17.64	92.29	80.00	97.19	79.20	5.31	-1.00

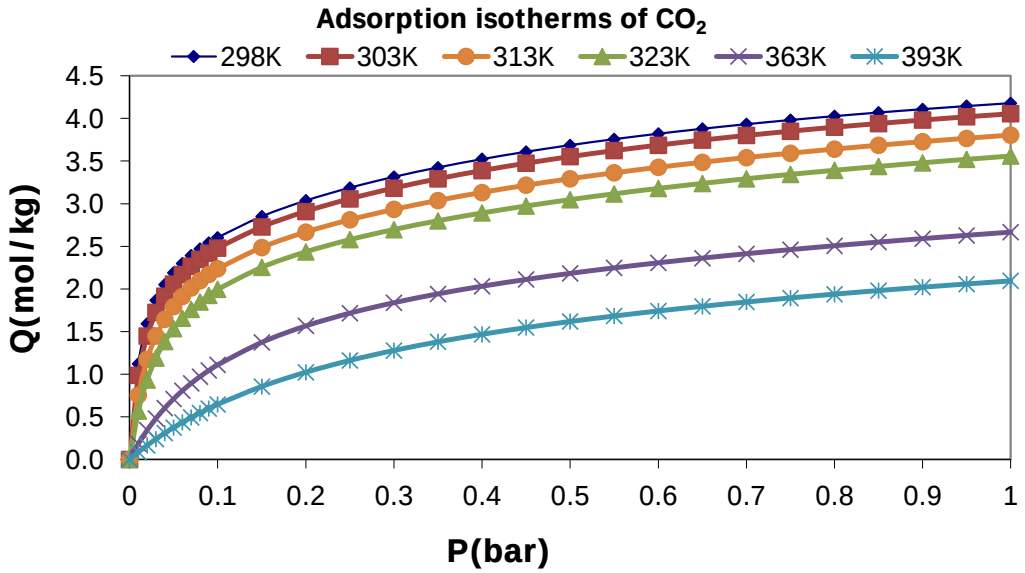

Figure 3.1. Adsorption isotherms of CO_2 on zeolite 13X at different temperatures.

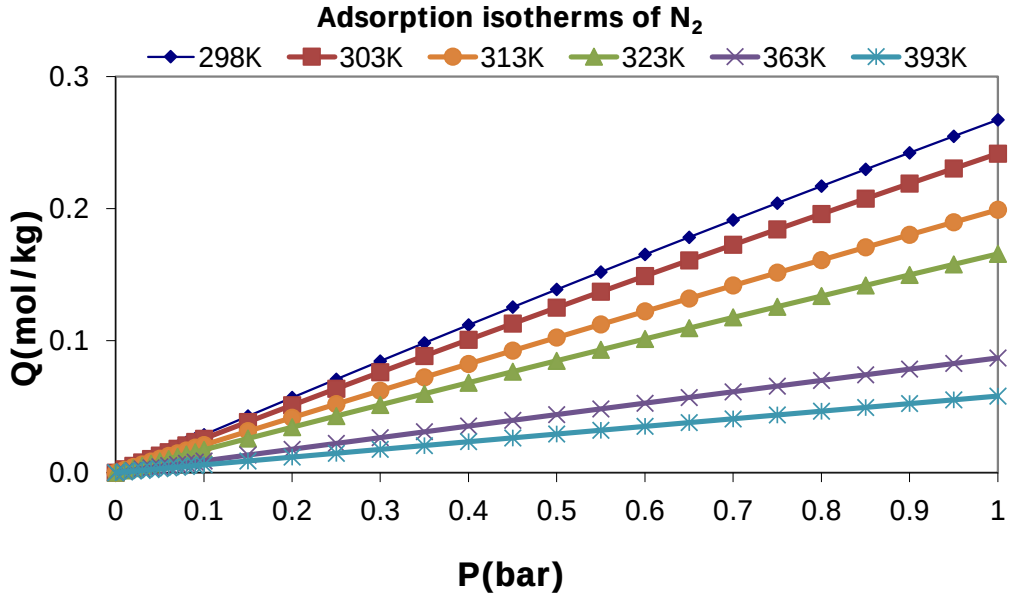

Figure 3.2. Adsorption isotherms of N_2 on zeolite 13X at different temperatures.

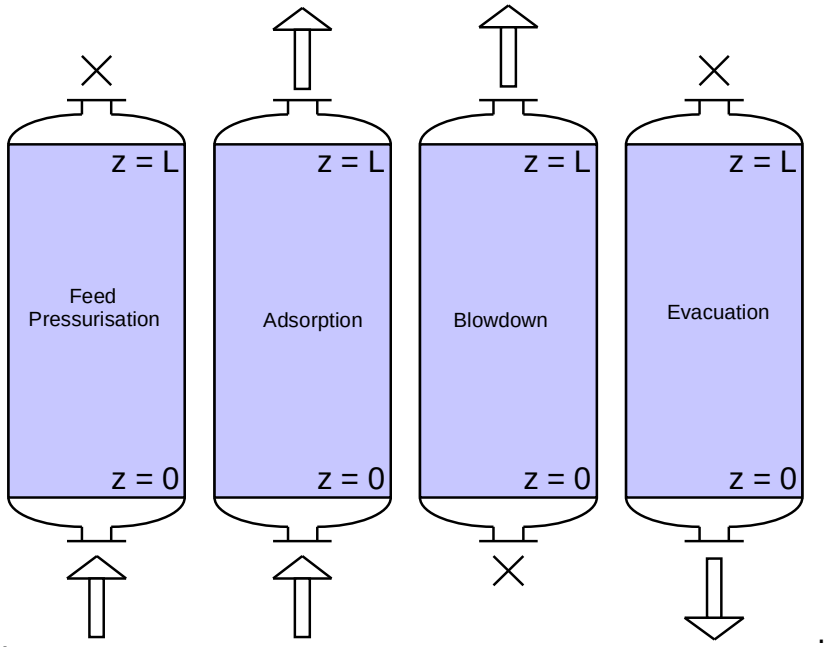

Figure 3.3. Sequence of operating steps for one-bed four-step PSA/VSA cycle configuration.

3.2. Parametric analysis

A systematic parametric analysis provides significant insight into the most critical design and operating variables, and their effect on process performance indicators. Several parametric studies have been reported in the literature for specific PSA/VSA systems.

The modelling framework has been applied in the same PSA/VSA process described in section 3.1 concerning the separation of CO_2 from dry flue gas (15% CO_2, 85% N_2) using zeolite 13X as adsorbent. The parameters studied in this work include feed flow rate, feed composition, feed pressure, blowdown pressure, evacuation pressure, bed length, particle radius and adsorption step duration. The effect of these parameters is well documented in the literature and the parametric studies performed in this work have been carried out only in cases when it was necessary to clarify the effect of certain parameter on the process performance. Thus, once the base case parameters have been selected, only one variable at the time has been varied, and its effect analyzed. A sensitivity study have been conducted to determine which properties are most important in order to improve process performance. The effects of feed flow rate, feed composition, feed pressure, blowdown pressure, evacuation pressure, bed length, particle radius and adsorption step duration on process performance indicators are shown in Figures 3.4 to 3.11.

As shown in Figure 3.4, CO_2 purity increased from 75.87% to 89.83% when the feed flow rate increased from 0.127 lt/s_stp to 0.476 lt/s_stp. Since the adsorption time is the same, increasing feed flow rate causes the increase of adsorption zone resulting in the increasing of CO_2 purity. However, the CO_2 recovery decreased from 99.90% to 63.61% due to the increase of feed flow rate, which is mainly due to the larger CO_2 losses when the feed flow rate is higher.

The CO_2 concentration in different streams where CO_2 capture can be employed ranges from 10% to 20% for different sources. In order to study the effect of feed concentration on the performance of the PSA/VSA process, the feed gas concentration has been varied from 10% to 20% while keeping all the other parameters the same. The main results are shown in Figure 3.5. The CO_2 purity increases, while the CO_2 recovery decreases with the rise of feed concentration.

In the PSA/VSA process, the energy consumption of the blower is one of the main components of total cost. High adsorption pressure results in high energy consumption of the blower, thus, the effect of the feed pressure has been studied, and it is illustrated in Figure 3.6. While the feed pressure rises from 4.52 bar to 8.52 bar, the CO_2 purity increases, too, as a direct result of more CO_2 being adsorbed and then released in the heavy product or "extract". In the meantime the CO_2 recovery decreases with the rise of feed pressure. This is in full agreement with the theory since for linear adsorption isotherms purity always increases for higher feed pressures. An increase in the feed pressure causes an increase in CO_2 purity since the adsorbent capacity increases as the pressure increases. On the other hand, as feed pressure increases, energy consumption also increases. Therefore, it is necessary to find the optimal feed pressure, which ensures feasible pressure equalization and co-current depressurization steps at minimum operating cost.

The impact of the intermediate pressure of the process (blowdown pressure) on the process performance has been investigated. Figure 3.7 indicates that as the blowdown pressure increases from 0.5 bar to 1 bar the CO_2 purity decreases and the CO_2 recovery increases.

The selection of evacuation pressure is an important variable since it governs the energy performance of the system. However, when a flue gas with atmospheric pressure is employed for adsorption, low evacuation pressure will be necessary to desorb CO_2. In Figure 3.8, it can be observed that both the CO_2 purity and the CO_2 recovery reduce with the increase of vacuum pressure. A small increase of vacuum pressure reduces the performance of the process significantly.

The effect of adsorbent bed length is illustrated in Figure 3.9. Both the CO_2 purity and the CO_2 recovery decrease with the increase of bed length. Increase in the bed length, while keeping all the other parameters the same, leads to an increase in the pressure drop, which results in an earlier breakthrough and degradation of the performance of the process.

The effect of particle radius is illustrated in Figure 3.10. Figure 3.10 indicates that as the particle radius increases, the CO_2 purity decreases and the CO_2 recovery increases. Particle size is an important design parameter whose influence on the separation performance can be qualitatively assessed according to the well-known

linear driving force (LDF) mechanism. The LDF mass transfer coefficient is inversely proportional to the square of particle radius and significantly affects the mass transfer within particles. On the other hand, the pressure drop is inversely proportional to the square of particle radius. So a decrease in particle radius leads to an increase in a pressure drop, which results in an earlier breakthrough and degradation of the performance of the process. As particle radius increases the CO_2 purity decreases as a direct result of less CO_2 being adsorbed and then released in the heavy product or “extract”.

The effect of adsorption step duration is illustrated in Figure 3.11. The CO_2 purity increases, while the CO_2 recovery decreases with the rise of adsorption step duration. As shown in Figure 3.11, CO_2 purity increased from 76.85% to 85.97% when the adsorption step duration increased from 30 sec to 70 sec. Since the feed flow rate is the same, increasing adsorption step duration causes the increase of adsorption zone resulting in the increasing of CO_2 purity. However, the CO_2 recovery decreased from 99.47% to 79.55% due to the increase of adsorption step duration, which is mainly due to the larger CO_2 losses when the adsorption step duration is higher.

The predictions of the mathematical model for the trends of CO_2 purity and CO_2 recovery are in full agreement with theory. Since the theory accurately portrays the overall behavior of the process, the transport mechanisms embodied in the theory may provide significant insight into phenomena that take place in a PSA/VSA process. In addition, by reviewing the results of the systematic parametric analysis, it is possible to gain an intuitive understanding of the relations between factors that affect process performance.

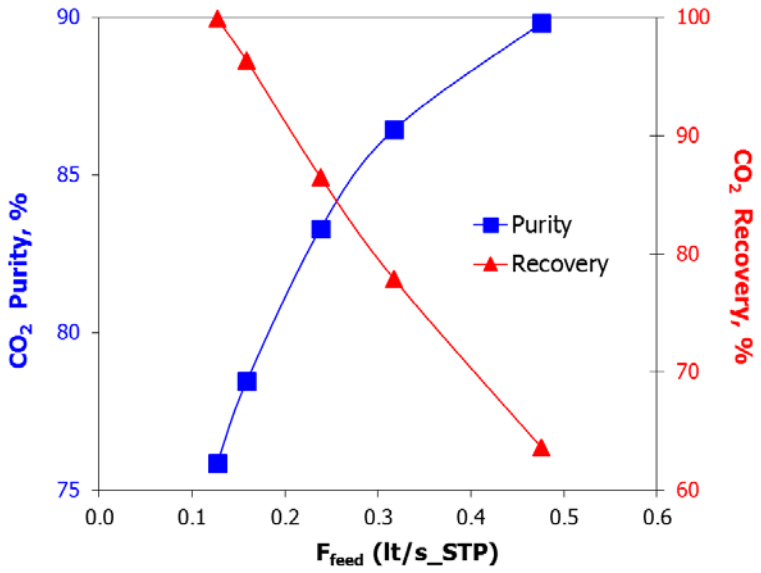

Figure 3.4. Effect of feed flow rate on PSA/VSA process performance indicators.

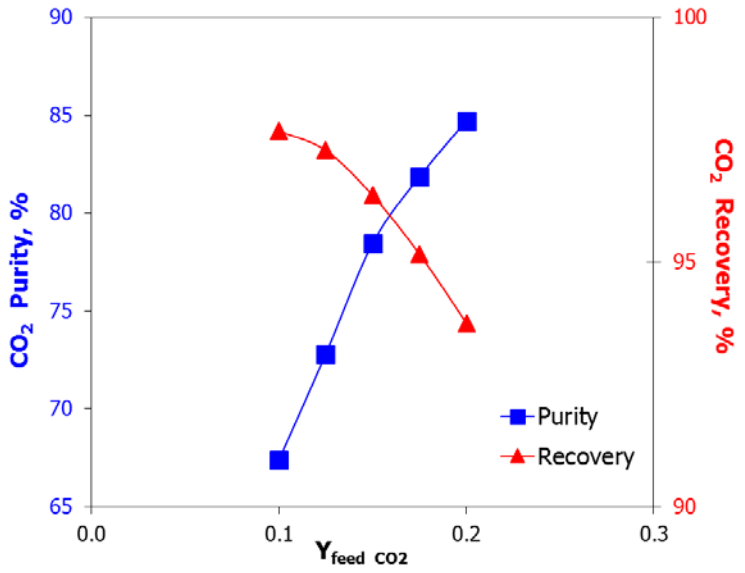

Figure 3.5. Effect of feed composition on PSA/VSA process performance indicators.

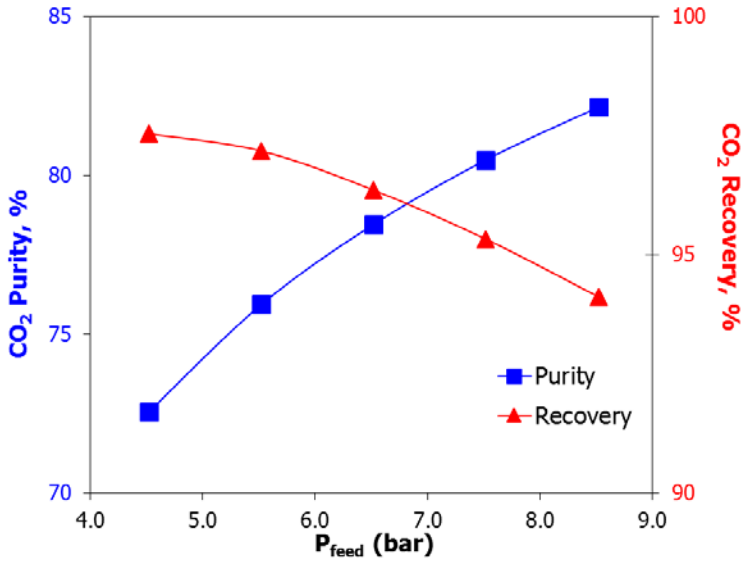

Figure 3.6. Effect of feed pressure on PSA/VSA process performance indicators.

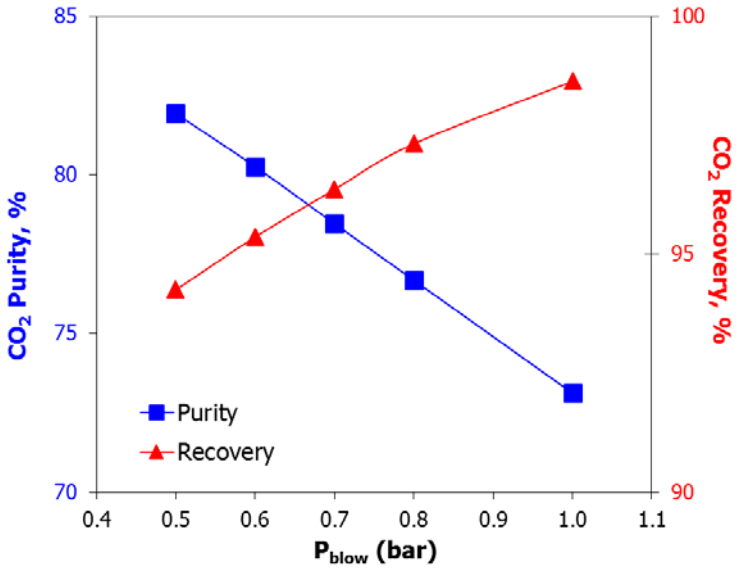

Figure 3.7. Effect of blowdown pressure on PSA/VSA process performance indicators.

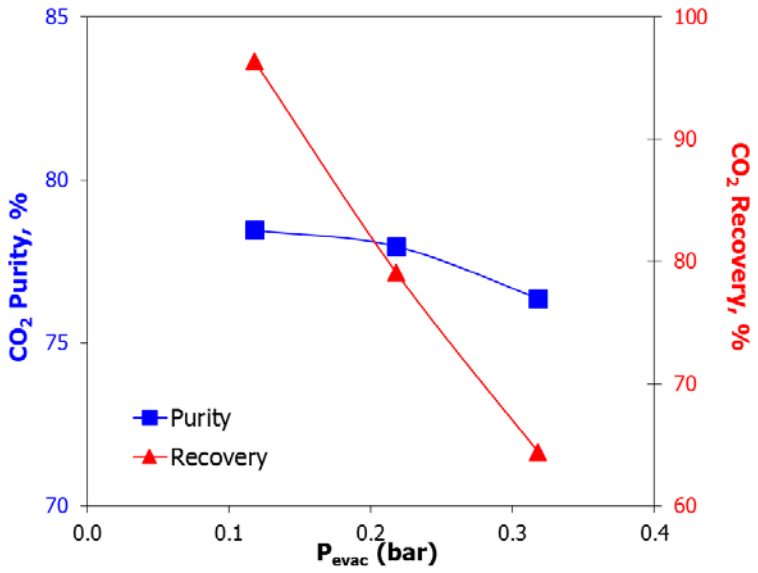

Figure 3.8. Effect of evacuation pressure on PSA/VSA process performance indicators.

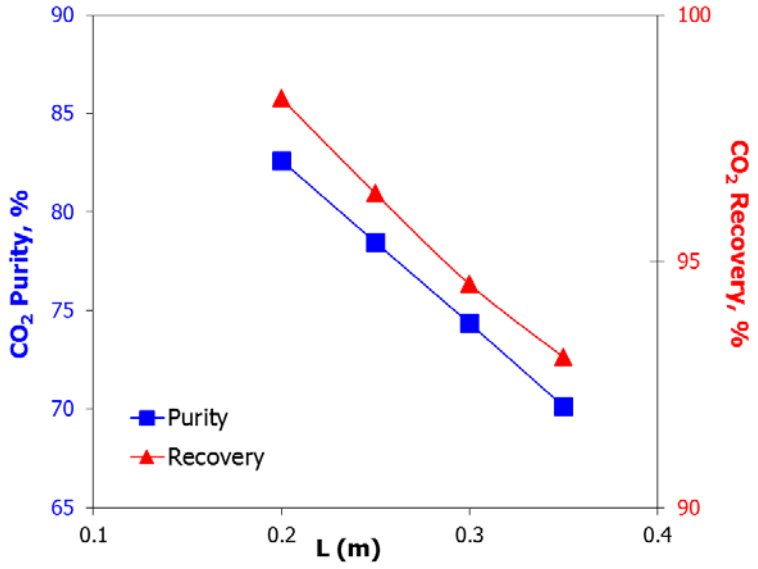

Figure 3.9. Effect of adsorbent bed length on PSA/VSA process performance indicators.

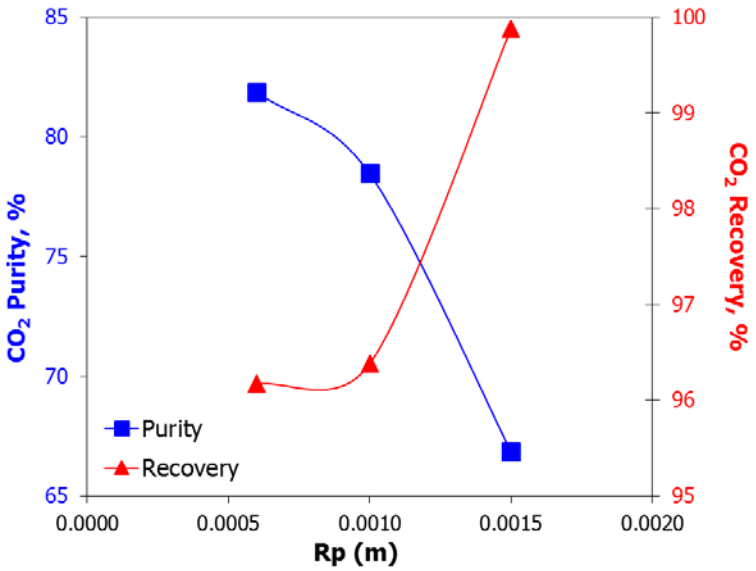

Figure 3.10. Effect of particle radius on PSA/VSA process performance indicators.

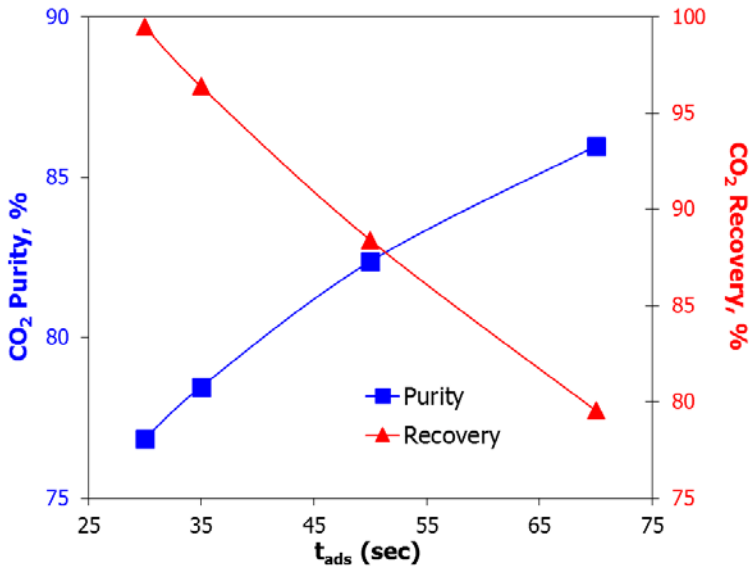

Figure 3.11. Effect of adsorption step duration on PSA/VSA process performance indicators.

3.3. Multi-bed PSA/VSA studies

3.3.1. Formulation of the optimisation problem

The objective of this study is to apply the optimisation framework on a PSA/VSA process concerning the CO_2 capture from dry flue gas in order to investigate the effect of multi-bed PSA/VSA configurations, number of pressure equalization steps, and additional operating steps that may significantly improve the overall process performance. The most commonly used process performance indicator CO_2 purity for specified minimum requirements in CO_2 recovery will be employed. In addition, in order to get a fair comparison between various multi-bed PSA/VSA configurations, it is necessary to define a set of conditions that have to be met.

Based on the parametric studies and the sensitivity analysis, the most significant process variables in this study are the feed pressure, the adsorbent bed geometry (length/diameter ratio), the particle radius and the feed flow rate, while the cycle time and operating step times will be fixed in all cycle configurations. Hence, the optimisation problem can be formulated as the maximization of CO_2 purity for a minimum requirement in CO_2 recovery, while optimising the number of adsorbent beds and cycle configuration, the feed pressure, the particle radius, the bed length to diameter ratio (for constant bed volume) and the feed flow rate. All studies have been carried out keeping the bed volume, the cycle time, the duration of operating steps and the gas valve parameters constant. In this way, it is possible to analyze the separation quality for a specified minimum requirement in CO_2 recovery and different process designs.

$$\text{max. } CO_2 \text{ purity} \tag{3.1}$$

$$\text{s. t. model equations}$$

$$CO_2 \text{ recovery} \geq 99.5\%$$

$$N_{beds} = [1,2,4,6]$$

$$\text{configuration} = [\text{C1}, \text{C2}, \text{C4}, \text{C6}]$$

$$1\ bar \leq P_{feed} \leq 8\ bar$$

$$0.5\ mm \leq R_p \leq 1.5\ mm$$

$$5 \leq \frac{L}{D} \leq 15$$

$$0.04\ lt/s\_stp\ \leq F_{feed} \leq 0.20\ lt/s\_stp$$

The above dynamic optimisation problem has been formulated and solved in the gPROMS™ modelling environment (PSE, 2011).

3.3.2. Optimisation results

The developed optimisation framework has been applied in the same PSA/VSA process described in section 3.1 concerning the separation of CO_2 from dry flue gas (15% CO_2, 85% N_2) using zeolite 13X as adsorbent. Four different PSA/VSA cycle configurations have been employed. The following sequence of steps served as a basis for all of them: pressurization with the feed stream co-currently (CoC), adsorption (Ads), pressure equalization (PED) (co-current depressurization to the other bed), co-current depressurization or blowdown (CoD), counter-current depressurization or evacuation (Evac), and pressure equalization (PER) (counter-current re-pressurization from the other bed). The cycle configurations differ only in the number of pressure equalization steps introduced. Cycle configurations of one, two, four and six beds have been simulated. Thus, one-bed cycle configuration (C1) contains no pressure equalization steps, two-bed cycle configuration (C2) involves one pressure equalization step, four-bed cycle configuration (C4) involves two pressure equalization steps and six-bed cycle configuration (C6) involves three pressure equalization steps. An overview of operating steps employed in these cycle configurations are presented in Table 3.4, Table 3.5, Table 3.6 and Table 3.7, respectively. The effect of number of adsorbent beds for constant cycle time on the separation quality has been analyzed. The following operating conditions have been selected: constant cycle time, and constant amount of feed processed per cycle. The input parameters for this optimisation study are given in Table 3.8.

The optimisation results are summarized in Table 3.9. A comparison of the optimisation results and the base case design (P_{feed} = 6.52 bar, R_p = 1 mm, L/D ratio = 11.4, F_{feed} = 0.07 lt/s_stp for cycle configuration C1, F_{feed} = 0.09 lt/s_stp for cycle configuration C2, F_{feed} = 0.12 lt/s_stp for cycle configuration C4, F_{feed} = 0.14 lt/s_stp for cycle configuration C6) is illustrated in Figures 3.12 to 3.16. It is clear from Figure 3.16, that with the proposed optimisation approach about 7% improvement of CO_2 purity has been achieved in all cycle configurations.

Table 3.4. One-bed four-step PSA/VSA cycle configuration C1.

	1	2a	2b	3	4b	4a
B-1	CoC	Ads	Ads	CoD	Evac	Evac

Table 3.5. Two-bed six-step PSA/VSA cycle configuration C2.

	1	2	3a	3b	4	5	6a	6b
B-1	PER1	CoC	Ads	Ads	PED1	CoD	Evac	Evac
B-2	PED1	CoD	Evac	Evac	PER1	CoC	Ads	Ads

Table 3.6. Four-bed eight-step PSA/VSA cycle configuration C4.

	1	2	3	4a	4b	5	6	7	8a	8b
B-1	PER2	PER1	CoC	Ads	Ads	PED1	PED2	CoD	Evac	Evac
B-2	Evac	Evac	PER2	PER1	CoC	Ads	Ads	PED1	PED2	CoD
B-3	PED2	CoD	Evac	Evac	PER2	PER1	CoC	Ads	Ads	PED1
B-4	Ads	PED1	PED2	CoD	Evac	Evac	PER2	PER1	CoC	Ads

Table 3.7. Six-bed ten-step PSA/VSA cycle configuration C6.

	1	2	3	4	5a	5b	6	7	8	9	10a	10b
B-1	PER3	PER2	PER1	CoC	Ads	Ads	PED1	PED2	PED3	CoD	Evac	Evac
B-2	Evac	Evac	PER3	PER2	PER1	CoC	Ads	Ads	PED1	PED2	PED3	CoD
B-3	PED3	CoD	Evac	Evac	PER3	PER2	PER1	CoC	Ads	Ads	PED1	PED2
B-4	PED1	PED2	PED3	CoD	Evac	Evac	PER3	PER2	PER1	CoC	Ads	Ads
B-5	Ads	Ads	PED1	PED2	PED3	CoD	Evac	Evac	PER3	PER2	PER1	CoC
B-6	PER1	CoC	Ads	Ads	PED1	PED2	PED3	CoD	Evac	Evac	PER3	PER2

Table 3.8. Input parameters for the optimisation study.

	C1	C2	C4	C6
PER3	-	-	-	20 s
PER2	-	-	24 s	20 s
PER1	-	30 s	24 s	20 s
CoC	40 s	30 s	24 s	20 s
Ads	80 s	60 s	48 s	40 s
PED1	-	30 s	24 s	20 s
PED2	-	-	24 s	20 s
PED3	-	-	-	20 s
CoD	40 s	30 s	24 s	20 s
Evac	80 s	60 s	48 s	40 s
	240 s	240 s	240 s	240 s

Table 3.9. Optimisation results.

Configuration	P_{feed}, (bar)	R_p, (mm)	L/D	F_{feed}, (lt/s_stp)	CO_2 Purity, %	CO_2 Recovery, %
C1	8.00	0.70	5.00	0.10	92.95	99.82
C2	8.00	1.00	5.22	0.14	92.37	99.85
C4	8.00	0.86	6.95	0.17	91.61	99.95
C6	8.00	0.74	7.82	0.20	91.25	99.94

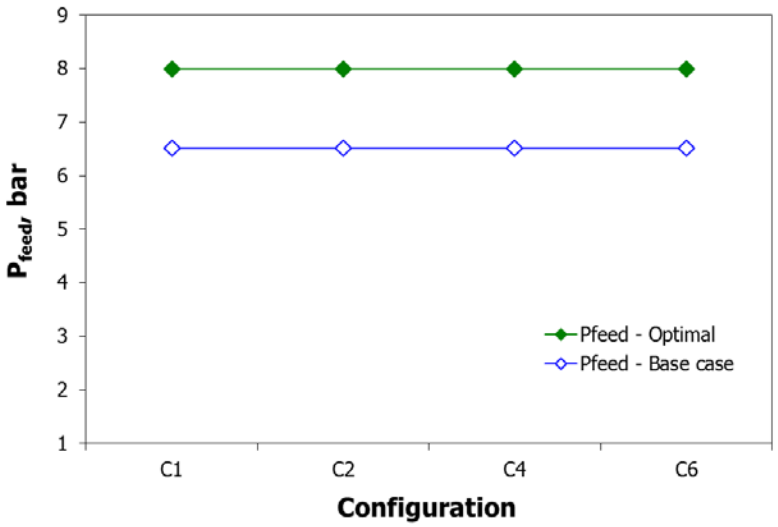

Figure 3.12. Optimal feed pressure.

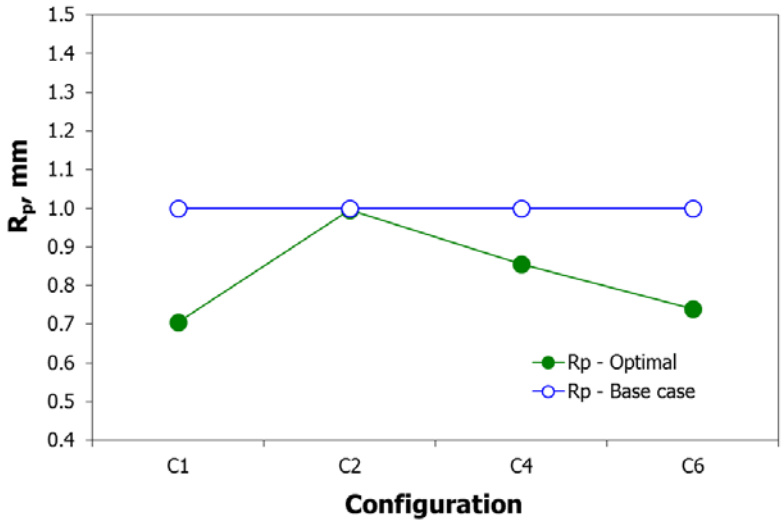

Figure 3.13. Optimal particle radius.

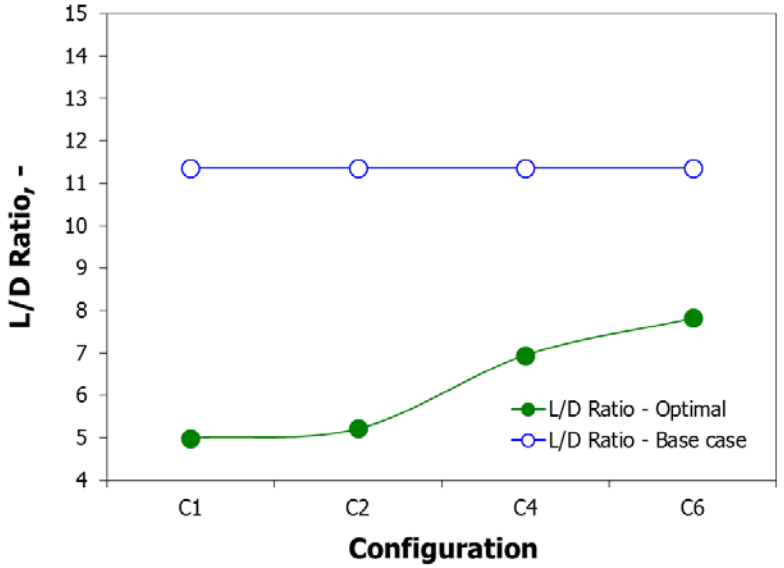

Figure 3.14. Optimal bed length to diameter ratio.

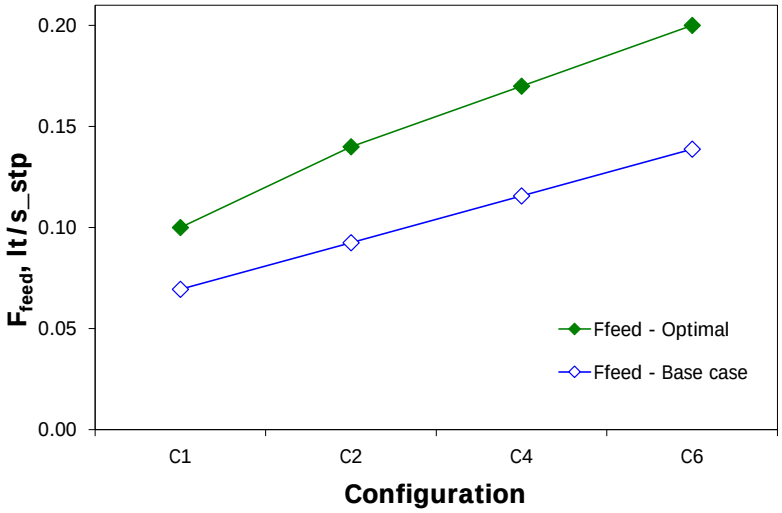

Figure 3.15. Optimal feed flow rate.

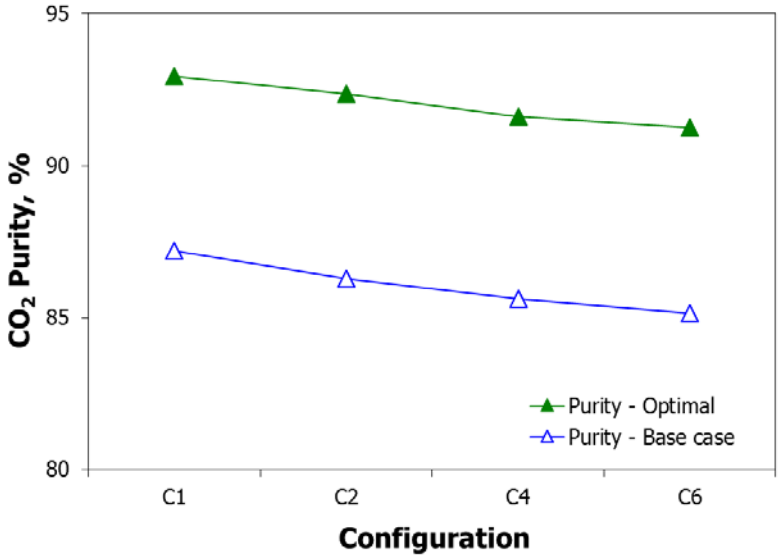

Figure 3.16. Optimal CO_2 purity.

3.4. Comparative evaluation of available adsorbents

3.4.1. Introduction

With the development of novel adsorbent materials, adsorption technology has become a potential tool for CO_2 capture from flue gases. There is a great variety of potential adsorbents currently considered for post-combustion CO_2 capture: zeolites, activated carbons, metal organic frameworks (MOFs), metal oxides, hydrotalcites, organic-inorganic hybrids, ZIFs, COFs, silica and alumina based materials. Recent studies suggest that adsorption processes using zeolites and MOFs with large internal surfaces are promising alternatives for CO_2 capture (Hasan *et al.,* 2012; Zhang *et al.,* 2008). The adsorption mechanism for these types of adsorbents is physisorption, where there is an interaction between the quadrupole moment of the gas and the polar adsorbent. CO_2 has a strong quadrupole moment ($13.4x10^{-40}$ Cm^2) while N_2 has a smaller but still significant quadrupole moment ($4.7x10^{-40}$ Cm^2) and therefore any adsorbent which adsorbs CO_2 will also adsorb appreciable amounts of N_2 (D'Alessandro *et al.,* 2010).

Most zeolites have a very strong adsorption affinity for CO_2 and therefore have nonlinear adsorption isotherms, relatively high CO_2 adsorption capacities and high CO_2/N_2 selectivity at low partial pressures. Commercial zeolite adsorbents are always bound together with clay or alumina to form a pellet or bead, which is a composite structure that contains both macropores and micropores. Hence, the overall mass transfer in zeolites is controlled by a combination of different diffusion mechanisms. Nevertheless, for the case of zeolite 13X, which is typically considered as a potential adsorbent for CO_2 capture, gas diffusion appears to be macropore controlled (Hu *et al.,* 2014). An effective screening method for selecting the most cost-effective zeolites for CO_2 capture using a computational framework that effectively combines material selection and process optimisation has been recently reported (Hasan *et al.,* 2013). In the last decade, MOFs have emerged as a new class of porous materials for CO_2 capture because of their unique features, such as large specific surface area and the corresponding high CO_2 adsorption capacity as well as regular pore size distributions. MOFs are assembled from metal clusters (e.g. square

shaped, trigonal, tetrahedral and octahedral) and organic linkers (e.g. carboxylates, imidazolates and tetrazolates). According to various combinations of metal clusters and organic linkers, an unlimited number of MOFs with different structures and functionalities can be synthesized (Nalaparaju *et al.,* 2015). The transport of CO_2 and N_2 in the MOFs particles can be safely considered as macropore controlled (Nalaparaju *et al.,* 2015).

Water reaches saturation levels on hydrophilic adsorbents, such as zeolites and MOFs, preventing them from adsorbing CO_2 and therefore a pre-layer is required to protect these adsorbents from the humidity. This reduces the percentage of the adsorbent bed containing the CO_2 adsorbent and additional vacuum work is required to regenerate the pre-layer. On the other hand, hydrophobic adsorbents, such as activated carbons, adsorb much smaller amounts of water and therefore humid flue gas can be processed using these adsorbents without any additional operating cost. Activated carbon beads are spherical and no binder material is used in their production. The spherical nature and hardness of activated carbon bead minimizes dust formation and attrition losses during adsorption and regeneration processes. Activated carbon beads also exhibit excellent fluidization properties both in gas and liquid applications. These characteristics make activated carbon bead the material of choice for higher performance in carbonaceous materials application (Shen *et al.,* 2011). However, activated carbons have typically lower CO_2 adsorption capacity and poorer CO_2/N_2 selectivity than zeolites and MOFs.

3.4.2. Process description

In the present study, a two-bed six-step VSA cycle configuration with light product pressurization and one pressure equalization step is considered. The use of one pressure equalization step improves primarily CO_2 recovery and CO_2 productivity from 1.2 up to 19% for the case of zeolite 13X as the feed flow rate increases from 0.056 to 0.185 lt/s_stp. A similar trend is observed in energy savings ranging from 2.8 up to 15%, respectively. Similar results are observed for the case of Mg-MOF-74, where the improvement is slightly smaller than that for the case of zeolite 13X. The sequence of the operating steps for the two-bed six-step cycle configuration is illustrated in Figure 3.17 and consist of: pressurization with the light product counter-currently (CC), adsorption (Ads), pressure equalization (PED) (co-current depressurization to the other bed), co-current depressurization or blowdown (CoD) to intermediate pressure, counter-current depressurization or evacuation (Evac) to low pressure and pressure equalization (PER) (counter-current re-pressurization from the other bed). The interaction between the beds during each operating step for the two-bed cycle configuration is illustrated in Figure 3.18.

In the current study it is assumed dry flue gas; however, actual flue gas emitted from power plants contains a considerable amount of humidity. More specifically, the dry flue gas mixture (85% N_2, 15% CO_2) is considered to be available at 1.10 bar pressure and at different temperatures 298 K, 313 K and 323 K while the blowdown pressure is set at 0.20 bar and the evacuation pressure is set at 0.02bar. At the beginning of the process, the adsorbent bed is saturated with pure N_2 at 1.10bar. The cycle time of the process is fixed at 240s and the operating time steps are fixed as follows: t_{CC}=20s, t_{Ads}=80s, t_{PED}=20s, t_{CoD}=20s, t_{Evac}=80s, t_{PER}=20s. It is important to note that the operating time steps are not independent variables, and in a typical multi-bed configuration, only the duration of one or two operating steps can be independently varied. When two-bed or multi-bed configurations are used the operating time steps must be correlated due to the need for synchronization of the adsorbent beds, although it was recently demonstrated that this constraint can be relaxed using idle/holding times for each adsorbent bed (Krishnamurthy *et al.,* 2014).

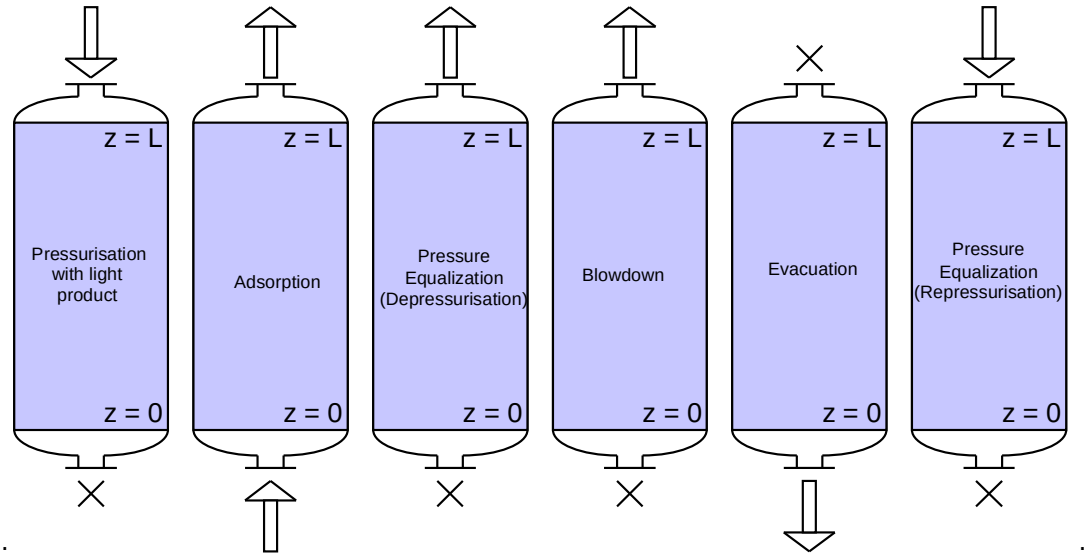

Figure 3.17. Sequence of operating steps for the two-bed six-step VSA cycle configuration.

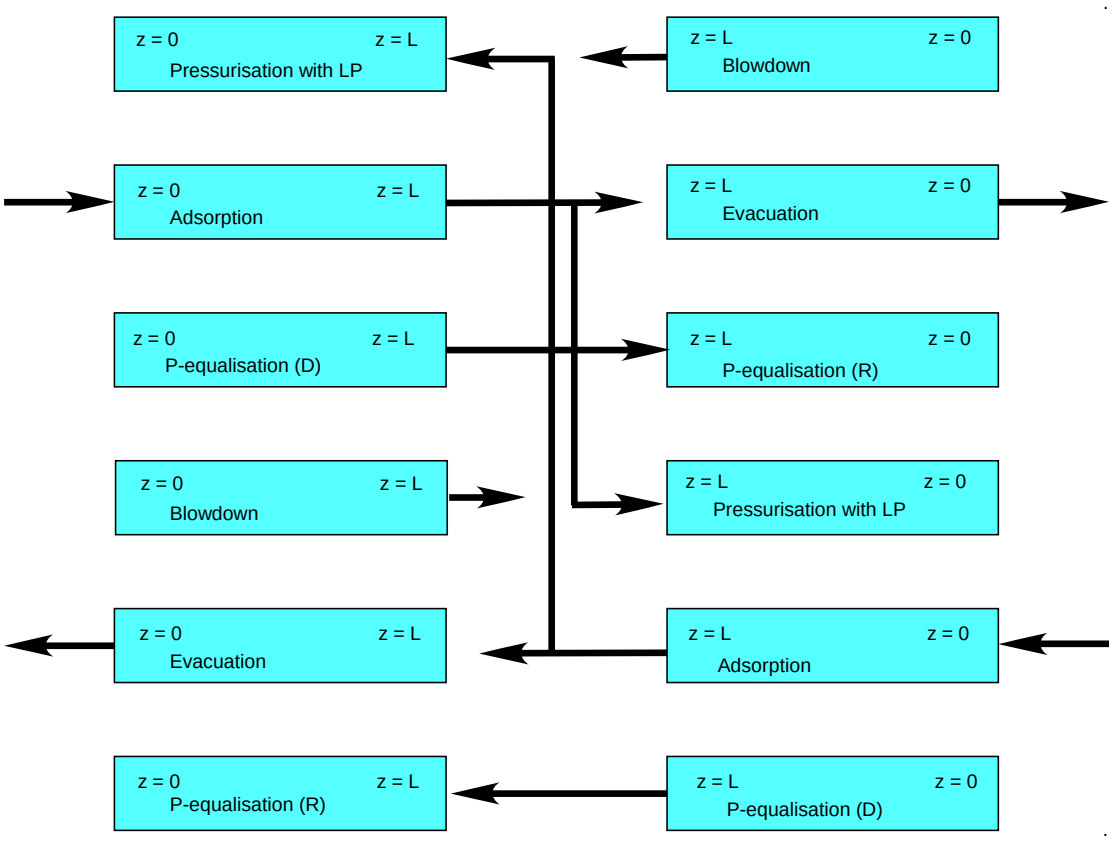

Figure 3.18. Interaction between the beds during each operating step for the two-bed cycle configuration.

3.4.3. Formulation of the optimisation problem

Optimisation is normally performed to improve the performance of a PSA/VSA process by locating the optimal values of several important process variables that control the process. Based on parametric studies and sensitivity analysis, the most significant process variables in this optimisation study are, feed pressure, feed flow rate, blowdown and evacuation pressure, while feed temperature, cycle time, operating step durations and adsorbent bed geometry are fixed in all cases under consideration. Optimisation studies have been performed at different feed temperatures. The main objective is to investigate the effect of feed temperature, feed pressure, feed flow rate, blowdown pressure and evacuation pressure on the overall process performance. The minimization of energy consumption for specified minimum requirements in CO_2 purity and CO_2 recovery is employed as the objective function.

Hence, the optimisation problem can be formulated as the minimization of energy consumption for specified minimum requirements in CO_2 purity and CO_2 recovery, while optimising the feed pressure, feed flow rate, blowdown pressure and evacuation pressure. Cycle time, duration of operating steps, adsorbent bed geometry and gas valve constants are kept constant in all cases under consideration at different feed temperatures:

$$\text{min. energy consumption} \tag{3.2}$$

$$\text{s.t. model equations}$$

$$CO_2 \text{ purity} \geq 90\%$$

$$CO_2 \text{ recovery} \geq 90\%$$

$$T_{feed} = [T_1, T_2, T_3, T_4]$$

$$1.1\ bar \leq P_{feed} \leq 1.5\ bar$$

$$0.048\ lt/s\_stp \leq F_{feed} \leq 0.480\ lt/s\_stp$$

$$0.11\ bar \leq P_{blow} \leq 0.70\ bar$$

$$0.01\ bar \leq P_{evac} \leq 0.10\ bar$$

The above dynamic optimisation problem has been formulated and solved in the gPROMS™ modelling environment (PSE, 2011).

3.4.4. Comparison and evaluation of available adsorbents

As a next step, the effect of the type of adsorbent on the PSA/VSA process performance for CO_2 removal from dry flue gas has been studied. Three different types of adsorbents have been selected: traditional ones, such as zeolite and activated carbon, and a novel adsorbent from the family of MOFs. The proposed modelling framework has been applied to compare these adsorbents for post-combustion CO_2 capture over a range of operating conditions (298 K, 313 K and 323 K) in terms of several process performance indicators.

More specifically, zeolite 13X has been considered as a representative of the zeolite group, which has been studied for more than two decades and is the current benchmark commercial adsorbent for CO_2 capture. The diffusion of CO_2 in commercial zeolite 13X beads is controlled by mass transport in the macropores, both under Knudsen and molecular diffusion regimes (Hu *et al.,* 2014). The parameters of the dual-site Langmuir adsorption isotherm of CO_2 and N_2 on zeolite 13X have been adopted from the work of Ko *et al.,* (2005) and are summarized in Table 3.10.

Activated carbons are promising adsorbents, since they have large specific surface area, they are water tolerant which is beneficial when working with wet flue gas, and can be produced with novel morphologies (monolith, bead, fiber, granular). Additionally, they are less expensive than other adsorbents like zeolites (Shen *et al.,* 2011). However, activated carbons have typically lower CO_2 adsorption capacity and poorer CO_2/N_2 selectivity than zeolites and MOFs. The parameters of the dual-site Langmuir adsorption isotherm of CO_2 and N_2 on activated carbon (AC) have been

adopted from the work of Maring and Webley (2013) and are summarized in Table 3.10.

Mg-MOF-74 [Mg_2(dobdc), (dobdc=1,4-dioxido-2,5-benzenedicarboxylate), ($Mg(C_4HO_3)(H_2O).4H_2O$), CPO-27-Mg] has received significant attention recently, since it has both high CO_2 adsorption capacity and high CO_2 adsorption affinity and is considered as a potential adsorbent in the present study. The parameters of the dual-site Langmuir adsorption isotherm of CO_2 and N_2 on Mg-MOF-74 have been adopted from the work of Mason *et al.,* (2011) and are summarized in Table 3.10.

The adsorption isotherms of CO_2 and N_2 on three potential adsorbents (zeolite 13X, AC, Mg-MOF-74) at T=313 K are illustrated in Figure 3.19. There are clearly both advantages and disadvantages with each of these potential adsorbents. The adsorption isotherm of CO_2 on zeolite 13X is steeper than the adsorption isotherm of CO_2 on activated carbon while the adsorption isotherm of CO_2 on Mg-MOF-74 is steeper than the adsorption isotherm of CO_2 on zeolite 13X. The simple visual inspection of the adsorption isotherms of the potential adsorbents shown in Figure 3.19 may suggest that Mg-MOF-74 is superior because of its high apparent CO_2 capacity. However, the N_2 capacity is similarly elevated and it is unclear initially which potential adsorbent would be the best for post-combustion CO_2 capture. The mixture selectivities of CO_2/N_2 at different temperatures and total pressure of 1 bar for the three potential adsorbents (zeolite 13X, AC, Mg-MOF-74), are presented in Figures 3.20, 3.21, 3.22, respectively. It is important to note that when the temperature is increased the selectivity of CO_2/N_2 decreases and the decrease is more pronounced for adsorbent Mg-MOF-74, at low mole fractions.

Other physical properties (density and heat capacity) of the adsorbents required for the process modelling and simulation have been adopted from the works of Ko *et al.,* (2005), Chue *et al.,* (1995), Wu *et al.,* (2009) and are summarized in Table 3.11. The parameters of the adsorbent bed model, have been adopted from the work of Ko *et al.,* (2005) and are summarized in Table 3.12. The adsorbent bed porosity is assumed to be 0.348 (porosity of randomly packed spherical beads), while the particle/bead porosity is assumed to be 0.38 for all adsorbents in the present study.

Table 3.10. Parameters of the dual-site Langmuir adsorption isotherm of different adsorbents.

	zeolite 13X (Ko *et al.*, 2005)		**AC** (Maring and Webley, 2013)		**Mg-MOF-74** (Mason *et al.*, 2011)		
	CO_2 (i = 1)	**N_2 (i = 2)**	**CO_2 (i = 1)**	**N_2 (i = 2)**	**CO_2 (i = 1)**	**N_2 (i = 2)**	**units**
$k_{1,i(1)}$	2.82	1.89	0.59	0.16	6.80	14.00	mol/Kg
$k_{2,i(1)}$	-3.50E-04	-2.25E-04	0	0	0	0	1/K
$k_{3,i(1)}$	2.83E-09	1.16E-09	4.05E-10	8.34E-08	2.44E-11	4.96E-10	1/Pa
$k_{4,i(1)}$	2598.20	1944.61	3776.76	1719.99	5051.72	2165.02	K
$k_{1,i(2)}$	3.97	1.89	7.51	41.30	9.90	0	mol/Kg
$k_{2,i(2)}$	-4.95E-03	-2.25E-04	0	0	0	0	1/K
$k_{3,i(2)}$	4.41E-09	1.16E-09	1.68E-09	7.98E-17	1.39E-10	0	1/Pa
$k_{4,i(2)}$	3594.07	1944.61	2381.53	6013.95	2886.70	0	K

Table 3.11. Physical properties of different adsorbents.

physical property	**zeolite 13X** (Ko *et al.*, 2005)	**AC** (Chue *et al.*, 1995)	**Mg-MOF-74** (Wu *et al.*, 2009)	**units**
particle density (ρ_p)	1159.4	800	909	kg/m3
heat capacity of particles (C_p^p)	504	1050	800	J/(kg·K)

Table 3.12. Parameters of adsorbent bed model.

parameter	**value**
adsorbent bed radius (R_{bed})	1.1×10^{-2} m
adsorbent bed length (L_{bed})	25×10^{-2} m
pore radius (R_{pore})	0.5×10^{-9} m
particle radius (R_p)	1.0×10^{-3} m
particle tortuosity (τ_p)	4.5
particle porosity (ε_p)	0.38
adsorbent bed void (ε_{bed})	0.348
universal gas constant (R)	8.314 J/(mol·K)
heat transfer coefficient of the wall ($k_{h,wall}$)	60 J/(m^2·K·s)
effective diffusivity of CO_2 ($D_{e,CO2}$)	1.087×10^{-8} m^2/s
effective diffusivity of N_2 ($D_{e,N2}$)	1.363×10^{-8} m^2/s

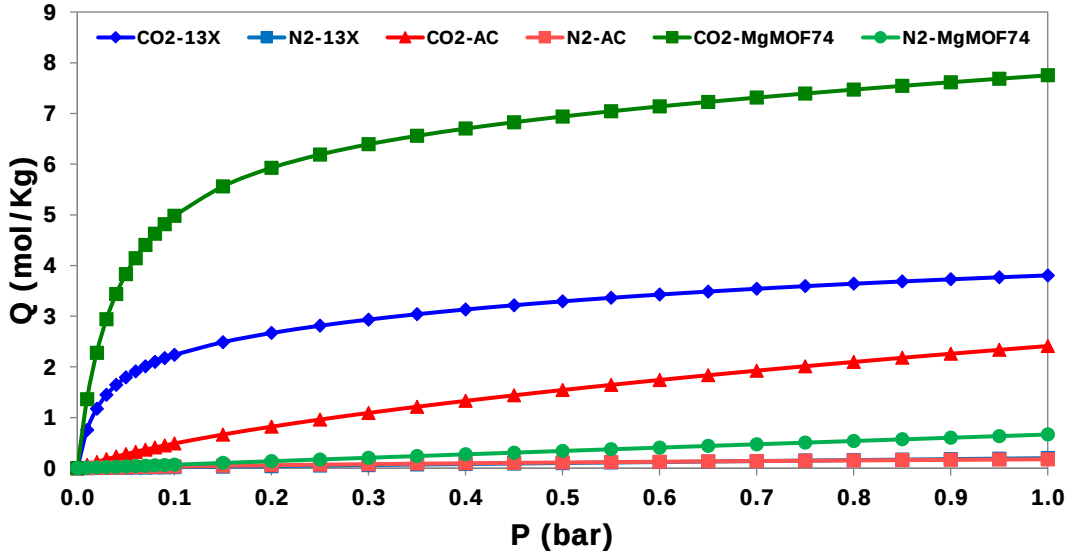

Figure 3.19. Adsorption isotherms of CO_2 and N_2 on potential adsorbents (zeolite 13X, AC, Mg-MOF-74) at T=313 K.

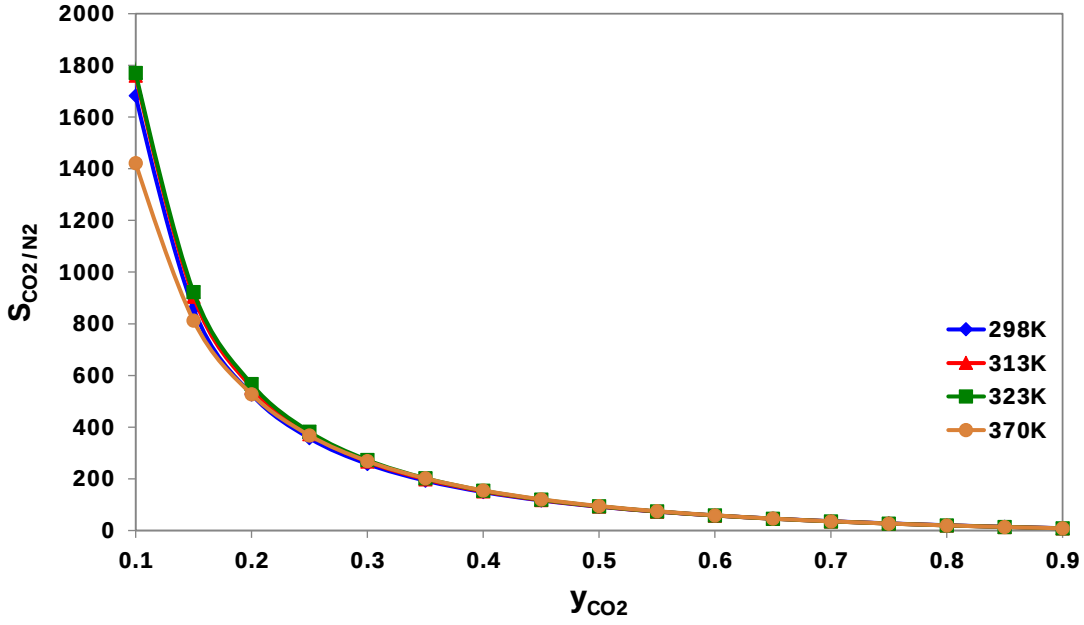

Figure 3.20. Mixture selectivity of CO_2/N_2 at different temperatures and total pressure of 1 bar for zeolite 13X.

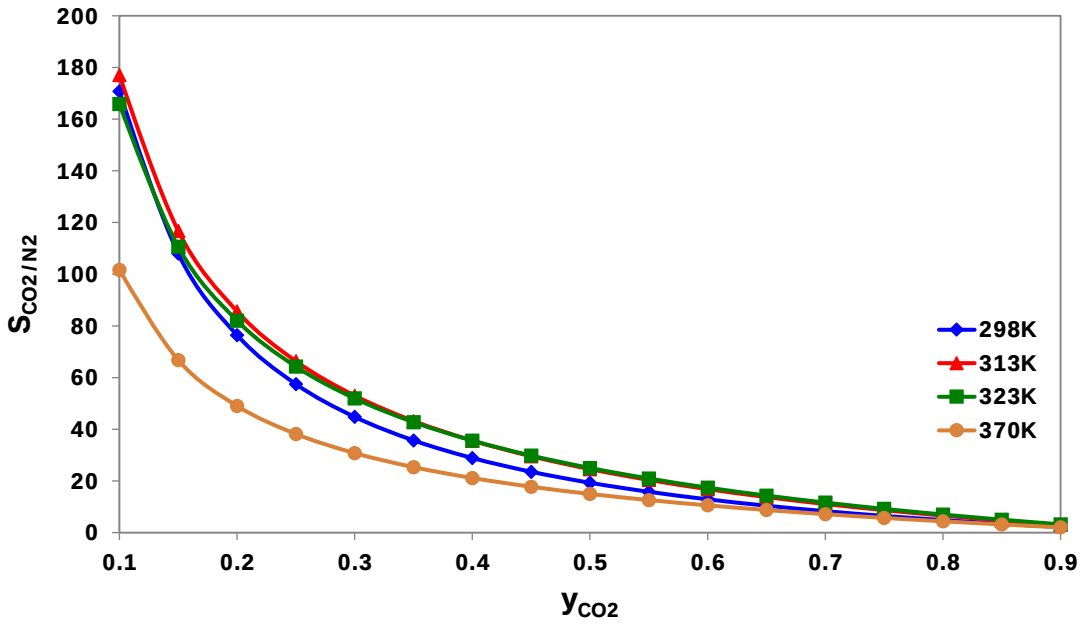

Figure 3.21. Mixture selectivity of CO_2/N_2 at different temperatures and total pressure of 1 bar for AC.

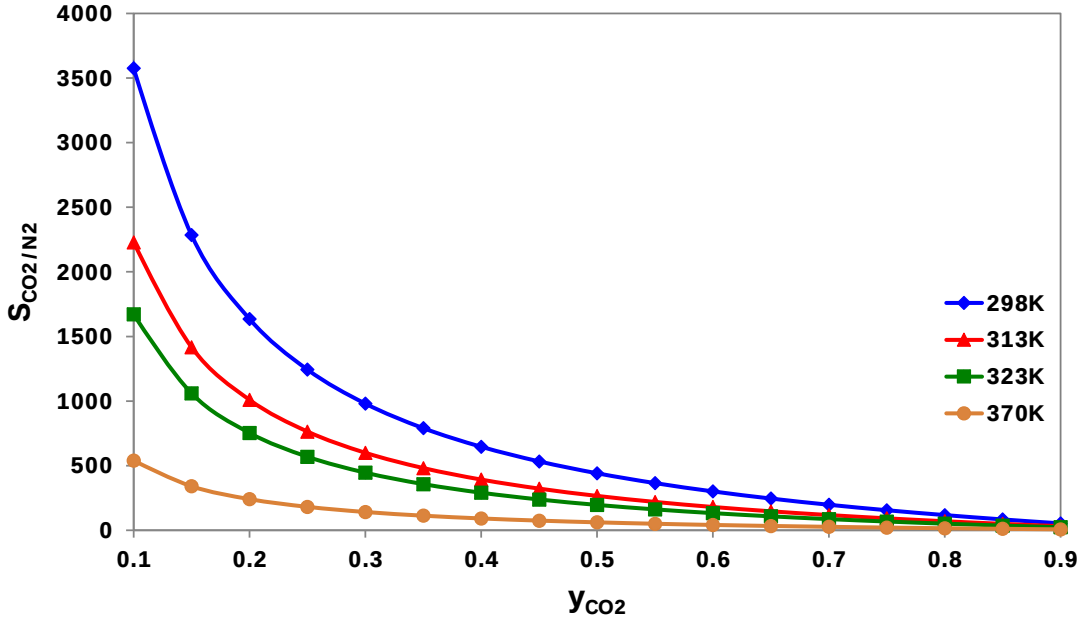

Figure 3.22. Mixture selectivity of CO_2/N_2 at different temperatures and total pressure of 1 bar for Mg-MOF-74.

The proposed modelling framework has been applied to estimate process performance indicators using each of the three potential adsorbents to objectively compare them over a range of feed flow rates at different feed temperatures. Simulation results in terms of various process performance indicators, for the three potential adsorbents (zeolite 13X, AC, Mg-MOF-74) are summarized in Table 3.13 at T_{feed}=298K, Table 3.14 at T_{feed}=313K, and Table 3.15 at T_{feed}=323K. There are also illustrated in Figures 3.23, 3.24 at T_{feed}=298K, Figures 3.25, 3.26 at T_{feed}=313K and Figures 3.27, 3.28 at T_{feed}=323K. The results clearly indicate that zeolite 13X yields the highest CO_2 purity, followed by Mg-MOF-74 and activated carbon over the full range of feed flow rates as illustrated in Figures 3.23, 3.25, 3.27. On the other hand, Mg-MOF-74 yields the highest CO_2 recovery followed by zeolite 13X and activated carbon over the full range of feed flow rates as shown in these figures. Mg-MOF-74, while showing higher CO_2 productivity than the other adsorbents as illustrated in Figures 3.24, 3.26, 3.28 has considerably lower energy requirement than activated carbon as shown in these figures and produces a much lower CO_2 purity than zeolite 13X due to significant N_2 adsorption and poor CO_2 desorption. Mg-MOF-74 has the highest CO_2 productivity, but most of the CO_2 is removed at a deeper vacuum level because of strong thermal effects and very nonlinear adsorption isotherm and therefore the energy requirement is at the same level as the zeolite 13X.

The comparison of the three adsorbents shows that zeolite 13X illustrates the best performance among the three adsorbents, in terms of CO_2 purity even though Mg-MOF-74 shows considerably higher CO_2 adsorption capacity (but in the meantime higher N_2 adsorption capacity and poor regeneration). On the other hand Mg-MOF-74 appears to be a promising adsorbent for CO_2 capture as it has considerably higher CO_2 productivity compared to the other two adsorbents.

The assessment of the adsorbent performance based on selectivities and working capacities are incorrect and misleading in many cases. The thermal effects and the relative amounts of CO_2 and N_2 adsorbed over the pressure range of interest must be taken into account. A single benchmark is probably insufficient to screen adsorbents and plots such as those shown in Figures 3.23-3.28 (in which adsordents are compared over a range of operating conditions) are appropriate in order to make adsorbent comparison. Although it is quite common to compare adsorbents based

Table 3.13. Effect of feed flow rate on process performance indicators at T=298 K employing different adsorbents (zeolite 13X, AC, Mg-MOF-74).

$F_{feed,}$ (lt/s_stp)	CO_2 Purity, %	CO_2 Recovery, %	CO_2 Productivity, (mol CO_2/Kg·s)	Energy, (KJ/mol CO_2)
zeolite 13X				
0.05	70.00	93.97	0.0014	74.61
0.06	74.81	93.56	0.0016	73.71
0.07	80.61	91.87	0.0020	73.63
0.09	86.15	88.12	0.0026	75.30
0.14	91.56	79.02	0.0035	81.95
0.19	93.96	68.92	0.0040	92.27
AC				
0.05	65.62	88.73	0.0019	78.55
0.06	69.77	85.94	0.0022	79.68
0.07	74.43	82.03	0.0026	81.91
0.09	78.98	73.24	0.0031	89.48
0.14	81.82	57.41	0.0036	110.57
0.19	82.35	45.76	0.0039	135.85
Mg-MOF-74				
0.05	44.59	96.73	0.0018	81.79
0.06	51.33	96.15	0.0021	78.79
0.07	60.84	95.40	0.0027	76.08
0.09	76.69	90.18	0.0034	75.32
0.14	88.66	78.92	0.0044	82.30
0.19	92.51	68.30	0.0051	93.06

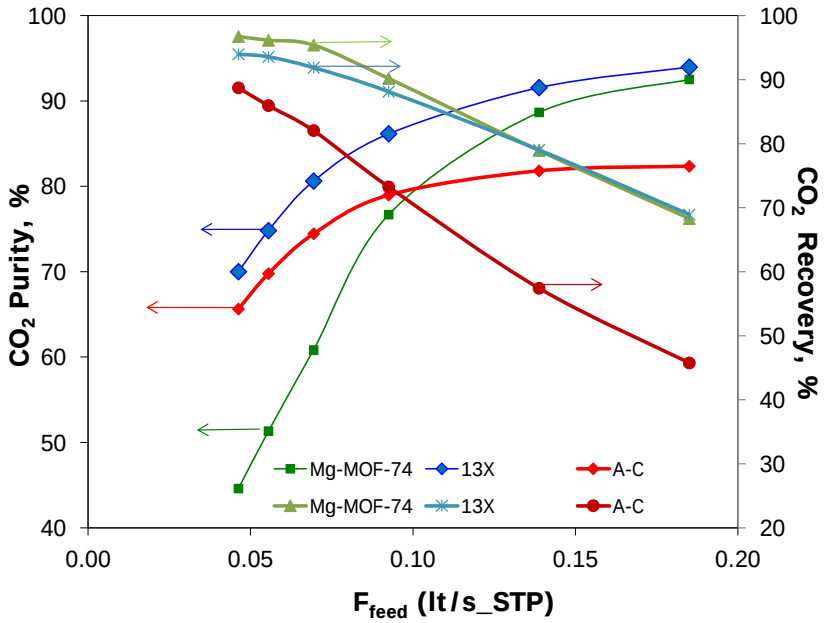

Figure 3.23. Effect of feed flow rate on CO_2 purity and CO_2 recovery at T=298 K.

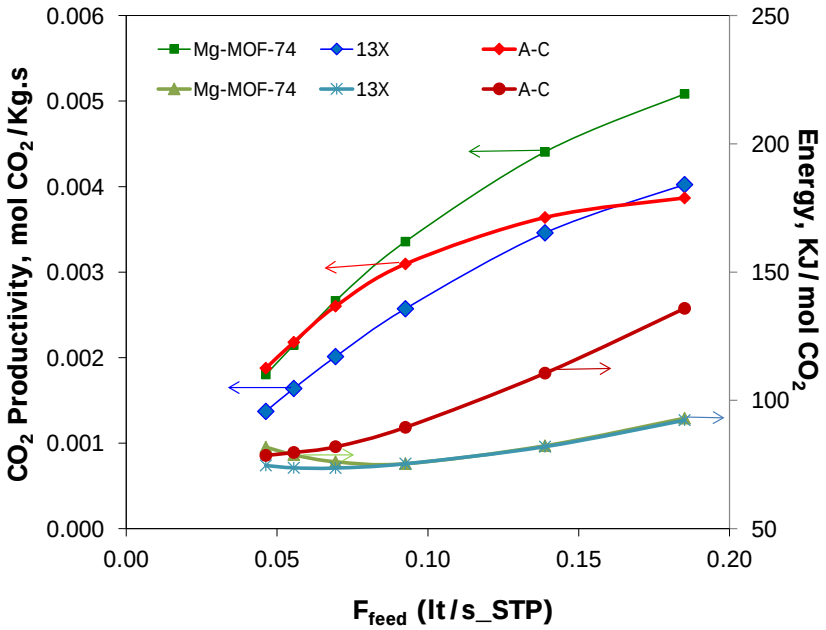

Figure 3.24. Effect of feed flow rate on CO_2 productivity and energy requirement at T=298 K.

Table 3.14. Effect of feed flow rate on process performance indicators at T=313 K employing different adsorbents (zeolite 13X, AC, Mg-MOF-74).

F_{feed}, (lt/s_stp)	CO_2 Purity, %	CO_2 Recovery, %	CO_2 Productivity, (mol CO_2/Kg·s)	Energy, (KJ/mol CO_2)
zeolite 13X				
0.05	75.55	93.04	0.0014	77.59
0.06	79.25	92.65	0.0016	77.04
0.07	83.55	91.10	0.0020	77.29
0.09	88.12	87.72	0.0026	79.04
0.14	92.82	79.40	0.0035	85.50
0.19	94.99	69.90	0.0041	95.51
AC				
0.05	77.13	83.94	0.0018	83.78
0.06	80.40	81.53	0.0021	85.66
0.07	83.94	77.48	0.0025	88.60
0.09	86.98	68.89	0.0029	97.85
0.14	88.47	52.17	0.0033	125.63
0.19	89.25	40.76	0.0034	157.71
Mg-MOF-74				
0.05	53.63	96.06	0.0018	82.19
0.06	59.34	95.45	0.0021	80.32
0.07	66.58	94.35	0.0026	78.74
0.09	77.03	90.19	0.0034	79.13
0.14	86.68	80.01	0.0045	85.78
0.19	90.74	69.73	0.0052	96.24

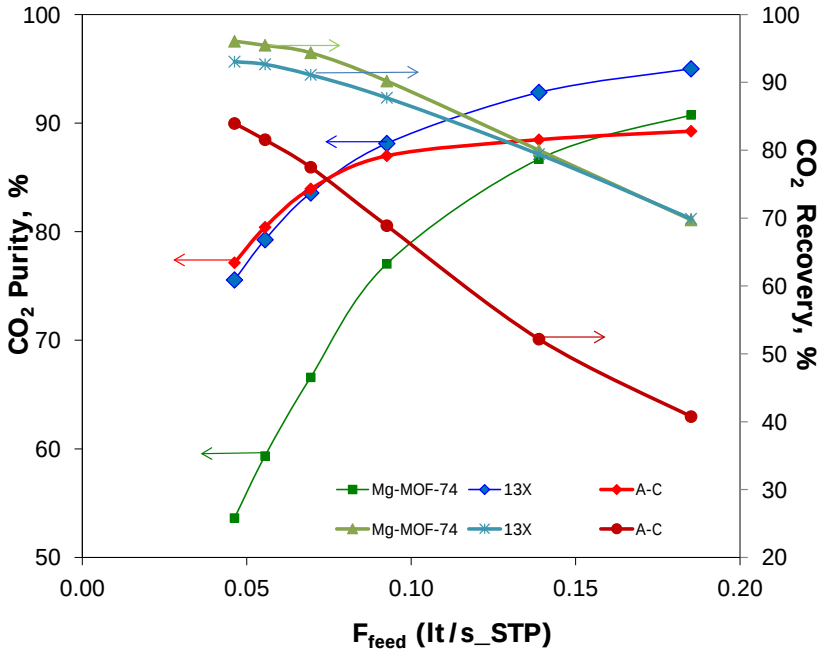

Figure 3.25. Effect of feed flow rate on CO_2 purity and CO_2 recovery at T=313 K.

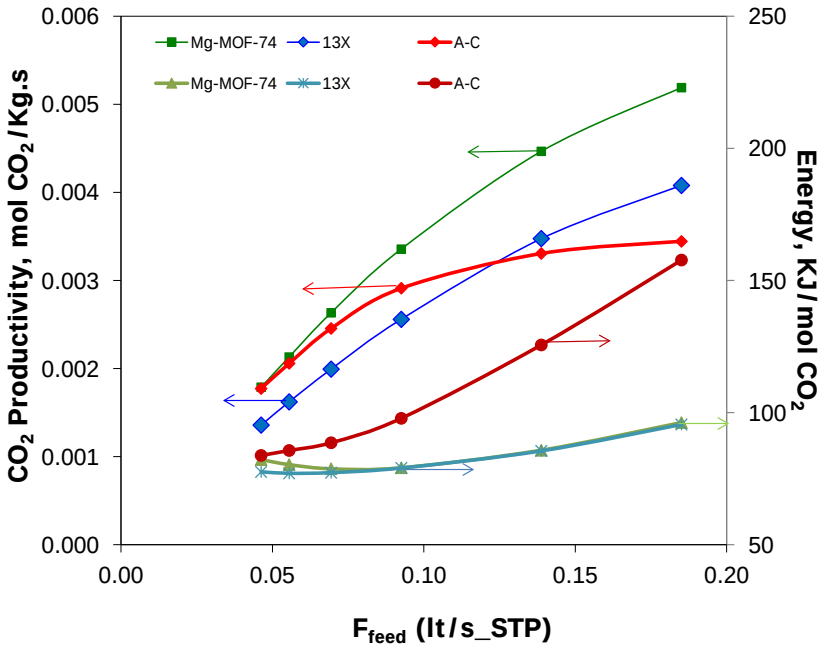

Figure 3.26. Effect of feed flow rate on CO_2 productivity and energy requirement at T=313 K.

Table 3.15. Effect of feed flow rate on process performance indicators at T=323 K employing different adsorbents (zeolite 13X, AC, Mg-MOF-74).

$F_{feed,}$ (lt/s_stp)	CO_2 Purity, %	CO_2 Recovery, %	CO_2 Productivity, (mol CO_2/Kg·s)	Energy, (KJ/mol CO_2)
zeolite 13X				
0.05	78.11	92.39	0.0013	79.91
0.06	81.39	92.01	0.0016	79.48
0.07	85.16	90.55	0.0020	79.85
0.09	89.23	87.39	0.0026	81.62
0.14	93.49	79.52	0.0035	88.00
0.19	95.51	70.39	0.0041	97.86
AC				
0.05	81.00	81.46	0.0017	87.97
0.06	83.88	78.56	0.0020	90.32
0.07	86.83	74.47	0.0024	94.22
0.09	89.00	65.02	0.0027	106.05
0.14	90.00	47.79	0.0030	140.33
0.19	90.29	37.09	0.0031	177.69
Mg-MOF-74				
0.05	58.73	95.23	0.0018	83.43
0.06	63.81	94.70	0.0021	81.97
0.07	70.10	93.63	0.0026	80.86
0.09	78.06	89.87	0.0033	81.70
0.14	86.48	80.39	0.0045	88.22
0.19	90.30	70.40	0.0052	98.56

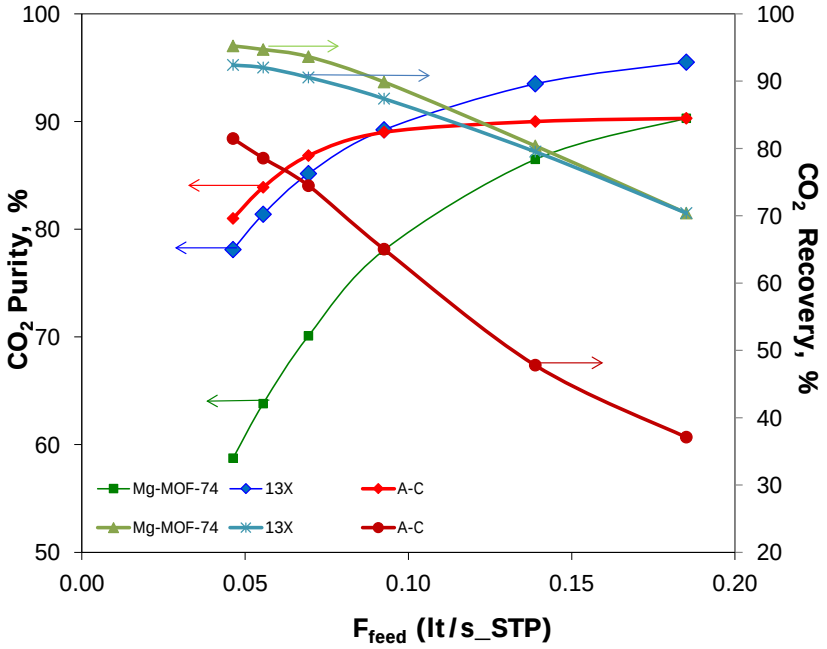

Figure 3.27. Effect of feed flow rate on CO_2 purity and CO_2 recovery at T=323 K.

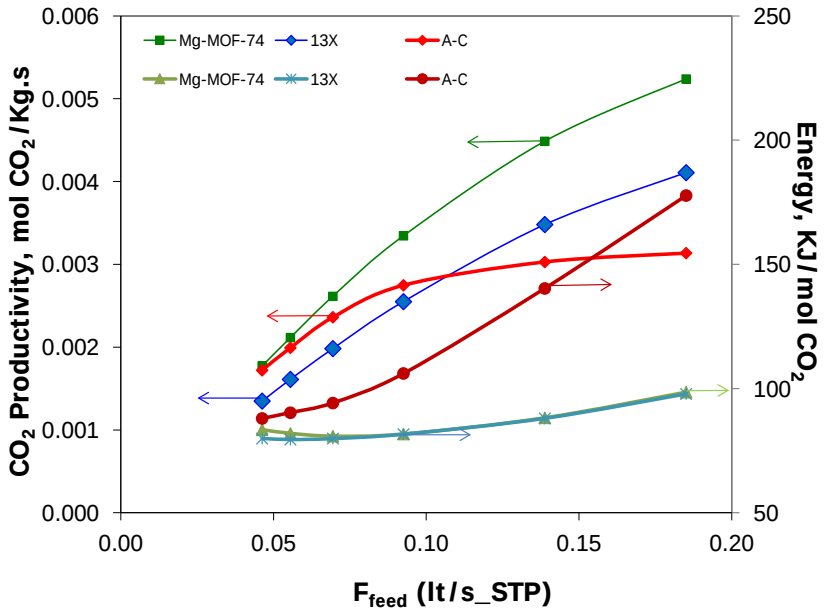

Figure 3.28. Effect of feed flow rate on CO_2 productivity and energy requirement at T=323 K.

on physicochemical properties such as equilibrium adsorption capacity and selectivity, the results from process simulations do not seem to support such a simple practice. Therefore, a detailed process modelling and simulation strategy such as the one described in this work, appears to be the most reliable way to assess the effectiveness of potential adsorbents for CO_2 capture and concentration. This study is useful both for material developers who want to demonstrate the potential of a new adsorbent as well as for process engineers who are selecting an adsorbent for a PSA/VSA process. The development of new adsorbent materials should focus on reduction in N_2 capacity (as it has relatively a higher impact on CO_2 purity) rather than on increase in CO_2 capacity.

3.4.5. Optimisation studies

Since zeolite 13X and Mg-MOF-74 adsorbents have shown some promising features as potential candidates for CO_2 removal from dry flue gas, it would be interesting to further explore their capabilities and improve their process performance. Hence, in addition to the simulation studies, process optimisation studies have been performed using the same VSA process described in section 3.4.2 above. Two different optimisation studies have been performed: (i) optimisation using zeolite 13X as adsorbent and (ii) optimisation using Mg-MOF-74 as adsorbent both at nearly atmospheric feed pressures. The objective of these cases is to minimize energy consumption for specified minimum requirements in CO_2 purity (90%) and CO_2 recovery (90%) at nearly atmospheric feed pressures. The minimum requirements for CO_2 purity and CO_2 recovery have been relaxed as a single-stage VSA process is considered.

The optimisation results of cases I and II for different temperatures are summarized in Table 3.16 and Table 3.17, respectively and illustrated in Figure 3.29 and Figure 3.30, respectively. The results of these cases reveal that, the minimum target of 90% in CO_2 purity and 90% in CO_2 recovery is met for the VSA process at nearly atmospheric pressures for both adsorbents. It is important to note that zeolite 13X has lower energy requirements than Mg-MOF-74, as can be seen from Figures 3.29 and 3.30, respectively, and this can be attributed mainly to the need for lower

blowdown and evacuation pressures when working with Mg-MOF-74 (around 0.11 and 0.015 bar, respectively) as opposed to zeolite 13X (around 0.215 and 0.025 bar, respectively). These differences in the optimal desorption pressures can be related to differences in CO_2 adsorption isotherm steepness and CO_2/N_2 selectivity at low pressures for each adsorbent, which may vary at different temperatures due to the different heat of adsorption between zeolite 13X and Mg-MOF-74. Thus, there is a complex relationship, between optimal process performance indicators and operating conditions, that varies between the two studied adsorbents.

Table 3.16. Optimisation results of case I (zeolite13X).

T_{feed}, (K)	P_{blow}, (bar)	P_{evac}, (bar)	P_{feed}, (bar)	F_{feed}, (lt/s_stp)	CO_2 Purity, %	CO_2 Recovery, %	Energy, (KJ/mol CO_2)
298	0.164	0.022	1.38	0.113	90.00	90.00	76.97
313	0.207	0.025	1.50	0.119	90.00	90.00	78.70
323	0.231	0.026	1.50	0.120	90.00	90.00	80.40
333	0.256	0.026	1.50	0.121	90.00	90.00	82.66

Table 3.17. Optimisation results of case II (Mg-MOF-74).

T_{feed}, (K)	P_{blow}, (bar)	P_{evac}, (bar)	P_{feed}, (bar)	F_{feed}, (lt/s_stp)	CO_2 Purity, %	CO_2 Recovery, %	Energy, (KJ/mol CO_2)
298	0.110	0.015	1.50	0.133	90.00	90.00	94.97
313	0.110	0.012	1.50	0.140	90.00	90.00	108.22
323	0.110	0.014	1.50	0.133	90.00	90.00	105.56
333	0.110	0.016	1.50	0.122	90.00	90.00	102.27

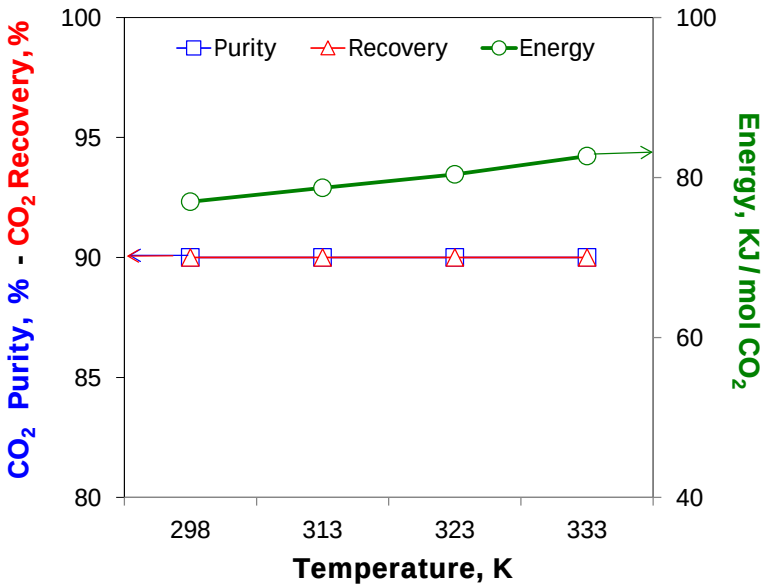

Figure 3.29. Effect of feed temperature on optimal CO_2 purity, CO_2 recovery and energy requirements of case I (zeolite 13X).

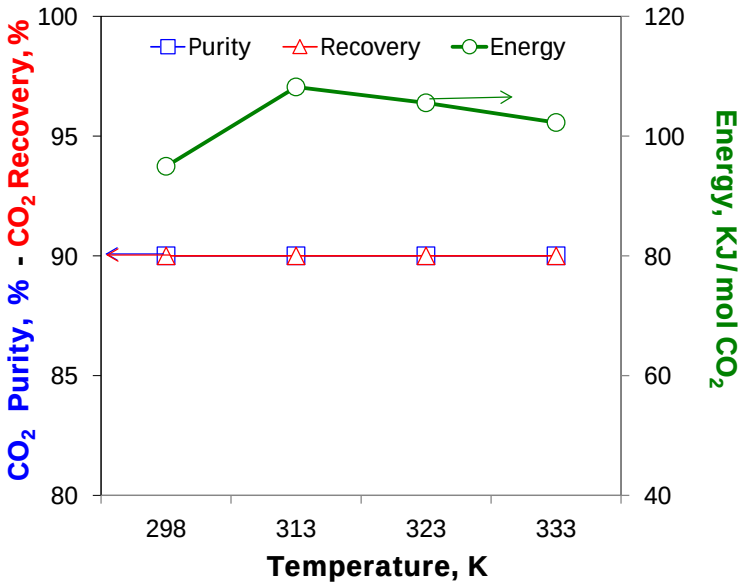

Figure 3.30. Effect of feed temperature on optimal CO_2 purity, CO_2 recovery and energy requirements of case II (Mg-MOF-74).

3.5. Concluding remarks

In this chapter the modelling framework has been validated against experimental and simulation data available from the literature. Model predictions are in good agreement in terms of several process performance indicators. Furthermore, a systematic parametric analysis has been performed to provide significant insight into the most critical design and operating parameters, and their effect on the process performance indicators. In addition, by reviewing the results of the parametric analysis it is possible to gain an intuitive understanding of the relations between factors that affect process performance.

A dynamic optimisation framework has been used to optimise a PSA/VSA process using zeolite 13X as adsorbent. The effect of multi-bed PSA/VSA configurations on the separation quality has been studied. Accordingly, in this chapter the developed modelling framework has been used for a comparative evaluation of three available potential adsorbents for CO_2 capture, namely, zeolite 13X, activated carbon and Mg-MOF-74. Systematic comparative simulations demonstrate that zeolite 13X illustrates the best process performance among the three adsorbents, in terms of CO_2 purity and CO_2 recovery. On the other hand, Mg-MOF-74 appears to be a promising adsorbent for CO_2 capture, as it has considerably higher CO_2 productivity compared to the other two adsorbents.

As a next step, zeolite 13X and Mg-MOF-74 have been selected for process optimisation to minimize energy consumption for specified minimum requirements in CO_2 purity and recovery at nearly atmospheric feed pressures. The optimisation results indicate that the minimum target of 90% in CO_2 purity and 90% in CO_2 recovery is met for the VSA process for both adsorbents. However, zeolite 13X illustrates lower energy requirements than Mg-MOF-74 and this can be attributed mainly to the need for lower desorption (blowdown and evacuation) pressures when working with Mg-MOF-74 as opposed to zeolite 13X. The differences in the optimal desorption pressures can be related to differences in the structure of CO_2/N_2 adsorption isotherms at low pressures for each adsorbent, at different temperatures, revealing a complex relationship between optimal process

performance indicators and operating conditions that varies among different adsorbents.

This study has demonstrated the difficulty to achieve the DOE target values for CO_2 purity and CO_2 recovery in a single-stage PSA/VSA process at nearly atmospheric feed pressure without employing deep vacuum levels. However such deep vacuum levels are not practically applied in industrial scale. In order to achieve the requested performance in terms of CO_2 purity and CO_2 recovery, the flue gas resulting from the combustion of coal needs to undergo an integrated two-stage P/VSA process. In this direction, an integrated two-stage P/VSA process will be studied in the next chapter in order to capture and concentrate CO_2 from flue gas obtaining CO_2 purity ≥ 95% and CO_2 recovery ≥ 90% at nearly atmospheric feed pressure, without employing deep vacuum desorption.

CHAPTER 4
SIMULATION AND OPTIMISATION OF AN INTEGRATED TWO-STAGE P/VSA PROCESS

4. Simulation and optimisation of an integrated two-stage P/VSA process

4.1. Introduction

In the previous chapter, it has been demonstrated the difficulty to achieve CO_2 purity ≥ 90% and CO_2 recovery ≥ 90% in a single-stage PSA/VSA process at nearly atmospheric feed pressure without employing deep vacuum levels. In order to achieve the DOE target values for CO_2 purity and CO_2 recovery an integrated two-stage P/VSA process has been considered in this chapter to capture and concentrate CO_2 from flue gas obtaining CO_2 purity ≥ 95% and CO_2 recovery ≥ 90% at nearly atmospheric feed pressure, without employing deep vacuum desorption.

In the previous chapter, the modelling framework has been employed for a comparative evaluation of three available potential adsorbents: zeolite 13X, activated carbon and Mg-MOF-74 considering the CO_2 capture from dry flue gas in a single-stage VSA process. Systematic comparative simulations demonstrated that zeolite 13X illustrated the best process performance among the three adsorbents, in terms of CO_2 purity and CO_2 recovery. On the other hand, Mg-MOF-74 appeared to be a promising adsorbent for CO_2 capture, as it illustrated a considerably higher CO_2 productivity compared to the other two adsorbents. These two adsorbents (zeolite 13X and Mg-MOF-74), which have shown some promising features as potential candidates for CO_2 removal from dry flue gas, have been selected in this chapter in an effort to develop a more efficient integrated two-stage P/VSA process.

In this chapter, an integrated two-stage P/VSA process for CO_2 capture from dry flue gas, using all the possible combinations of these two adsorbents has been considered, to study the effect of adsorbent type on process performance characteristics. Furthermore, process optimisation studies have been performed to minimize energy consumption for specified minimum requirements in CO_2 purity and recovery. Optimisation studies are normally performed to improve the performance of the proposed integrated two-stage P/VSA process by locating the optimal values of several important process variables that control the process.

The CO_2 purity of an integrated two-stage P/VSA process is the CO_2 purity of the second stage, while the CO_2 recovery equals to the CO_2 recovery of the first stage multiplied by the CO_2 recovery of the second stage. The overall energy consumption of the integrated two-stage P/VSA process is the sum of the energy consumptions of the first and second stage. For example if CO_2 recovery of the first stage is 90% and CO_2 recovery of the second stage is 90%, the CO_2 recovery of an integrated two-stage P/VSA process is 81%. If the CO_2 recovery values at each stage increase from 90% to 95%, the overall CO_2 recovery will meet the desired target of 90%. Thus, the aim of the first stage is to achieve the highest possible CO_2 recovery (above 95%). On the other hand, it is not possible to achieve simultaneously high CO_2 purity as a trade-off. Hence, at the first stage, CO_2 is concentrated to 40-60% and then it is further concentrated to 95% at the second stage. The CO_2 purity in product gas should be more than 95% in order to reduce the costs of CO_2 compression, liquefaction, transportation and storage.

4.2. Process description

An integrated two-stage P/VSA process for post-combustion CO_2 capture from dry flue gas has been employed in the present study. The first stage consists of a two-bed six-step cycle configuration while the second stage consists of a two-bed five-step cycle configuration. The sequence of the operating steps for the two-bed cycle configuration of the first stage is illustrated in Figure 4.1 and consists of pressurization with feed co-currently (CoC), adsorption (Ads), pressure equalization (PED) (co-current depressurization to the other bed), counter-current blowdown (Blow), counter-current purge with N_2 rich light product (Purge) and pressure equalization (PER) (counter-current re-pressurization from the other bed). Since the main objective of the first stage is to obtain the highest possible CO_2 recovery (above 95%), a CO_2 rinse (heavy reflux) step has not been used, since it would cause a significant decrease in CO_2 recovery. The sequence of the operating steps for the two-bed cycle configuration of the second stage is illustrated in Figure 4.2 and consists of pressurization with feed co-currently (CoC), adsorption (Ads), pressure equalization (PED), counter-current blowdown (Blow) and pressure equalization (PER). Due to potential high pressure of adsorption step in the second stage, pressure equalization has been employed to save energy. Since the main objective of the second stage is to obtain the highest possible CO_2 purity (above 95%), N_2 purge (light reflux) step has not been used, since it would dilute the heavy product and decrease the CO_2 purity.

Simulation studies have been performed of the above mentioned two-stage P/VSA process for post-combustion CO_2 capture from dry flue gas (85% N_2, 15% CO_2) using all possible combinations of two different types of adsorbents (zeolite 13X and Mg-MOF-74). The diffusion of CO_2 in commercial zeolite 13X beads appears to be macropore controlled (Hu *et al.,* 2014). The parameters of the dual-site Langmuir adsorption isotherm and the isosteric heats of adsorption of CO_2 and N_2 on zeolite 13X have been adopted from the work of Ko *et al.,* (2005) and are summarized in Table 4.1. Mg-MOF-74 [Mg_2(dobdc), (dobdc=1,4-dioxido-2,5-benzenedicarboxylate), ($Mg(C_4HO_3)(H_2O).4H_2O$), CPO-27-Mg] has received significant attention recently, since it has both high CO_2 adsorption capacity and high CO_2 adsorption affinity and it

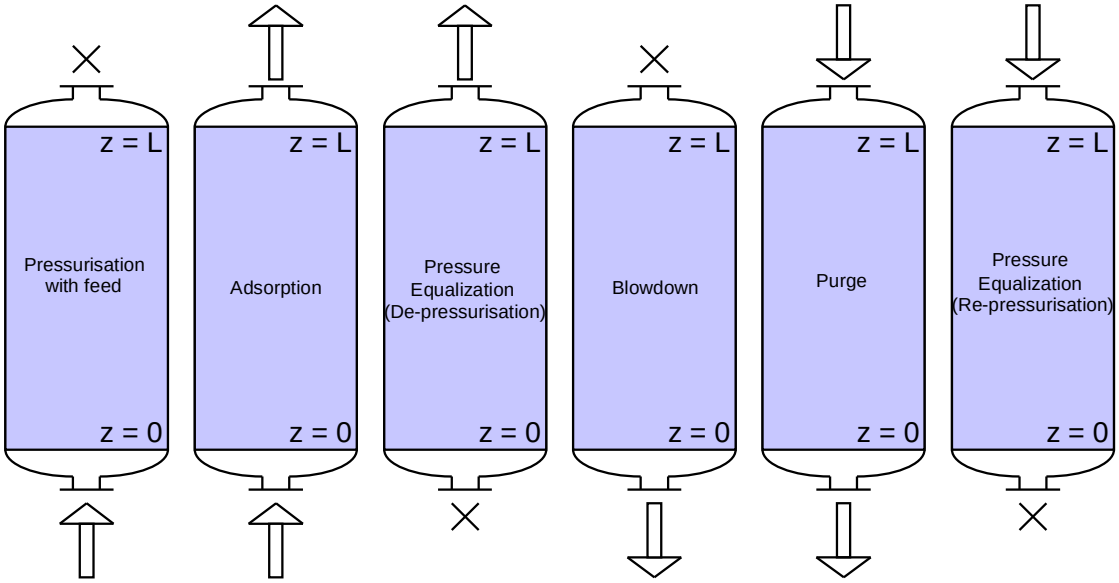

Figure 4.1. Sequence of operating steps for the cycle configuration (two-bed six-step) of the first stage.

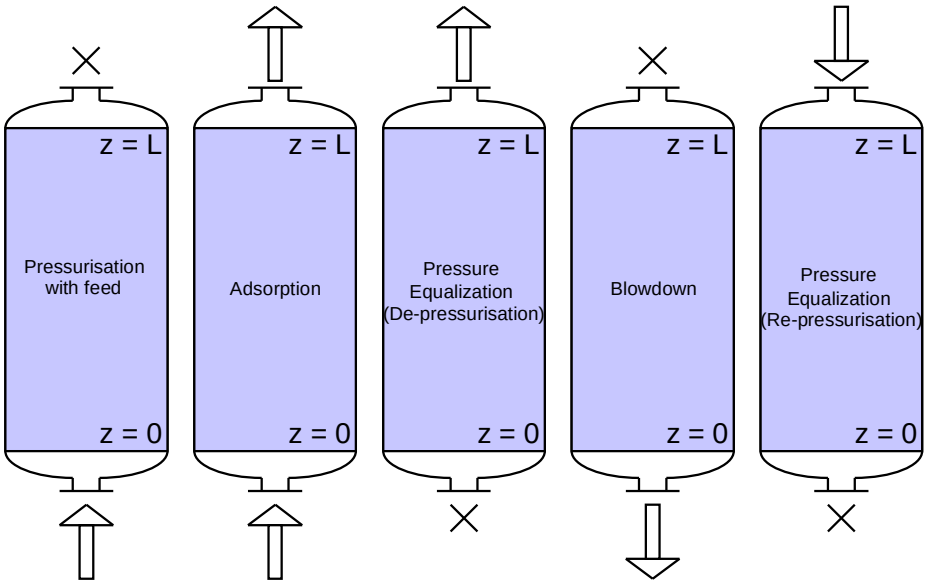

Figure 4.2. Sequence of operating steps for the cycle configuration (two-bed five-step) of the second stage.

Table 4.1. Parameters of the dual-site Langmuir adsorption isotherm and isosteric heats of adsorption of adsorbents.

	zeolite 13X (Ko *et al.*, 2005)		**Mg-MOF-74** (Mason *et al.*, 2011)		
	CO_2 (i = 1)	**N_2 (i = 2)**	**CO_2 (i = 1)**	**N_2 (i = 2)**	**units**
$k_{1,i(1)}$	2.82	1.89	6.80	14.00	mol/Kg
$k_{2,i(1)}$	-3.50E-04	-2.25E-04	0	0	1/K
$k_{3,i(1)}$	2.83E-09	1.16E-09	2.44E-11	4.96E-10	1/Pa
$k_{4,i(1)}$	2598.20	1944.61	5051.72	2165.02	K
$k_{1,i(2)}$	3.97	1.89	9.90	0	mol/Kg
$k_{2,i(2)}$	-4.95E-03	-2.25E-04	0	0	1/K
$k_{3,i(2)}$	4.41E-09	1.16E-09	1.39E-10	0	1/Pa
$k_{4,i(2)}$	3594.07	1944.61	2886.70	0	K
$\Delta H_{ads\ (i)}$	-21601.5	-16167.5	-42000	-18000	J/mol

Table 4.2. Physical properties of adsorbents.

physical property	**zeolite 13X** (Ko *et al.*, 2005)	**Mg-MOF-74** (Wu *et al.*, 2009)	**units**
adsorbent density (ρ^s)	1870	1466.1	kg/m^3
particle density (ρ^p)	1159.4	909	kg/m^3
heat capacity of particles ($C_p^{\ p}$)	504	800	J/(kg·K)

Table 4.3. Parameters used in simulations of an integrated two-stage P/VSA process.

parameter	**value**
first stage adsorbent bed length (L)	1 m
first stage adsorbent bed diameter (D)	8.8×10^{-2} m
second stage adsorbent bed length (L)	1 m
second stage adsorbent bed diameter (D)	4.4×10^{-2} m
pore radius (R_{pore})	0.5×10^{-9} m
particle radius (R_p)	1.0×10^{-3} m
particle tortuosity (τ_p)	4.5
particle porosity (ε_p)	0.38
adsorbent bed porosity (ε_{bed})	0.348
universal gas constant (R)	8.314 J/(mol·K)
heat transfer coefficient of the wall ($k_{h,wall}$)	60 J/(m^2·K·s)
effective diffusivity of CO_2 ($D_{e,CO2}$)	1.087×10^{-8} m^2/s
effective diffusivity of N_2 ($D_{e,N2}$)	1.363×10^{-8} m^2/s

has been considered as a potential adsorbent in the present study. The transport of CO_2 and N_2 in the MOF particles can be safely considered as macropore controlled (Nalaparaju *et al.,* 2015). The parameters of the dual-site Langmuir adsorption isotherm and the isosteric heats of adsorption of CO_2 and N_2 on Mg-MOF-74 have been adopted from the work of Mason *et al.,* (2011) and are summarized in Table 4.1. Other physical properties of the adsorbents particles required for the process modelling and simulation studies have been adopted from the works of Ko *et al.,* (2005) and Wu *et al.,* (2009) and are summarized in Table 4.2.

A typical flue gas from coal-fired power plants contains N_2, CO_2, H_2O, and minor impurities such as SO_x and NO_x. In the present study, it is assumed that H_2O, SO_x, and NO_x have been removed during the pretreatment process (desulfurization and dehumidification unit), so that the feed flue gas consists of CO_2 and N_2 at near atmospheric pressure. More specifically, the dry flue gas mixture is fed to the separation unit at 1.10 bar pressure and at 313 K temperature while the blowdown pressure is set to 0.10 bar and the purge to feed ratio to 0.30 for the first stage. Note that the same temperature and pressure conditions hold for the second stage of the process. It should be also noted that the blowdown pressure has been selected at 0.10 bar, according to previous studies (Kikkinides *et al.,* 1993; Liu *et al.,* 2011; Na *et al.,* 2001; Na *et al.,* 2002; Takamura *et al.,* 2001). From a physicochemical point of view, the value of this pressure depends primarily on the shape of the adsorbent isotherm and the need to achieve proper adsorbent bed regeneration. On the other hand, there are important equipment constraints and energy requirements that prohibit the use of deep vacuum particularly for industrial applications.

At the beginning of the process, the adsorbent beds are saturated with pure N_2 at 1.10 bar. The parameters used in simulation of an integrated two-stage P/VSA process are listed in Table 4.3. The dimensions of the adsorbent beds of the second stage are smaller than that of the first stage since the feed flow rate is now much smaller. It is important to note that in a typical multi-bed configuration, the operating time steps are not independent variables and must be correlated due to the need for synchronization of the adsorbent beds, although it was recently demonstrated that this constraint can be relaxed using idle times for each adsorbent

bed (Krishnamurthy *et al.,* 2014). The cycle time of the first stage is fixed at 240s and the operating time steps are fixed as follows: t_{CoC}=20s, t_{Ads}=80s, t_{PED}=20s, t_{Blow}=20s, t_{Purge}=80s, t_{PER}=20s. The cycle time of the second stage is fixed at 240s and the operating time steps are fixed as follows: t_{CoC}=20s, t_{Ads}=80s, t_{PED}=20s, t_{Blow}=100s, t_{PER}=20s. The operating time of adsorption step is only 80s of the total cycle time of 240s at both stages. It should be clarified that the multi-bed process cycle configuration and the durations of the operating steps have not been optimised due to the computational complexity. The durations of the operating steps have been selected based on simulations and previous studies. Specific attention has been placed in order to take into account the time interactions between two beds during each operating step. At the first stage the operating time steps are selected as follows: $t_{Ads}=4t_{CoC}$, $t_{PED}=t_{CoC}$, $t_{Blow}=t_{CoC}$, $t_{Purge}=t_{Ads}$, $t_{PER}=t_{PED}$. At the second stage the operating time steps are selected as follows: $t_{Ads}=4t_{CoC}$, $t_{PED}=t_{CoC}$, $t_{Blow}=t_{Ads}+t_{CoC}$, $t_{PER}=t_{PED}$. Due to no constant feed flow rate entering the second stage, a tank is required to accumulate the product gas coming from the first stage and provide a constant feed flow rate to the second stage.

4.3. Formulation of the optimisation problem

In an integrated two-stage P/VSA process, the output extract stream of the first stage is the input feed stream of the second stage. Thus, the overall process optimisation of the integrated two-stage P/VSA process is quite a complicated task because the two stages are coupled with each other. The problem of simultaneously optimising the operating conditions in an integrated two-stage P/VSA multi-bed process is computationally intractable with current optimisation techniques. So, in this study the two stages are optimised separately. First the optimisation problem of the first stage has been considered and the optimal results of the first stage are used as input parameters to the optimisation problem of the second stage. According to the preliminary simulation studies performed in this work, the first stage consumes more energy than the second stage. The decision variables of the optimisation problem include feed pressure, feed flow rate, blowdown pressure, purge to feed ratio and length to diameter ratio.

4.3.1. Optimisation of the first stage

The main objective in the optimisation study of the first stage is to investigate the effect of feed pressure, feed flow rate, blowdown pressure, purge to feed ratio and length to diameter ratio on the overall process performance. The objective function employed is the minimization of energy consumption for specified minimum requirements in CO_2 purity and CO_2 recovery. Preliminary simulations studies demonstrated that it is difficult to achieve the DOE target values for CO_2 purity and CO_2 recovery of an integrated two-stage P/VSA process at nearly atmospheric feed pressure, with a moderate vacuum of 0.10 bar when the CO_2 purity of the first stage is less than 50%. The main target of the first stage is to achieve the highest possible CO_2 recovery (above 97.4%) with a corresponding CO_2 purity (40-60%) as a trade-off.

$$\text{min. energy consumption} \tag{4.1}$$

$$\text{s. t. model equations}$$

$$40\% \leq CO_2 \text{ purity} \leq 60\%$$

$$CO_2 \text{ recovery} \geq 97.4\%$$

$$1.1\ bar \leq P_{feed} \leq 1.5\ bar$$

$$36\ SLPM \leq F_{feed} \leq 360\ SLPM$$

$$0.1\ bar \leq P_{blow} \leq 0.2\ bar$$

$$0.1 \leq P/F \quad \leq 1$$

$$2.5 \leq L/D \quad \leq 20$$

The above dynamic optimisation problem has been formulated and solved in the gPROMS™ modelling environment (PSE, 2011).

4.3.2. Optimisation of the second stage

The optimisation of the second stage can be formulated as the minimization of energy consumption for specified minimum requirements in CO_2 purity and CO_2 recovery, while optimising feed pressure, blowdown pressure and length to diameter ratio. The main target of the second stage is to obtain the highest possible CO_2 purity (above 95%) with a corresponding highest possible CO_2 recovery (above 92.5%).

$$\text{min. energy consumption} \tag{4.2}$$

$$\text{s.t. model equations}$$

$$\text{CO}_2 \text{ purity} \geq 95\%$$

$$\text{CO}_2 \text{ recovery} \geq 92.5\%$$

$$1.1\ bar \leq P_{feed} \leq 2.5\ bar$$

$$0.1\ bar \leq P_{blow} \leq 0.2\ bar$$

$$2.5 \leq L/D \quad \leq 20$$

The above dynamic optimisation problem has been formulated and solved in the gPROMS™ modelling environment (PSE, 2011). The optimal values of process variables should be optimally decided in order to minimize energy consumption for specified minimum requirements in CO_2 purity (95%) and CO_2 recovery (90%) of the integrated two-stage P/VSA process. Note that the CO_2 purity of the integrated two-stage P/VSA process is that of the second stage, while the overall CO_2 recovery is the product of CO_2 recoveries of the first and second stage. Although the target value of CO_2 recovery of the second stage is smaller than the target value of CO_2 recovery of the first stage the overall CO_2 recovery must meet the DOE requirements of 90%.

4.4. Results and discussion

4.4.1. Comparison and evaluation of combinations of adsorbents

Figure 4.3 shows the adsorption isotherms of CO_2 and N_2 on zeolite 13X and Mg-MOF-74 at T=313 K. Clearly there are both advantages and disadvantages associated with each of these two potential adsorbents. The adsorption isotherm of CO_2 on Mg-MOF-74 is steeper than that on zeolite 13X. A simple visual inspection of the adsorption isotherms of the potential adsorbents may suggest that Mg-MOF-74 is superior because of its high apparent CO_2 capacity. However, the N_2 capacity is similarly elevated and initially it is unclear which potential adsorbent would be the best for the integrated two-stage P/VSA process. The working capacities for the adsorption of CO_2 and N_2 on zeolite 13X and Mg-MOF-74 are estimated using pure component isotherms for the first and the second P/VSA unit and are summarized in Table 4.4. It is found that the CO_2 working capacity on Mg-MOF-74 is higher than that on zeolite 13X and therefore theoretically, Mg-MOF-74 looks as a better adsorbent material for the first and the second P/VSA unit. Nevertheless, in the present study, the choice of adsorbent materials packed in the first and the second unit, is not based on a simple comparison of CO_2/N_2 adsorption isotherms and working capacities of the two adsorbents for each capture unit. For the precise choice of adsorbents, both the competitive adsorption equilibrium and the adsorption/desorption kinetics should be taken into account. Thus, detailed process modelling and simulation provide the most reliable way to evaluate both qualitatively and quantitatively potential adsorbents for each capture unit.

As a next step, all possible combinations of the two selected adsorbents have been employed in an integrated two-stage P/VSA process. The modelling framework has been applied to estimate process performance indicators (CO_2 purity, CO_2 recovery, CO_2 productivity and energy requirements) using each of the four potential combinations of adsorbents over a range of feed flow rates. Four different process simulation studies have been performed using the following combinations of adsorbents for the first and second stage of the P/VSA process: (I) zeolite 13X – zeolite 13X, (II) zeolite 13X – Mg-MOF-74, (III) Mg-MOF-74 – zeolite 13X and (IV) Mg-

MOF-74 – Mg-MOF-74. The simulation results of cases I, II, III and IV are summarized in Table 4.5 and illustrated in Figure 4.4. Systematic comparative simulations demonstrated that zeolite 13X had a better performance than Mg-MOF-74, in terms of CO_2 purity and CO_2 recovery (Nikolaidis *et al.,* 2016). As the main target of the first stage is to achieve the highest possible CO_2 recovery (above 95%) with a corresponding CO_2 purity (40-60%), the choice of zeolite 13X as adsorbent at the first stage can significantly improve the process performance in terms of CO_2 purity and CO_2 recovery, as it is summarized in Table 4.5. On the other hand, even though Mg-MOF-74 shows considerably higher CO_2 adsorption capacity (but in the meantime higher N_2 adsorption capacity and poor regeneration), the choice of Mg-MOF-74 as adsorbent at the first stage cannot improve the process performance in terms of CO_2 purity and CO_2 recovery, as it is summarized in Table 4.5. This observation seems to indicate that the increased N_2 adsorption capacity is rather detrimental compared to the increased CO_2 adsorption capacity in accordance with similar conclusions reported in the literature (Khurana and Farooq, 2016; Rajagopalan *et al.,* 2016). This observation provides an important physical insight into the factors that need to be taken into account during design, synthesis and development of potential novel adsorbent materials for more efficient CO_2 capture. This remark also explains why the combination of adsorbents zeolite 13X – Mg-MOF-74 of case II has a better performance than the combination of adsorbents Mg-MOF-74 – zeolite 13X of case III, in terms of CO_2 purity and CO_2 recovery, as it is also illustrated in Figure 4.4. The results of the comparison of the four potential combinations of adsorbents clearly indicate that the combination of adsorbents zeolite 13X – Mg-MOF-74 of case II illustrates the best performance in terms of CO_2 purity and recovery followed by the use of zeolite 13X at both stages of the process of case I, over the full range of feed flow rates. The simulation results also reveal that the remaining two combinations of adsorbents corresponding to cases III and IV, appear to have a much worse performance in terms of CO_2 purity and CO_2 recovery. It is important to note that all simulation studies do not meet the target levels established for all combinations of adsorbents. Hence, in the remaining part of this work the optimisation studies will be focused on the most promising combinations of adsorbents, which correspond to

Table 4.4. Working capacities for the adsorption of CO_2 and N_2 on zeolite 13X and Mg-MOF-74.

		A stage			B stage		
adsorbent	**gas**	**adsorption capacity (mole/Kg)**	**desorption capacity (mole/Kg)**	**working capacity (mole/Kg)**	**adsorption capacity (mole/Kg)**	**desorption capacity (mole/Kg)**	**working capacity (mole/Kg)**
zeolite 13X	CO_2	2.56	1.79	0.77	3.36	2.24	1.12
	N_2	0.187	0.011	0.176	0.112	0.001	0.111
Mg-MOF-74	CO_2	5.69	3.83	1.86	7.04	4.98	2.06
	N_2	0.624	0.035	0.589	0.374	0.004	0.370

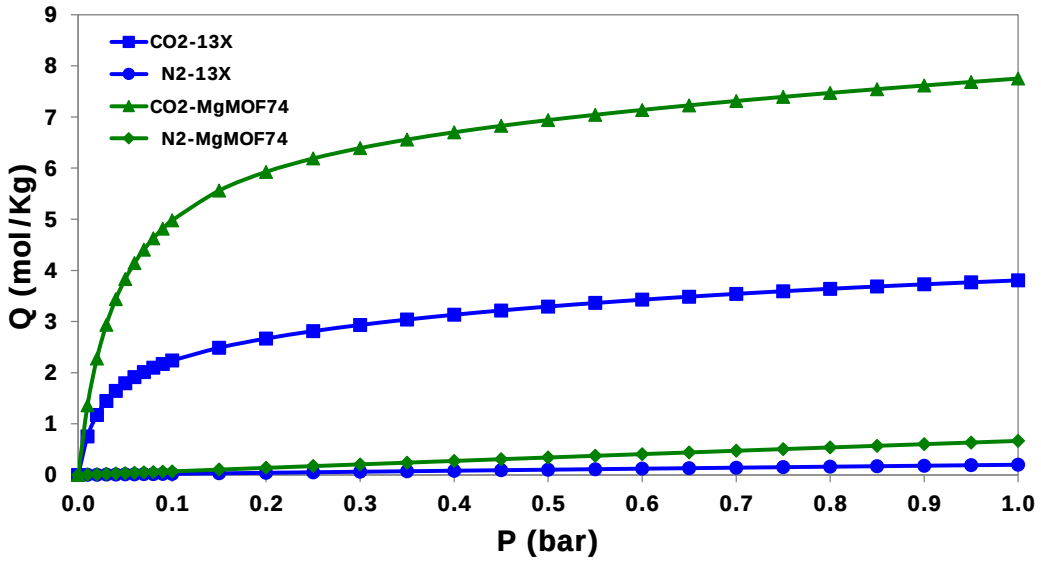

Figure 4.3. Adsorption isotherms of CO_2 and N_2 on zeolite 13X and Mg-MOF-74 at T=313 K.

Table 4.5. Simulation results of cases I, II, III and IV for different combinations of adsorbents.

A stage (P_{feed}=1.1 bar, P_{blow}=0.1 bar, P/F=0.3)			B stage (P_{feed}=1.1 bar, P_{blow}=0.1 bar)		integrated two-stage			
Ffeed (SLPM)	CO_2 Purity, %	CO_2 Recovery, %	CO_2 Purity, %	CO_2 Recovery, %	CO_2 Purity, %	CO_2 Recovery, %	CO_2 Productivity (mol CO_2/Kg·h)	Energy (MJ/Kg CO_2)
zeolite 13X			**zeolite 13X**		**(zeolite 13X – zeolite 13X)**			
133.3	50.58	94.33	93.86	88.94	93.86	83.90	1.53	0.64
152.3	53.84	92.12	95.71	88.40	95.71	81.43	1.70	0.62
177.7	58.46	88.10	97.75	87.33	97.75	76.94	1.94	0.58
213.2	61.70	83.90	97.67	85.44	97.67	71.68	2.16	0.57
266.5	64.34	78.44	98.30	79.14	98.30	62.08	2.29	0.56
355.3	66.33	70.46	98.46	71.34	98.46	50.27	2.43	0.55
zeolite 13X			**Mg-MOF-74**		**(zeolite 13X – Mg-MOF-74)**			
133.3	50.58	94.33	96.84	81.22	96.84	76.61	1.47	0.64
152.3	53.84	92.12	97.61	79.58	97.61	73.31	1.60	0.61
177.7	58.46	88.10	98.25	77.78	98.25	68.52	1.76	0.58
213.2	61.70	83.90	98.65	73.24	98.65	61.45	1.88	0.57
266.5	64.34	78.44	98.89	66.94	98.89	52.51	1.99	0.56
355.3	66.33	70.46	99.05	59.19	99.05	41.71	2.07	0.56
Mg-MOF-74			**zeolite 13X**		**(Mg-MOF-74 – zeolite 13X)**			
133.3	38.44	91.71	90.83	81.14	90.83	74.41	1.55	0.78
152.3	41.02	90.43	92.92	80.83	92.92	73.09	1.73	0.74
177.7	46.14	87.16	95.21	80.95	95.21	70.56	2.00	0.68
213.2	53.80	79.19	96.75	83.26	96.75	65.93	2.31	0.62
266.5	58.37	72.06	97.10	81.21	97.10	58.52	2.57	0.60
355.3	61.42	58.45	97.44	79.42	97.44	46.42	2.73	0.59
Mg-MOF-74			**Mg-MOF-74**		**(Mg-MOF-74 – Mg-MOF-74)**			
133.3	38.44	91.71	92.24	73.04	92.24	66.98	1.48	0.78
152.3	41.02	90.43	93.92	71.11	93.92	64.30	1.61	0.74
177.7	46.14	87.16	95.95	70.64	95.95	61.57	1.82	0.68
213.2	53.80	79.19	97.72	71.87	97.72	56.91	2.06	0.62
266.5	58.37	72.06	98.39	68.31	98.39	49.22	2.24	0.60
355.3	61.42	58.45	98.69	66.03	98.69	38.59	2.34	0.59

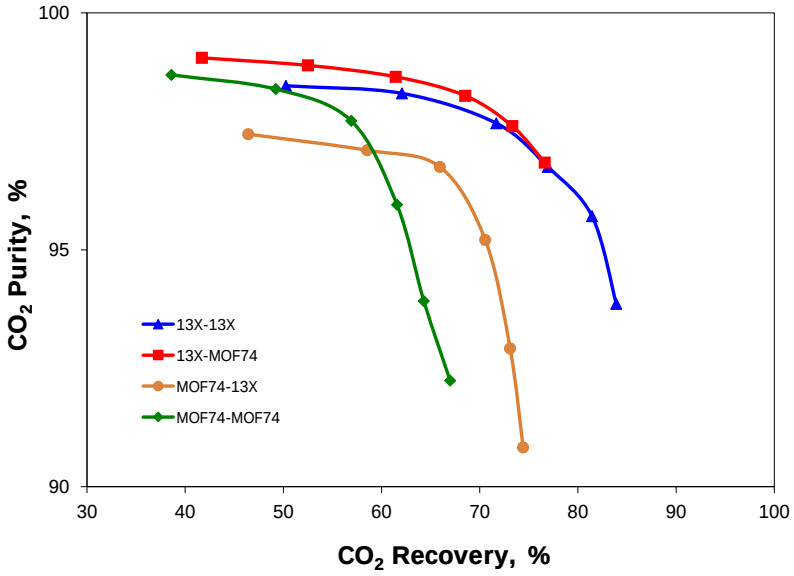

Figure 4.4. Simulation results of all possible combinations of two different types of adsorbents.

cases I and II, in order to obtain 95% CO_2 purity and 90% CO_2 recovery of the integrated two-stage P/VSA process.

It should be also emphasized that there is a complex relation between process performance indicators and operating conditions that varies among the different combinations of adsorbents. Such a relation cannot be quantified by a simple comparison of CO_2/N_2 adsorption isotherms and physicochemical properties such as selectivity data and equilibrium working capacities. Therefore, detailed process modelling and simulation, provide a reliable way to systematically assess the effectiveness of potential combinations of adsorbents for CO_2 capture of the integrated two-stage P/VSA process.

4.4.2. Optimisation studies

Since the use of zeolite 13X at both stages of the process (case I) and the combination of adsorbents zeolite 13X – Mg-MOF-74 (case II) have shown some promising features as potential candidates for CO_2 capture from dry flue gas, it would be interesting to further improve their process performance characteristics by employing process optimisation studies to minimize energy consumption for specified minimum requirements in CO_2 purity and CO_2 recovery. Hence, in addition to the simulation studies, process optimisation studies have been performed in cases I and II, employing the same integrated two-stage P/VSA process described in section 4.2 above. The objective of the optimisation studies is to minimize energy consumption for specified minimum requirements in CO_2 purity and CO_2 recovery of the integrated two-stage P/VSA process at nearly atmospheric feed pressures, following the optimisation strategy analyzed in section 4.3 above. All optimisation studies have been carried out at constant feed temperature, adsorbent bed volume, cycle time, duration of operating steps and gas valve parameters.

The first stage employing zeolite 13X as adsorbent (similar in both optimisation studies) produces an enriched stream of 54.67% CO_2 with a CO_2 recovery of 97.41% at a desorption pressure of 0.10 bar. The second stage employs also zeolite 13X produces an enriched stream of 95.46% CO_2 with a CO_2 recovery of 92.52% at a desorption pressure of 0.10 bar. The integrated two-stage P/VSA process (zeolite 13X – zeolite 13X) leads to a CO_2 purity of 95.46% and a CO_2 recovery of 90.12% with CO_2 productivity 2.67 mol CO_2/Kg·h. The total energy requirements are 0.63 MJ/Kg CO_2 (case I). On the other hand, in case II, if Mg-MOF-74 is used in the second stage a concentrated stream of 97.57% CO_2 is produced with a CO_2 recovery of 92.56% at a desorption pressure of 0.10 bar. The integrated two-stage P/VSA process (zeolite 13X – Mg-MOF-74) results in a CO_2 purity of 97.57%, CO_2 recovery of 90.16% and CO_2 productivity of 3.09 mol CO_2/Kg·h. The total energy requirements are 0.70 MJ/Kg CO_2 (case II). The optimal dimensions of the adsorbent beds in the first stage are, L=0.364m, D=0.146m, while the corresponding optimal dimensions of the second stage are, L=0.292m, D=0.103m, in both optimisation studies.

The optimisation results of cases I and II are summarized in Table 4.6. The flow charts of the optimised integrated two-stage P/VSA process of cases I and II are illustrated in Figures 4.5 and 4.6, respectively. The pressure history profiles of the optimised first and second stage of case I are illustrated in Figures 4.7 and 4.8, respectively. The temperature history profiles of the optimised first and second stage of case I at different positions of the adsorbent bed are illustrated in Figures 4.9 and 4.10, respectively. The breakdown of energy consumption among the different operating steps of the optimised first and second stage of case I are illustrated in Figures 4.11 and 4.12, respectively. The energy consumption at the blower is reduced with the increase of the purge to feed ratio. On the contrary, the energy consumption at the vacuum pump is increased with the increase of the purge to feed ratio. Because of these two competitive effects, there is an optimum purge to feed ratio, which minimizes the energy consumption of the first stage. The effluent stream from the second stage can be recycled to the inlet of the first stage as it brings about the same characteristics with the feed stream in order to further increase the CO_2 recovery from the dry flue gas, as it is illustrated in Figure 4.13. The results of the optimisation studies reveal that, the minimum target of 95% in CO_2 purity and 90% in CO_2 recovery is met for the integrated two-stage P/VSA process, at nearly atmospheric pressures for both combinations of adsorbents, without the need to employ deep vacuum. It is important to note that the combination of adsorbents zeolite 13X **–** Mg-MOF-74 produces a higher CO_2 productivity (around 16%) compared to the use of zeolite 13X at both stages due to the use of Mg-MOF-74 which has a considerably higher CO_2 equilibrium working capacity compared to zeolite 13X. On the other hand, the use of zeolite 13X at both stages has lower energy requirements (around 10%) than the combination of adsorbents zeolite 13X **–** Mg-MOF-74 and this can be attributed mainly to the need for higher feed pressure at the second stage when working with Mg-MOF-74 (around 2.24 bar) as opposed to zeolite 13X (around 1.33 bar).

The performances of previous literature studies (Haghpanah *et al.,* 2014; Leperi *et al.,* 2016; Liu *et al.,* 2011; Riboldi and Bolland, 2015; Shen *et al.,* 2012; Wang *et al.,* 2012; Wang *et al.,* 2013a) employing two successive P/VSA units are summarized in Table 4.7 and compared with the results of this work. It should be noted that the

energy consumption requirements of this work are comparative and in most cases compare favorably with previous literature contributions (Haghpanah *et al.,* 2014; Leperi *et al.,* 2016; Liu *et al.,* 2011; Shen *et al.,* 2012; Wang *et al.,* 2013a). Table 4.7 also summarizes the cycle times of previously studied two-stage P/VSA processes as well as the overall CO_2 productivity, where available. It is important to note that the optimised two-stage P/VSA process leads to a significantly higher CO_2 productivity comparing with all previous contributions, due to the use of much shorter cycle times. The total energy consumption (0.53 MJ/Kg CO_2) in the work of Wang *et al.,* (2012) is lower than that of this study, but illustrates a lower CO_2 productivity (0.71 mol CO_2/Kg·h). This can be attributed to the use of relatively long cycle times at both stages of the process (900s at the first stage and 860s at the second stage). This leads to larger adsorbent bed units and also higher adsorbent replacement costs. Furthermore, it is important to note that the total energy requirements of the proposed integrated two-stage P/VSA process are lower than those obtained from competitive amine absorption processes (1.04 MJ/Kg CO_2) (DOE/NETL, 2015). This suggests that adsorption processes are efficient and economically attractive for the industrial application of CO_2 capture from flue gas. The main advantage of physical adsorption over chemical absorption is its simple and energy efficient operation and regeneration which can be simply achieved by a pressure swing.

Table 4.6. Optimisation results of cases I and II for different combinations of adsorbents.

	F_{feed}, (SLPM)	P_{feed}, (bar)	P_{blow}, (bar)	L/D	P/F	CO_2 Purity, %	CO_2 Recovery, %	CO_2 Productivity, (mol CO_2/Kg·h)	Energy, (MJ/Kg CO_2)
case I (zeolite 13X – zeolite 13X)									
A stage	230.2	1.1	0.1	2.5	0.82	54.67	97.41	7.22	0.39
B stage	61.5	1.33	0.1	2.84	0	95.46	92.52	18.69	0.24
integrated two-stage						95.46	90.12	2.67	0.63
case II (zeolite 13X – Mg-MOF-74)									
A stage	230.2	1.1	0.1	2.5	0.82	54.67	97.41	7.22	0.39
B stage	61.5	2.24	0.1	2.84	0	97.57	92.56	25.84	0.31
integrated two-stage						97.57	90.16	3.09	0.70

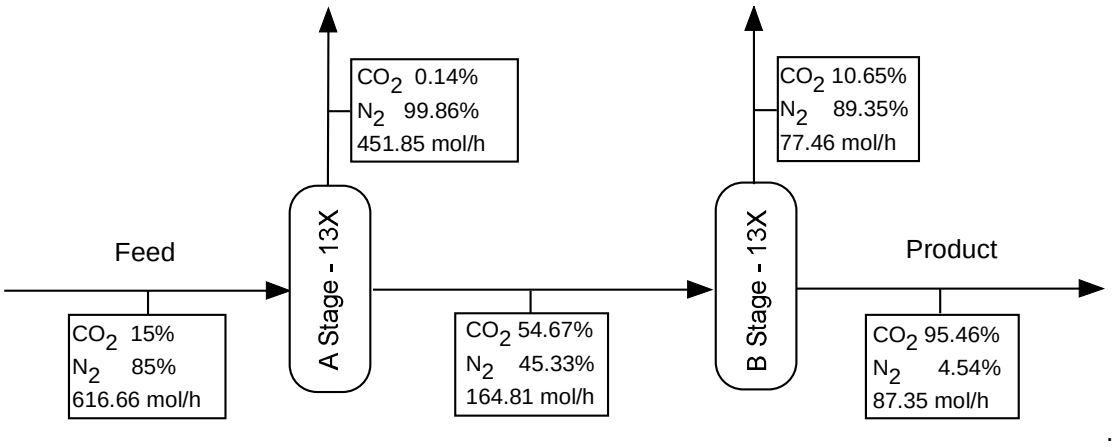

Figure 4.5. Flow chart of the optimised integrated two-stage P/VSA process of case I.

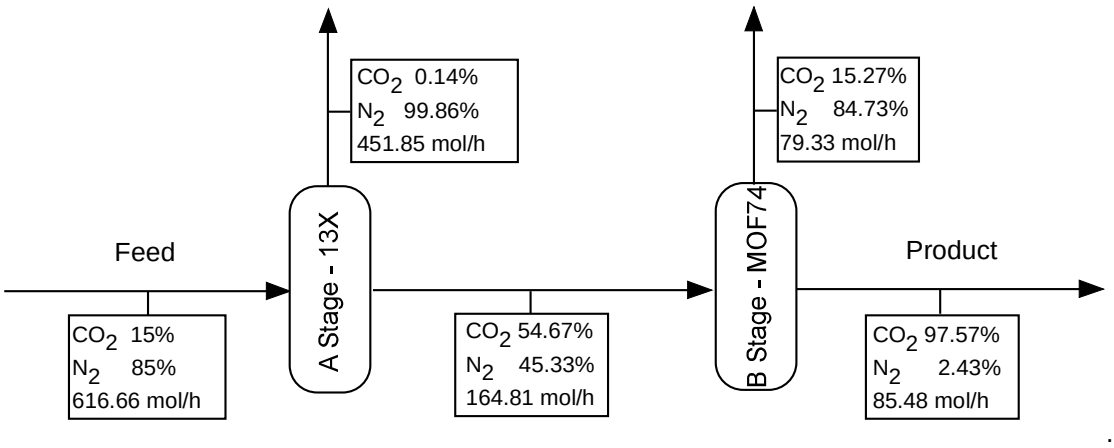

Figure 4.6. Flow chart of the optimised integrated two-stage P/VSA process of case II.

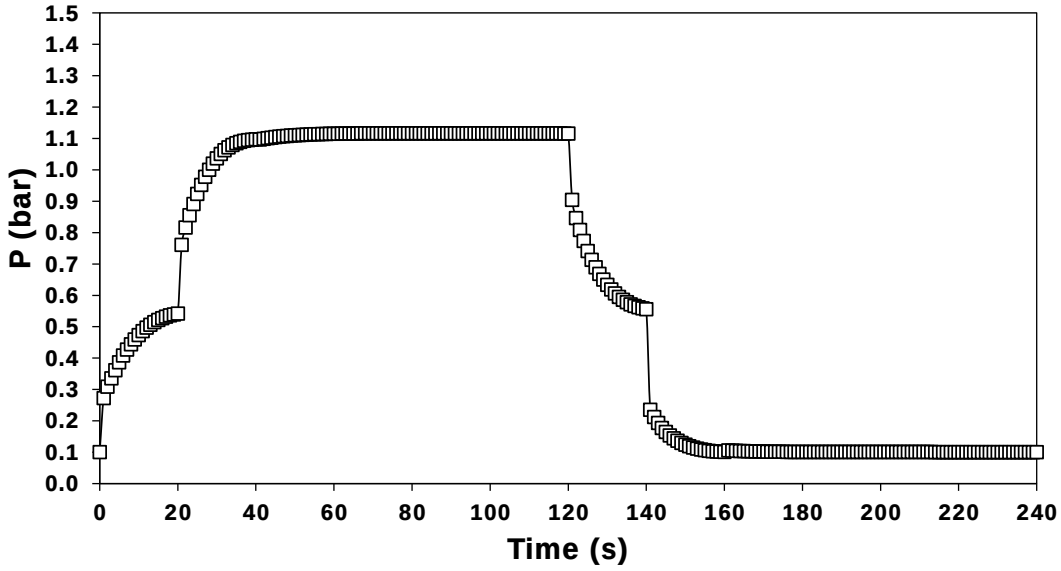

Figure 4.7. Pressure history profile of the optimised first stage of case I.

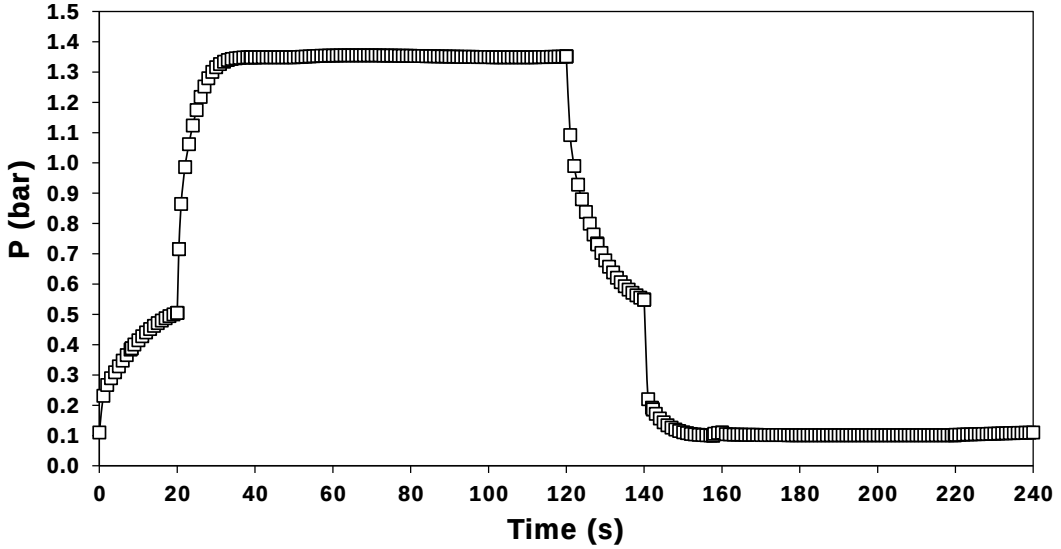

Figure 4.8. Pressure history profile of the optimised second stage of case I.

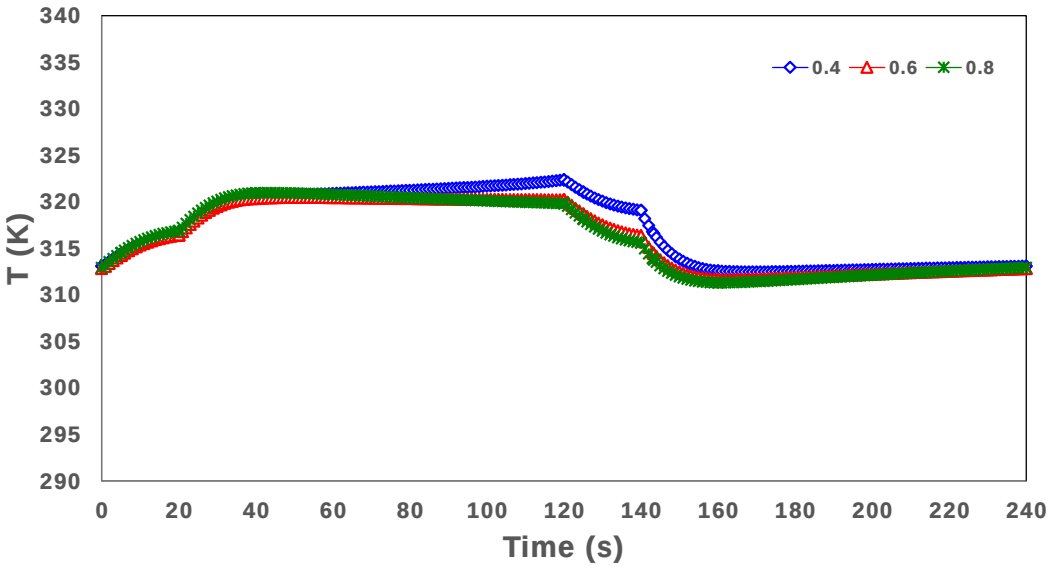

Figure 4.9. Temperature history profile of the optimised first stage of case I at different positions (0.4, 0.6 and 0.8 of the adsorbent bed length).

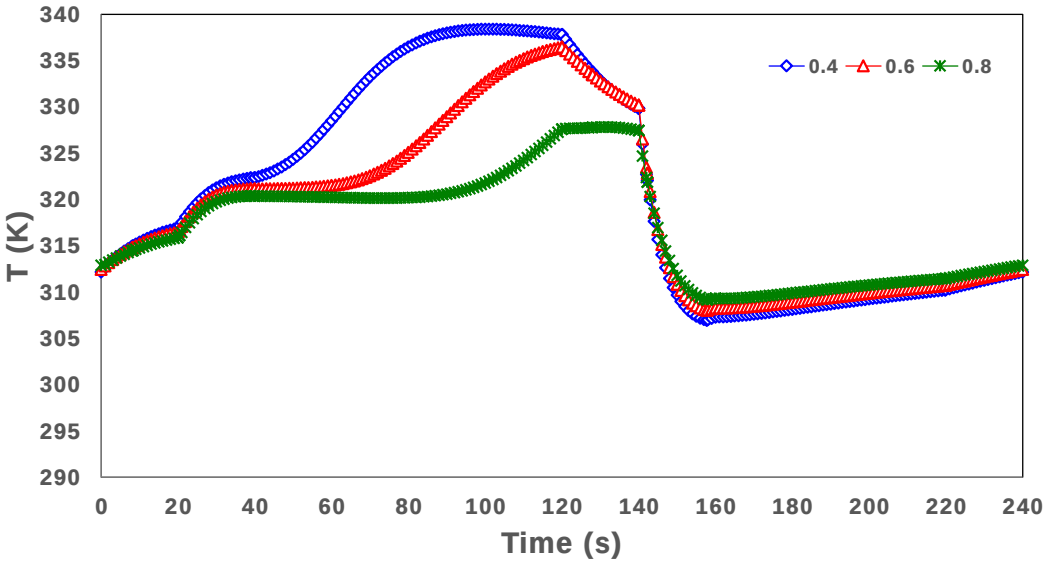

Figure 4.10. Temperature history profile of the optimised second stage of case I at different positions (0.4, 0.6 and 0.8 of the adsorbent bed length).

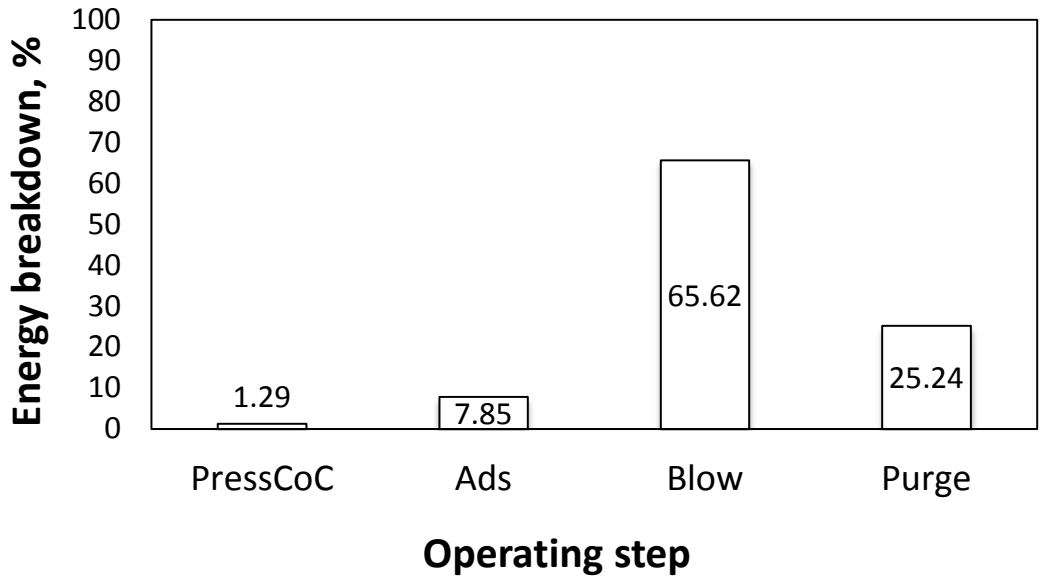

Figure 4.11. Energy breakdown of the operating steps of optimised first stage of case I.

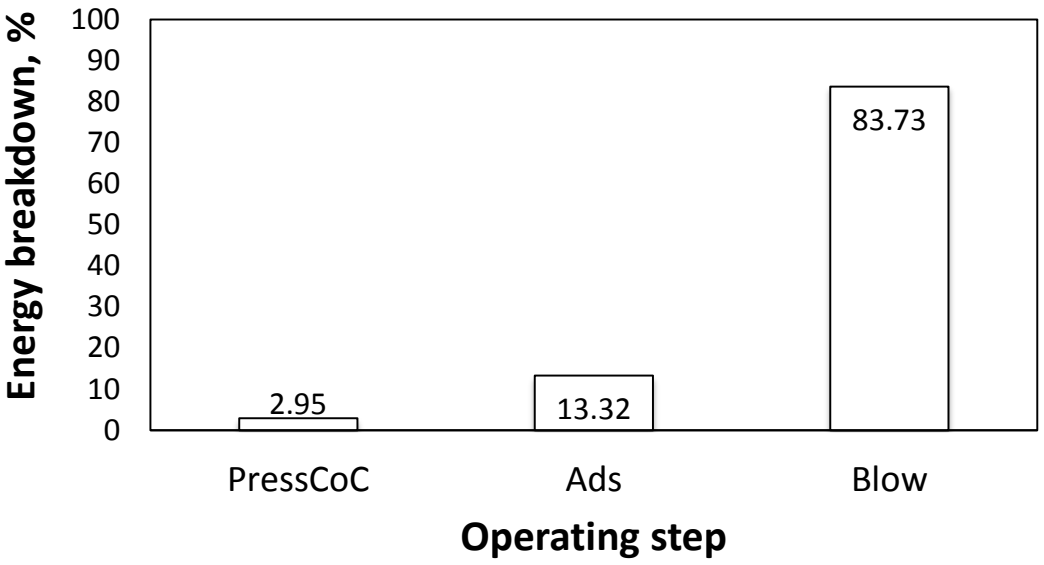

Figure 4.12. Energy breakdown of the operating steps of optimised second stage of case I.

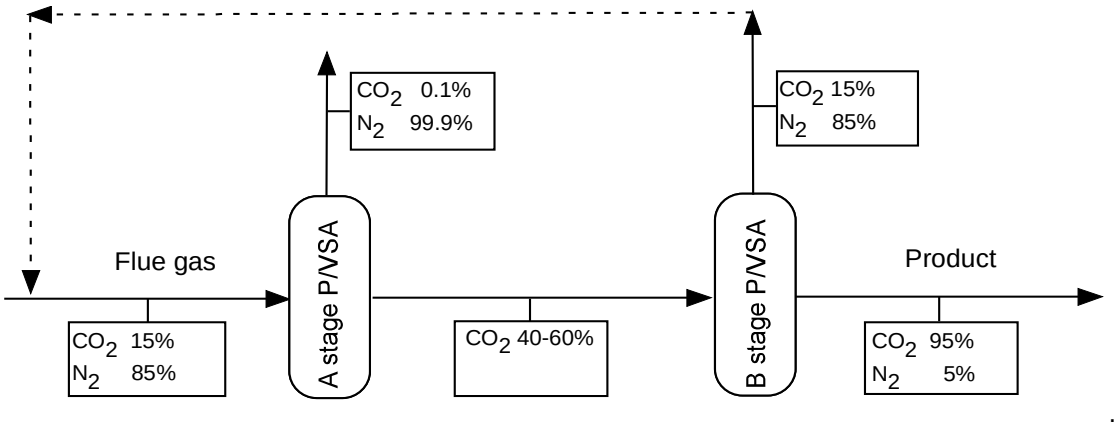

Figure 4.13. Flow chart of an integrated two-stage P/VSA process.

Table 4.7. Performance comparison of two successive P/VSA units reported in the literature.

two-stage P/VSA configuration	adsorbents	cycle time, s	P_{feed}, bar	P_{blow}, bar	CO_2 Purity, %	CO_2 Recovery, %	CO_2 Productivity, (mol CO_2/Kg·h)	Energy, (MJ/Kg CO_2)	Reference
3-bed 5-step/ 2-bed 6-step	5A-5A	900-860	1.50-1.50	0.10-0.15	96.05	91.05	0.33	0.65	(Liu *et al.,* 2011)
3-bed 5-step/ 2-bed 6-step	13XAPG-13XAPG	900-860	1.50-1.50	0.10-0.10	96.54	93.35	0.71	0.53	(Wang *et al.,* 2012)
2-bed 4-step/ 2-bed 5-step	AC-AC	560-620	1.30-3.45	0.10-0.10	95.29	74.36	0.85	0.72	(Shen *et al.,* 2012)
3-bed 8-step/ 2-bed 6-step	13X-AC	780-560	1.16-1.23	0.08-0.20	95.60	90.20	-	2.44	(Wang *et al.,* 2013a)
3-bed 5-step/ 2-bed 5-step	5A-5A	2106-1760	1.00-2.00	0.10-0.10	95.10	90.14	-	-	(Riboldi and Bolland, 2015)
1-bed 4-step/ 1-bed 4-step	CMS-CMS	443-412	1.00-1.00	0.04-0.07	90.00	89.94	-	0.96	(Haghpanah *et al.,* 2014)
1-bed 4-step/ 1-bed 4-step	13X-13X	1113-806	1.49-2.76	0.10-0.13	95.00	90.00	0.49	1.13	(Leperi *et al.,* 2016)
2-bed 6-step/ 2-bed 5-step	13X-13X	240-240	1.10-1.33	0.10-0.10	95.46	90.12	2.67	0.63	**This study**
2-bed 6-step/ 2-bed 5-step	13X-MgMOF74	240-240	1.10-2.24	0.10-0.10	97.57	90.16	3.09	0.70	**This study**

4.5. Concluding remarks

In this chapter an integrated two-stage P/VSA process for CO_2 capture from dry flue gas has been simulated and optimised using the modelling framework in order to obtain CO_2 purity ≥ 95% and CO_2 recovery ≥ 90% at nearly atmospheric feed pressure, without employing deep vacuum desorption. Two different promising adsorbents (zeolite 13X and Mg-MOF-74) have been considered and all possible combinations of them have been examined. Systematic comparative simulations demonstrate that the combination of adsorbents zeolite 13X − Mg-MOF-74 illustrates the best process performance, in terms of CO_2 purity and CO_2 recovery, followed by the use of zeolite 13X at both stages of the integrated two-stage P/VSA process.

As a next step, these two different combinations of adsorbents have been selected for process optimisation studies to minimize the energy consumption for specified minimum requirements in CO_2 purity and CO_2 recovery at nearly atmospheric feed pressures. The resulting CO_2 purity and recovery of the integrated two-stage P/VSA process in both optimisation studies meet the target levels established for both combinations of adsorbents at different pressure conditions thus resulting in different energy requirements and CO_2 productivities. These differences reveal a complex relation between optimal process performance, operating conditions and combinations of adsorbents and cannot be quantified by simple comparison of CO_2/N_2 adsorption isotherms, selectivity data and equilibrium working capacities. The results indicate that the energy requirements of this study are comparable or lower than that in previously studied two-stage P/VSA processes. On the other hand, the optimised process relies on relatively shorter cycle times and thus leads to significantly higher CO_2 productivities compared with all previous literature studies. In summary the proposed optimised integrated two-stage P/VSA process is a promising technology for CO_2 capture due to its relatively lower energy consumption and higher CO_2 productivity. This indicates that from the energy consumption point of view the two-stage P/VSA process may compare favorably with the monoethanolamine (MEA) absorption process.

CHAPTER 5
EVALUATION OF NEW ADSORBENTS

5. Evaluation of potential new adsorbents

5.1. Introduction

The capture capacity is a key property of an adsorbent since, for example, a 1 GW coal fired power plant emits approximately 800-900 tons of CO_2 per hour and the scale of the adsorbent bed unit is inversely proportional to the capture capacity and directly proportional to the cycle time. Nevertheless, as fast cycles are approached, mass and heat transfer limitations become important. Also critical is the rate at which flue gas can be fed through the system and the corresponding pressure drop associated with the adsorbent bed and gas lines. More specifically, in rapid P/VSA processes, very low pressure drops through the adsorbent beds are needed to achieve fast pressurization, pressure equalization and purge/evacuation steps. Since CO_2/N_2 selectivity is equilibrium driven, then the improved adsorbent material must have a small characteristic thickness (or size in the case of beads) to limit macropore mass transfer resistances, but this in turn will increase pressure drop.

It has been previously demonstrated that the CO_2 purity and CO_2 recovery are closely related to the vacuum pressure selected in the P/VSA process. This process constraint imposes a practical limit on the value of Henry's law constant for CO_2, which is essentially the steepness of the CO_2 isotherm at very low pressures, so materials with high absolute capacities may have relatively low working capacities for this species. Furthermore, for post-combustion carbon capture the energy to compress the entire flue gas well above atmospheric pressure would be too high, so a high CO_2 absolute capacity at pressures above atmospheric is useless. The above arguments suggest that an improved adsorbent must not only exhibit high CO_2 capacity and CO_2/N_2 selectivity at atmospheric pressure, but it should also have low to medium Henry's law constant for CO_2. The latter parameter reflects the steepness

of the CO_2 isotherm and from a physicochemical point of view is related to the magnitude of the energy interaction potential and hence the heat of adsorption for CO_2 at the fluid-solid interface.

A large number of promising adsorbents for CO_2 capture are reported almost daily. The assessment of an adsorbent can be done either by the simple visual inspection of the adsorption isotherms of the adsorbent or by the calculation of pure component selectivities. These are poor indicators of process performance which are incorrect and misleading in many cases. Another way in order to have a reliable assessment of an adsorbent is the integrated material and process modelling and simulation which requires detailed knowledge of the P/VSA process. With the development of new adsorbent materials, adsorption technology has become a potential tool for CO_2 capture from flue gases. New adsorbents are typically first synthesized in very small quantities where adsorption isotherms, porosity, density, and surface area can be measured. However, a much larger quantity (several hundred grams) is required to perform breakthrough and lab scale P/VSA experiments and therefore process modelling and simulation plays a critical role in adsorbent evaluation. On the other hand, detailed process modelling is computationally expensive, requiring the solution of a large-scale coupled set of mixed partial differential and algebraic equations (PDAEs) with cyclic boundary conditions.

In this chapter simulation studies have been performed of a single-stage P/VSA process for post-combustion CO_2 capture from dry flue gas, using different degrees of perturbation on the zeolite 13X isotherm in order to study and evaluate potential new zeolite 13X-based adsorbents. Furthermore, process optimisation studies have been performed to minimize energy consumption for specified minimum requirements in CO_2 purity and CO_2 recovery. Optimisation studies are normally performed to improve the performance of a single-stage P/VSA process by identifying the optimal values of several important process variables that control the process.

5.2. Process description

A single-stage P/VSA process for post-combustion CO_2 capture from dry flue gas has been employed. More specifically, a two-bed six-step P/VSA cycle configuration with light product pressurization has been considered. The sequence of the operating steps for the two-bed six-step P/VSA cycle configuration is illustrated in Figure 5.1 and consists of: pressurization with the light product counter-currently (CC), adsorption (Ads), pressure equalization (PED) (co-current depressurization to the other bed), co-current depressurization or blowdown (Blow) to intermediate pressure, counter-current depressurization or evacuation (Evac) to lowest pressure and pressure equalization (PER) (counter-current re-pressurization from the other bed). The interactions between two beds during each operating step are shown in Figure 5.2. Due to potential high pressure of the adsorption step, a pressure equalization step has been employed to save energy. Since the main objective of the process is to obtain the highest possible CO_2 purity (above 95%) and the highest possible CO_2 recovery (above 90%), a light reflux step (N_2 purge) has not been used, since it would dilute the heavy product and decrease the CO_2 purity and a heavy reflux step (CO_2 rinse) has not been used, since it would cause a significant decrease in CO_2 recovery.

In a typical multi-bed configuration, the operating time steps are not independent variables and must be correlated due to the need for synchronization of the beds, although it was recently demonstrated that this constraint can be relaxed using idle times for each bed (Krishnamurthy *et al.,* 2014). The cycle time of the process is fixed at 240s and the operating time steps are fixed as follows: t_{CC}=20s, t_{Ads}=80s, t_{PED}=20s, t_{Blow}=20s, t_{Evac}=80s, t_{PER}=20s. The durations of the operating steps have been selected based on previous simulation studies as follows: $t_{Ads}=4t_{CC}$, $t_{PED}=t_{CC}$, $t_{Blow}=t_{CC}$, $t_{Evac}=t_{Ads}$, $t_{PER}=t_{PED}$. Specific attention has been placed in order to take into account the time interactions between two beds during each operating step. More specifically, the dry flue gas (85% N_2, 15% CO_2) mixture has been considered to be available at 0.128 lt/s_stp flowrate, 1.46 bar pressure and 313 K temperature. The blowdown pressure has been set to 0.11 bar, the evacuation pressure has been 0.015 bar and the length to diameter ratio has been 8.72 in all simulation studies.

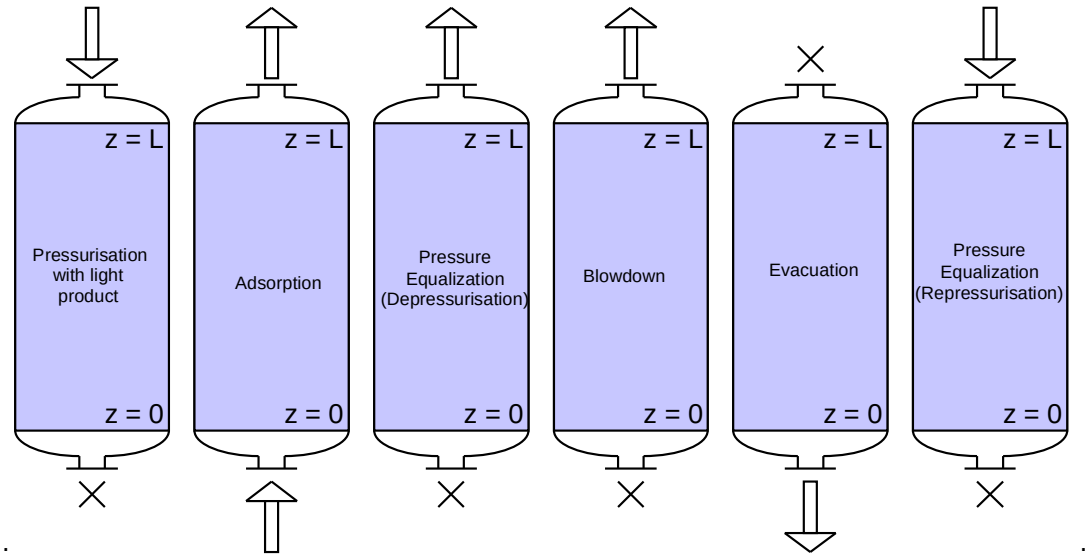

Figure 5.1. Sequence of operating steps for the two-bed six-step P/VSA cycle configuration.

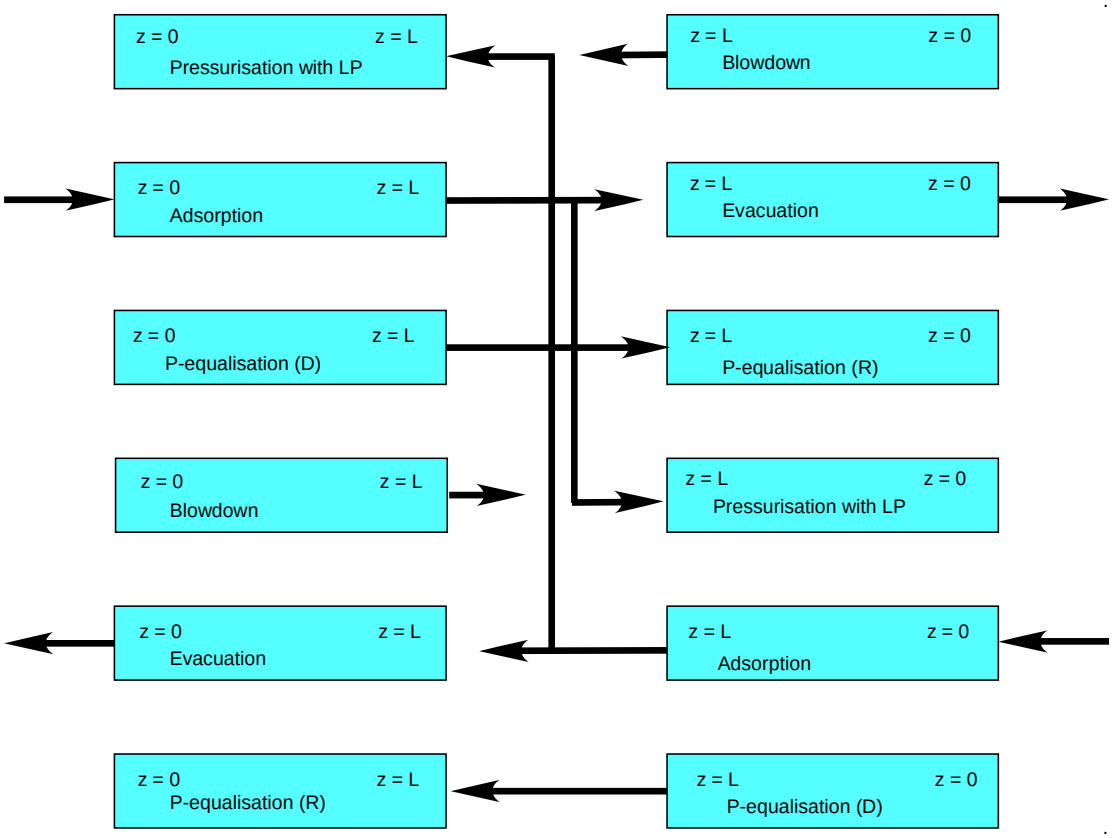

Figure 5.2. Interactions between two beds during each operating step.

5.3. Formulation of the optimisation problem

The main objective is to investigate the effect of feed temperature, feed pressure, feed flow rate, blowdown pressure, evacuation pressure, length to diameter ratio, CO_2 perturbation factor and N_2 perturbation factor of the dual-site Langmuir isotherm parameters on the overall process performance. Hence, the optimisation problem can be formulated as the minimization of energy consumption for specified minimum requirements in CO_2 purity and CO_2 recovery, while optimising the above process variables. Cycle time, operating step durations, bed volume and gas valve constants are kept constant in all cases under consideration for different feed temperatures:

$$\text{min. energy consumption} \tag{5.1}$$

$$\text{s. t. model equations}$$

$$CO_2 \text{ purity} \geq 95\%$$

$$CO_2 \text{ recovery} \geq 90\%$$

$$1.1 \text{ bar} \leq P_{feed} \leq 2.0 \text{ bar}$$

$$0.05 \text{ lt/s\_stp} \leq F_{feed} \leq 0.50 \text{ lt/s\_stp}$$

$$0.11 \text{ bar} \leq P_{blow} \leq 0.50 \text{ bar}$$

$$0.015 \text{ bar} \leq P_{evac} \leq 0.10 \text{ bar}$$

$$3.24 \leq L/D \leq 22.72$$

$$1.0 \leq P_{factor\_CO2} \leq 1.4$$

$$0.6 \leq P_{factor\_N2} \leq 1.0$$

The above dynamic optimisation problem has been formulated and solved in the gPROMS™ modelling environment (PSE, 2011).

5.4. Results and discussion

5.4.1. Comparison and evaluation of potential new adsorbents

In the present study, the choice of the adsorbent material packed in a single-stage P/VSA capture unit, has not been based on a simple comparison of CO_2/N_2 adsorption isotherms and working capacities of the potential adsorbents. For the precise choice of adsorbent, both the competitive adsorption equilibrium and the adsorption/desorption kinetics should be taken into account. More specifically, zeolite 13X has been considered as a representative of the zeolite group, which has been studied for more than two decades and it is the current benchmark commercial adsorbent for CO_2 capture. Most zeolites have a very strong adsorption affinity for CO_2 and therefore have nonlinear adsorption isotherms, relatively high CO_2 adsorption capacities and high CO_2/N_2 selectivity at low partial pressures. Commercial zeolite adsorbents are always bound together with clay or alumina to form a pellet or bead, which is a composite structure that contains both macropores and micropores. Hence, the overall mass transfer in zeolites is controlled by a combination of different diffusion mechanisms. Zeolite 13X beads appears to have large pore dimensions to limit mass transfer resistances, thermal stability, mechanical stability, and recyclability. The diffusion of CO_2 in commercial zeolite 13X beads appears to be macropore controlled (Ling *et al.,* 2015). The parameters of the dual-site Langmuir adsorption isotherm and the isosteric heats of adsorption of CO_2 and N_2 on zeolite 13X have been adopted from the work of Ko *et al.,* (2005) and are summarized in Table 5.1. The physical properties of zeolite 13X have been adopted also from the work of Ko *et al.,* (2005) and are presented in Table 5.2. All the parameters required for process modelling, simulation and optimisation studies of the P/VSA process are listed in Table 5.3.

Simulation studies have been performed using different degrees of perturbation on the zeolite 13X isotherm (modified zeolite 13X-based adsorbent) in order to study and evaluate potential new zeolite 13X-based adsorbents and compare them. The physical properties (density, heat capacity) and the saturation capacities of CO_2 and N_2 of the modified zeolite 13X-based adsorbent have been taken identical to that of

zeolite 13X. The adsorption isotherms of CO_2 with different degrees of perturbation on the zeolite 13X isotherm at T=313 K are illustrated in Figure 5.3, while the adsorption isotherms of N_2 with different degrees of perturbation on the zeolite 13X isotherm at T=313 K are shown in Figure 5.4. The proposed modelling framework has been applied to estimate process performance indicators (CO_2 purity, CO_2 recovery, CO_2 productivity and energy requirements) employing different degrees of perturbation on the zeolite 13X isotherm in a single-stage P/VSA process. More specifically, three different process simulation studies have been performed using the following degrees of perturbation on the zeolite 13X isotherm: (I) CO_2 and N_2 perturbation on the zeolite 13X isotherm, (II) N_2 perturbation without CO_2 perturbation on the zeolite 13X isotherm and (III) CO_2 perturbation without N_2 perturbation on the zeolite 13X isotherm. The simulation results illustrating the effect of various degrees of CO_2 and N_2 perturbation on the zeolite 13X isotherm on process performance indicators are summarized in Table 5.4 and also illustrated in Figures 5.5 and 5.6. The simulation results illustrating the effect of various degrees of N_2 perturbation without CO_2 perturbation on the zeolite 13X isotherm on process performance indicators are summarized in Table 5.5 and also illustrated in Figures 5.7 and 5.8. Finally, the simulation results illustrating the effect of various degrees of CO_2 perturbation without N_2 perturbation on the zeolite 13X isotherm on process performance indicators are summarized in Table 5.6 and also illustrated in Figures 5.9 and 5.10. The results of the comparison of different degrees of perturbation on the zeolite 13X isotherm clearly indicate that a positive CO_2 perturbation on the zeolite 13X isotherm, as well as a negative N_2 perturbation on the zeolite 13X isotherm lead to an increase of the CO_2 purity with a corresponding decrease in the CO_2 recovery. The simulation results also reveal that a positive CO_2 perturbation on the zeolite 13X isotherm and a negative N_2 perturbation on the zeolite 13X isotherm result in a decrease of the energy requirements and CO_2 productivity as well. Therefore, for more efficient CO_2 capture, it is crucial to develop new adsorbent materials with an increased CO_2 adsorption capacity and a decreased N_2 adsorption capacity in the meantime. This study is useful for material developers who want to demonstrate the potential of a new adsorbent for a P/VSA process. The development of new adsorbent materials should focus on reduction in N_2 capacity

(as it has relatively a higher impact on CO_2 purity) rather than on increase in CO_2 capacity.

It is important to note that all simulation studies do not meet the target levels established for all potential new adsorbents resulting from different degrees of perturbation on the zeolite 13X isotherm (modified zeolite 13X-based adsorbents). Hence, in the remaining part of this study the optimisation studies will be focused on the investigation of more promising potential new adsorbent materials in order to find the optimal CO_2 and N_2 perturbation factors on the 13X zeolite isotherm while minimizing energy consumption for specified minimum requirements in CO_2 purity and CO_2 recovery of a single-stage P/VSA process.

Table 5.1. Parameters of the dual-site Langmuir adsorption isotherm and isosteric heats of adsorption of zeolite 13X.

	zeolite 13X (Ko *et al.*, 2005)		
	CO_2 (i = 1)	**N_2 (i = 2)**	**units**
$k_{1,i(1)}$	2.82	1.89	mol/Kg
$k_{2,i(1)}$	-3.50E-04	-2.25E-04	1/K
$k_{3,i(1)}$	2.83E-09	1.16E-09	1/Pa
$k_{4,i(1)}$	2598.20	1944.61	K
$k_{1,i(2)}$	3.97	1.89	mol/Kg
$k_{2,i(2)}$	-4.95E-03	-2.25E-04	1/K
$k_{3,i(2)}$	4.41E-09	1.16E-09	1/Pa
$k_{4,i(2)}$	3594.07	1944.61	K
$\Delta H_{ads\,(i)}$	-21601.5	-16167.5	J/mol

Table 5.2. Physical properties of zeolite 13X.

Physical property	**zeolite 13X** (Ko *et al.*, 2005)	**units**
adsorbent density (ρ^s)	1870	kg/m^3
particle density (ρ^p)	1159.4	kg/m^3
heat capacity of particles ($C_p^{\,p}$)	504	$J/(kg{\cdot}K)$

Table 5.3. Parameters used in simulation and optimisation studies of the P/VSA process.

parameter	**value**
pore radius (R_{pore})	0.5×10^{-9} m
particle radius (R_p)	1.0×10^{-3} m
particle tortuosity (τ_p)	4.5
particle porosity (ε_p)	0.38
adsorption bed porosity (ε_{bed})	0.348
universal gas constant (R)	8.314 J/(mol·K)
heat transfer coefficient of wall ($k_{h,wall}$)	60 $J/(m^2{\cdot}K{\cdot}s)$
effective diffusivity of CO_2 ($D_{e,CO2}$)	1.087×10^{-8} m^2/s
effective diffusivity of N_2 ($D_{e,N2}$)	1.363×10^{-8} m^2/s

Table 5.4. Effect of CO_2 and N_2 perturbation on the zeolite 13X isotherm on process performance indicators.

CO_2 perturbation, %	N_2 perturbation, %	P_{factor_CO2}	P_{factor_N2}	CO_2 Purity, %	CO_2 Recovery, %	CO_2 Productivity, (mol CO_2/Kg.h)	Energy, (MJ/Kg CO_2)
-20	-20	0.80	0.80	97.97	88.90	13.04	0.96
-15	-15	0.85	0.85	97.26	89.06	13.06	0.97
-10	-10	0.90	0.90	96.55	89.46	13.09	0.98
-5	-5	0.95	0.95	95.77	89.96	13.11	1.00
0	0	1.00	1.00	95.00	90.00	13.12	1.03
5	5	1.05	1.05	94.05	90.23	13.14	1.05
10	10	1.10	1.10	92.49	90.42	13.15	1.08

Table 5.5. Effect of N_2 perturbation on the zeolite 13X isotherm on process performance indicators.

CO_2 perturbation, %	N_2 perturbation, %	P_{factor_CO2}	P_{factor_N2}	CO_2 Purity, %	CO_2 Recovery, %	CO_2 Productivity, (mol CO_2/Kg.h)	Energy, (MJ/Kg CO_2)
0	-30	1.00	0.70	98.23	89.59	13.07	0.94
0	-20	1.00	0.80	97.81	89.55	13.06	0.95
0	-10	1.00	0.90	96.91	89.62	13.07	0.98
0	0	1.00	1.00	95.00	90.00	13.12	1.03
0	10	1.00	1.10	88.58	91.08	13.29	1.15

Table 5.6. Effect of CO_2 perturbation on the zeolite 13X isotherm on process performance indicators.

CO_2 perturbation, %	N_2 perturbation, %	P_{factor_CO2}	P_{factor_N2}	CO_2 Purity, %	CO_2 Recovery, %	CO_2 Productivity, (mol CO_2/Kg.h)	Energy, (MJ/Kg CO_2)
-20	0	0.80	1.00	94.00	90.70	13.30	1.06
-10	0	0.90	1.00	94.19	90.35	13.20	1.05
0	0	1.00	1.00	95.00	90.00	13.12	1.03
10	0	1.10	1.00	96.00	89.24	13.02	1.00
20	0	1.20	1.00	96.52	89.00	12.98	0.99
30	0	1.30	1.00	97.02	88.99	12.98	0.97

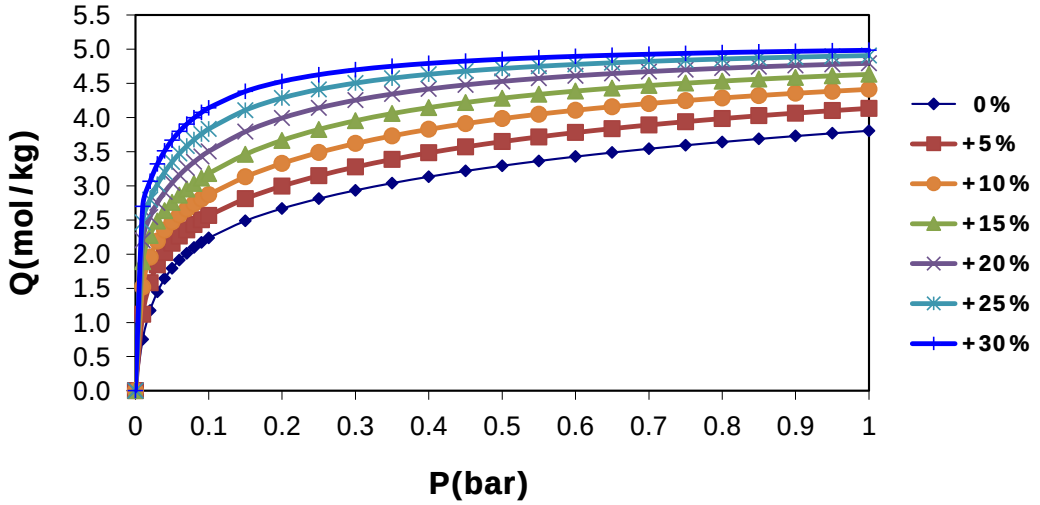

Figure 5.3. Adsorption isotherms of CO_2 with perturbations on the zeolite 13X isotherm at T=313 K.

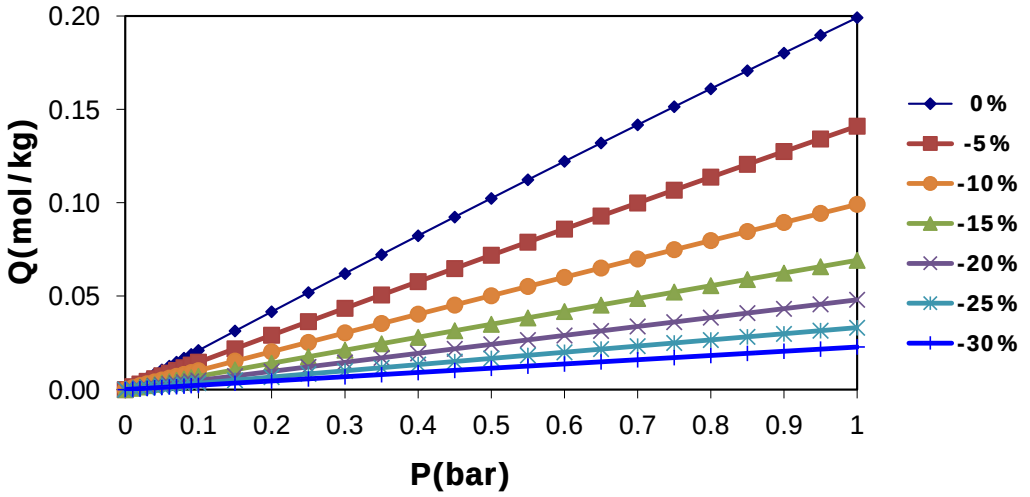

Figure 5.4. Adsorption isotherms of N_2 with perturbations on the zeolite 13X isotherm at T=313 K.

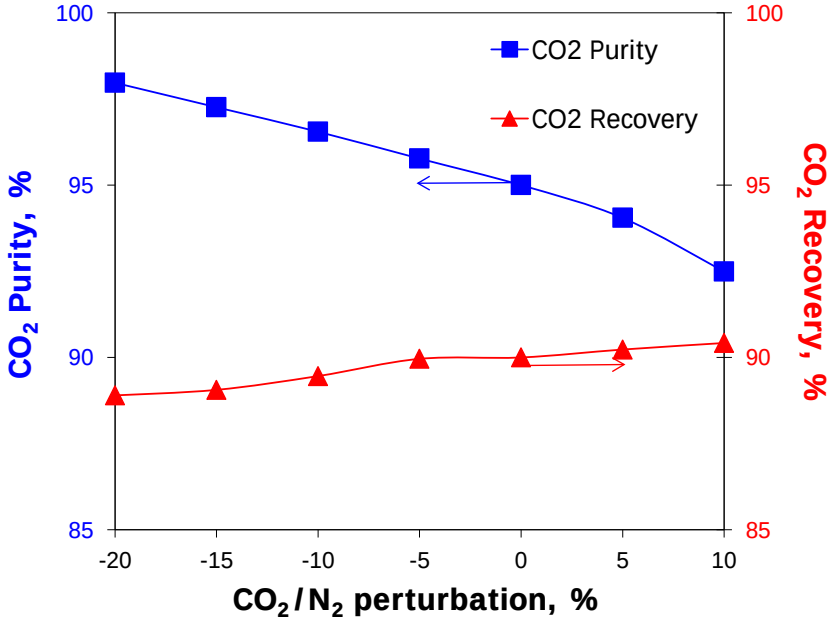

Figure 5.5. Effect of CO_2 and N_2 perturbation on the zeolite 13X isotherm on CO_2 purity and CO_2 recovery.

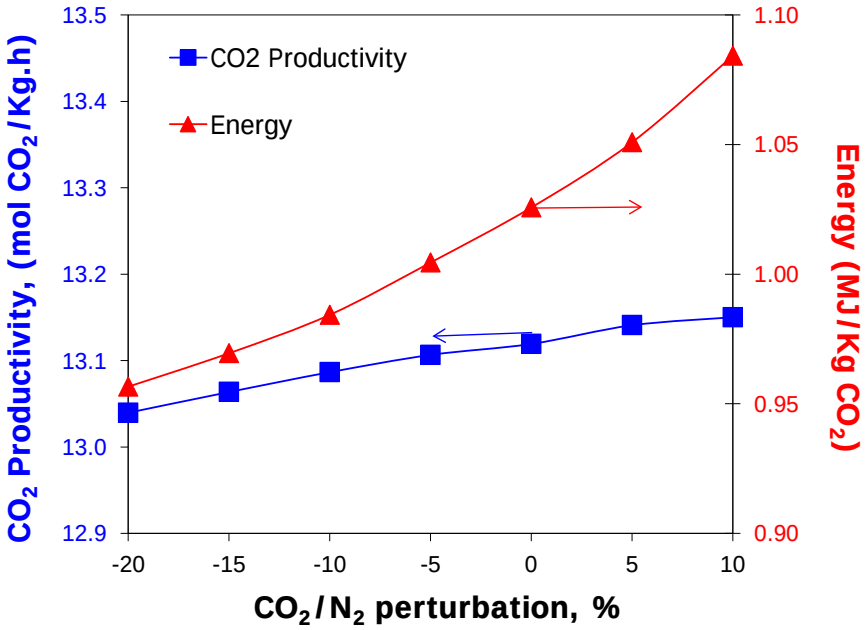

Figure 5.6. Effect of CO_2 and N_2 perturbation on the zeolite 13X isotherm on CO_2 productivity and energy requirements.

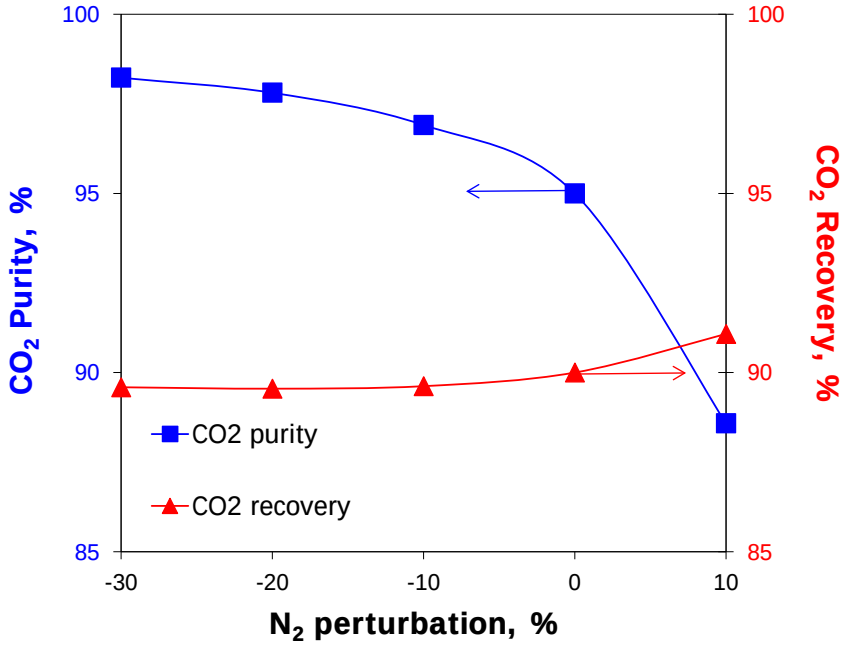

Figure 5.7. Effect of N_2 perturbation on the zeolite 13X isotherm on CO_2 purity and CO_2 recovery.

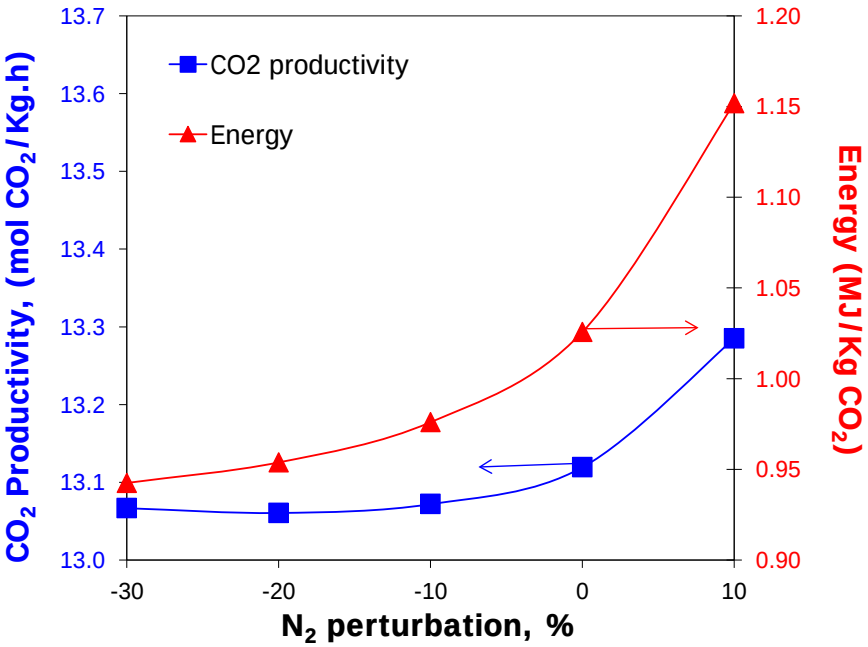

Figure 5.8. Effect of N_2 perturbation on the zeolite 13X isotherm on CO_2 productivity and energy requirements.

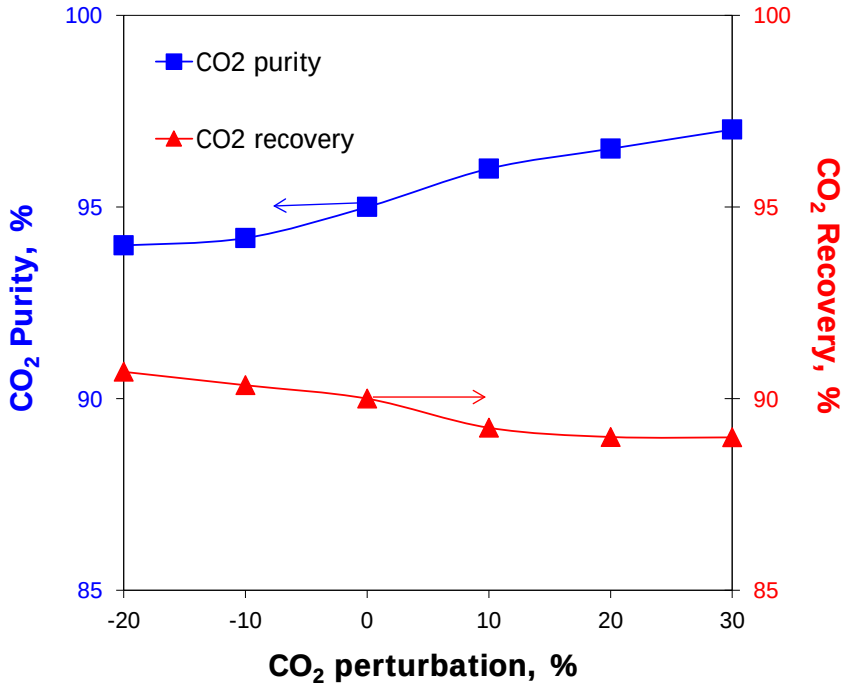

Figure 5.9. Effect of CO_2 perturbation on the zeolite 13X isotherm on CO_2 purity and CO_2 recovery.

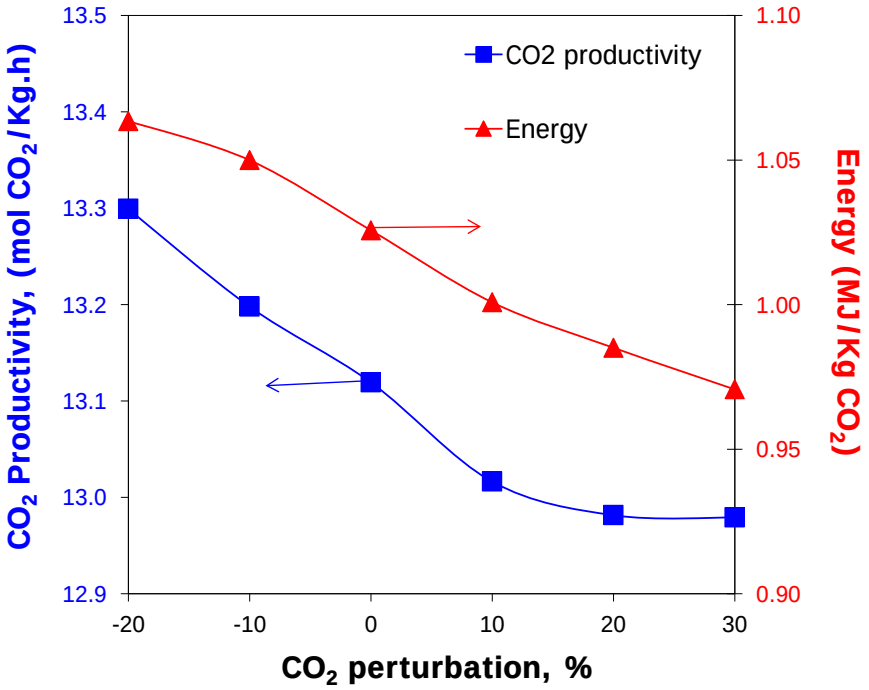

Figure 5.10. Effect of CO_2 perturbation on the zeolite 13X isotherm on CO_2 productivity and energy requirements.

5.4.2. Optimisation studies

Since the use of zeolite 13X and modified zeolite 13X-based adsorbents resulting from perturbation on the 13X zeolite isotherm have shown some promising features as potential candidates for CO_2 capture, it would be interesting to further improve the process performance characteristics and minimize energy consumption for specified minimum requirements in CO_2 purity and CO_2 recovery. A single-stage P/VSA process as described in section 5.2 above has been optimised for two different cases: case I employing zeolite 13X and case II with the modified zeolite 13X-based adsorbent, based on the optimisation strategy presented in section 5.3. The optimisation results of cases I and II are summarized in Tables 5.7 and 5.8, respectively. The effect of feed temperature on optimal CO_2 purity, CO_2 recovery and energy requirements of cases I and II is graphically illustrated in Figures 5.11 and 5.12, respectively. In case II, the optimal CO_2 perturbation factor of the dual-site Langmuir isotherm parameters of zeolite 13X is 1.30, while the optimal N_2 perturbation factor of the dual-site Langmuir isotherm parameters of zeolite 13X is 0.70. The corresponding optimal parameters of the dual-site Langmuir adsorption isotherm and isosteric heats of adsorption of the new adsorbent material (modified zeolite 13X-based adsorbent) of case II are summarized in Table 5.9. The adsorption isotherms of CO_2 and N_2 on zeolite 13X and modified zeolite 13X-based adsorbent at T=313 K are illustrated in Figure 5.13. The results of the optimisation studies reveal that the minimum target of 95% in CO_2 purity and 90% in CO_2 recovery is met for a single-stage P/VSA process, for both potential adsorbents. It is important to note that the modified zeolite 13X-based adsorbent has lower energy requirements (around 10%) than zeolite 13X, as illustrated in Figures 5.11 and 5.12. This can be attributed mainly to the need for lower blowdown and evacuation pressures when working with zeolite 13X (around 0.11 and 0.015 bar, respectively) as opposed to the modified zeolite 13X-based adsorbent (around 0.50 and 0.030 bar, respectively). These differences in the optimal desorption pressures are related to differences in the CO_2 adsorption isotherm steepness and the CO_2/N_2 selectivity at low partial pressures for each adsorbent.

Table 5.7. Optimisation results of case I (zeolite 13X).

T_{feed}, K	P_{blow}, bar	P_{evac}, bar	P_{feed}, bar	F_{feed}, lt/s_stp	L/D	P_{factor_CO2}	P_{factor_N2}	CO_2 Purity, %	CO_2 Recovery, %	CO_2 Productivity, ($molCO_2/Kg.h$)	Energy, ($MJ/KgCO_2$)
298	0.11	0.015	1.46	0.128	8.72	1.00	1.00	95.00	90.00	13.10	1.00
313	0.11	0.015	1.46	0.128	8.72	1.00	1.00	95.00	90.00	13.12	1.03
323	0.11	0.015	1.47	0.129	8.72	1.00	1.00	95.45	90.00	13.16	1.05
333	0.11	0.015	1.49	0.129	8.72	1.00	1.00	95.90	90.00	13.19	1.08

Table 5.8. Optimisation results of case II (modified zeolite 13X-based adsorbent).

T_{feed}, K	P_{blow}, bar	P_{evac}, bar	P_{feed}, bar	F_{feed}, lt/s_stp	L/D	P_{factor_CO2}	P_{factor_N2}	CO_2 Purity, %	CO_2 Recovery, %	CO_2 Productivity, ($molCO_2/Kg.h$)	Energy, ($MJ/KgCO_2$)
298	0.50	0.030	1.75	0.105	3.24	1.30	0.70	95.61	90.00	10.72	0.89
313	0.50	0.030	1.75	0.105	3.24	1.30	0.70	95.63	90.00	10.73	0.93
323	0.50	0.030	1.76	0.107	3.24	1.30	0.70	95.80	90.00	10.94	0.97
333	0.50	0.030	1.77	0.107	3.24	1.30	0.70	95.90	90.00	10.96	1.00

Table 5.9. Parameters of the dual-site Langmuir adsorption isotherm and isosteric heats of adsorption of new adsorbent material (modified zeolite 13X-based adsorbent).

	modified zeolite 13X-based adsorbent		
	CO_2 (i = 1)	**N_2 (i = 2)**	**units**
$k_{1,i(1)}$	2.82	1.89	mol/Kg
$k_{2,i(1)}$	-3.50E-04	-2.25E-04	1/K
$k_{3,i(1)}$	3.68E-09	8.14E-10	1/Pa
$k_{4,i(1)}$	3377.66	1361.22	K
$k_{1,i(2)}$	3.97	1.89	mol/Kg
$k_{2,i(2)}$	-4.95E-03	-2.25E-04	1/K
$k_{3,i(2)}$	5.73E-09	8.14E-10	1/Pa
$k_{4,i(2)}$	4672.29	1361.22	K
$\Delta H_{ads\ (i)}$	-28081.9	-11317.2	J/mol

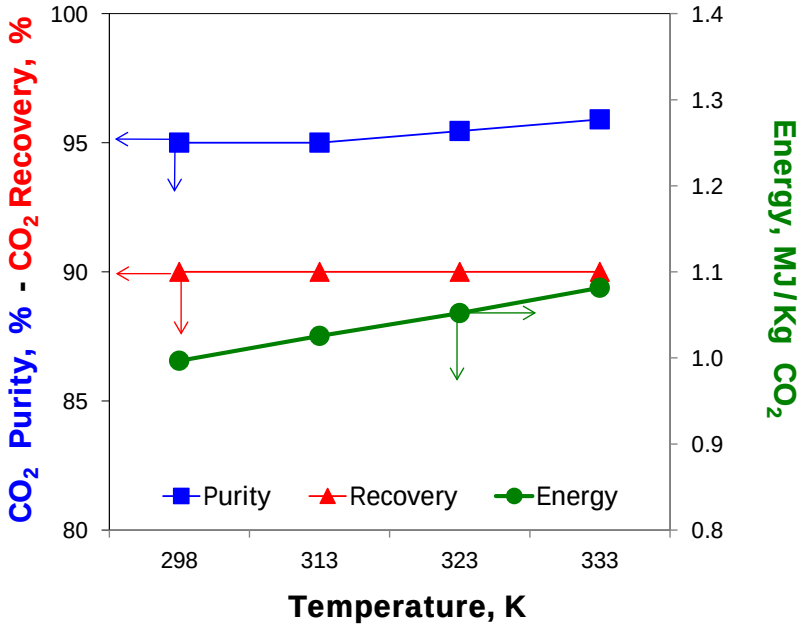

Figure 5.11. Effect of feed temperature on optimal CO_2 purity, CO_2 recovery and energy requirements of case I (zeolite 13X).

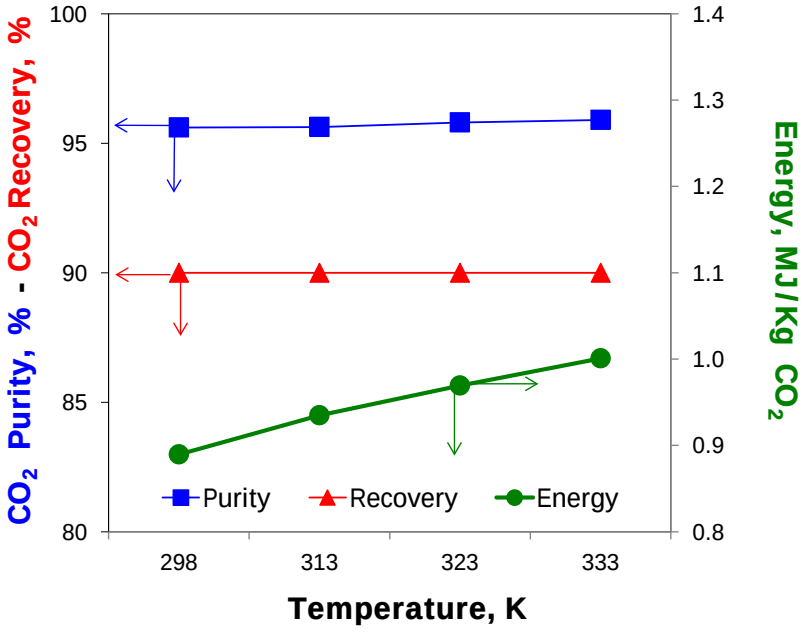

Figure 5.12. Effect of feed temperature on optimal CO_2 purity, CO_2 recovery and energy requirements of case II (modified zeolite 13X-based adsorbent).

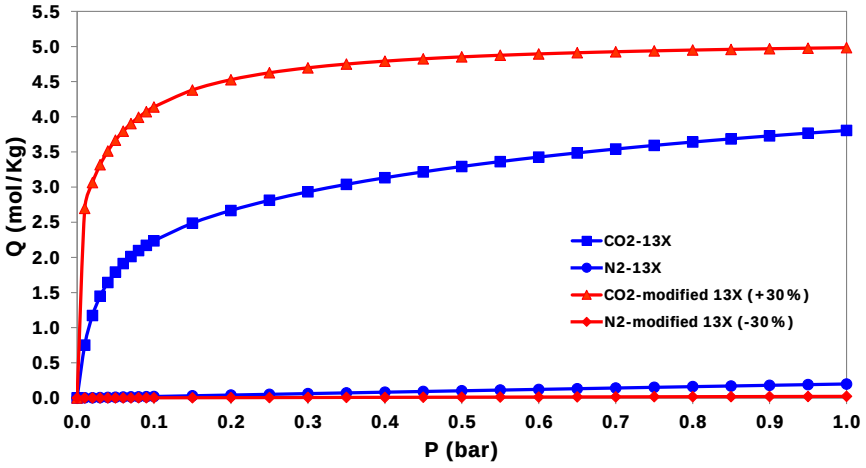

Figure 5.13. Adsorption isotherms of CO_2 and N_2 on zeolite 13X and modified zeolite 13X-based adsorbent at T=313 K.

It should be noted that the performance of a P/VSA process is not only determined by the adsorbent employed for the separation but also affected by the process engineering design. The most challenging process engineering design is the decision of a cycle configuration and operating conditions (Ling *et al.,* 2015). Evidently, further work must be done to explore in detail the effect of other process variables including the duration of operating steps and overall cycle time, adsorbent bed geometry, more complex cycle configurations, etc.

5.4. Concluding remarks

In this chapter a single-stage P/VSA process for CO_2 capture from dry flue gas has been simulated and optimised in order to study and evaluate potential new adsorbents. First zeolite 13X, the current benchmark commercial adsorbent for CO_2 capture has been considered. The proposed modelling framework has been used to study and evaluate potential new adsorbents resulting from perturbation on the 13X zeolite isotherm. The results from systematic comparative simulation studies reveal that a modified zeolite 13X-based adsorbent material appears to lead to a better process performance compared with the original zeolite 13X.

As a next step, zeolite 13X and the modified zeolite 13X-based adsorbent have been selected for process optimisation studies. The objective has been to minimize energy consumption for specified minimum requirements in CO_2 purity and CO_2 recovery. The results indicate that the targets are met for both potential adsorbents resulting in different energy requirements and CO_2 productivities. The proposed optimised modified zeolite 13X-based adsorbent seems to be a promising adsorbent material for CO_2 capture because of its relatively lower energy consumption comparing with that of the original zeolite 13X. This is due to higher blowdown and evacuation pressure levels which can be potential implemented in industrial practice.

Finally, it is important to note the complex relations between optimal process performance, operating conditions and adsorbents design, which cannot be quantified by a simple comparison of CO_2/N_2 adsorption isotherms, selectivity data and equilibrium working capacities. Evidently, detailed process modelling, simulation and optimisation, provide the most reliable and robust way to evaluate both qualitatively and quantitatively potential new adsorbents of a single-stage P/VSA process for efficient CO_2 capture. It is clear that, the modelling framework can also help process and material engineers to study, evaluate, design and develop new tailor-made adsorbent materials engineered for enhanced CO_2 separation.

CHAPTER 6
CONCLUSIONS & FUTURE DIRECTIONS

6. Conclusions and future directions

6.1. Conclusions

A mathematical modelling framework has been developed for the simulation and optimisation of PSA/VSA processes for post-combustion CO_2 capture from dry flue gas. The core of the modelling framework represents a detailed adsorbent bed model relying on a coupled set of mixed partial differential and algebraic equations (PDAEs) for mass, heat and momentum balance at both bulk gas and particle level, equilibrium isotherm equations, transport and thermo-physical properties of the gas mixture and boundary conditions according to the operating steps. The proposed modelling equations have been implemented in the gPROMS™ modelling environment.

The modelling framework has been validated against experimental and simulation data available from the literature. Model predictions are in good agreement in terms of several process performance indicators. Furthermore, a systematic parametric analysis has been performed to provide significant insight into the most critical design and operating parameters, and their effect on the process performance indicators. In addition, by reviewing the results of the parametric analysis it is possible to gain an intuitive understanding of the relations between factors that affect process performance.

A dynamic optimisation framework has been used to optimise a PSA/VSA process using zeolite 13X as adsorbent. The effect of multi-bed PSA/VSA configurations on the separation quality has been studied. The developed modelling framework has been used for a comparative evaluation of three available potential adsorbents for CO_2 capture, namely, zeolite 13X, activated carbon and Mg-MOF-74. Systematic comparative simulations demonstrate that zeolite 13X illustrates the best process performance among the three adsorbents, in terms of CO_2 purity and CO_2 recovery.

On the other hand, Mg-MOF-74 appears to be a promising adsorbent for CO_2 capture, as it has considerably higher CO_2 productivity compared to the other two adsorbents.

As a next step, zeolite 13X and Mg-MOF-74 have been selected for process optimisation to minimize energy consumption for specified minimum requirements in CO_2 purity and recovery at nearly atmospheric feed pressures. The optimisation results indicate that the minimum target of 90% in CO_2 purity and 90% in CO_2 recovery is met for the VSA process for both adsorbents. However, zeolite 13X illustrates lower energy requirements than Mg-MOF-74 and this can be attributed mainly to the need for lower desorption (blowdown and evacuation) pressures when working with Mg-MOF-74 as opposed to zeolite 13X. The differences in the optimal desorption pressures can be related to differences in the structure of CO_2/N_2 adsorption isotherms at low pressures for each adsorbent, at different temperatures, revealing a complex relationship between optimal process performance indicators and operating conditions that varies among different adsorbents.

Furthermore, an integrated two-stage P/VSA process for CO_2 capture from dry flue gas has been simulated and optimised using the modelling framework in order to obtain CO_2 purity ≥ 95% and CO_2 recovery ≥ 90% at nearly atmospheric feed pressure, without employing deep vacuum desorption. Two different promising adsorbents (zeolite 13X and Mg-MOF-74) have been considered and all possible combinations of them have been examined. Systematic comparative simulations demonstrate that the combination of adsorbents zeolite 13X − Mg-MOF-74 illustrates the best process performance, in terms of CO_2 purity and CO_2 recovery, followed by the use of zeolite 13X at both stages of the integrated two-stage P/VSA process.

As a next step, these two different combinations of adsorbents have been selected for process optimisation studies to minimize the energy consumption for specified minimum requirements in CO_2 purity and CO_2 recovery at nearly atmospheric feed pressures. The resulting CO_2 purity and recovery of the integrated two-stage P/VSA process in both optimisation studies meet the target levels established for both combinations of adsorbents at different pressure conditions thus resulting in

different energy requirements and CO_2 productivities. These differences reveal a complex relation between optimal process performance, operating conditions and combinations of adsorbents and cannot be quantified by simple comparison of CO_2/N_2 adsorption isotherms, selectivity data and equilibrium working capacities. The results indicate that the energy requirements of this study are comparable or lower than that in previously studied two-stage P/VSA processes. On the other hand, the optimised process relies on relatively shorter cycle times and thus leads to significantly higher CO_2 productivities compared with all previous literature studies. In summary the proposed optimised integrated two-stage P/VSA process is a promising technology for CO_2 capture due to its relatively lower energy consumption and higher CO_2 productivity. This indicates that from the energy consumption point of view the two-stage P/VSA process may compare favorably with the monoethanolamine (MEA) absorption process.

Finally, a single-stage P/VSA process for CO_2 capture from dry flue gas has been simulated and optimised in order to study and evaluate potential new adsorbents. First zeolite 13X, the current benchmark commercial adsorbent for CO_2 capture has been considered. The proposed modelling framework has been used to study and evaluate potential new adsorbents resulting from perturbation on the 13X zeolite isotherm. The results from systematic comparative simulation studies reveal that a modified zeolite 13X-based adsorbent material appears to lead to a better process performance compared with the original zeolite 13X.

Then, zeolite 13X and the modified zeolite 13X-based adsorbent have been selected for process optimisation studies. The objective has been to minimize energy consumption for specified minimum requirements in CO_2 purity and CO_2 recovery. The results indicate that the targets are met for both potential adsorbents resulting in different energy requirements and CO_2 productivities. The proposed optimised modified zeolite 13X-based adsorbent seems to be a promising adsorbent material for CO_2 capture because of its relatively lower energy consumption comparing with that of the original zeolite 13X. This is due to higher blowdown and evacuation pressure levels which can be potential implemented in industrial practice.

This thesis illustrates also the complex relations between optimal process performance, operating conditions and adsorbents design, which cannot be

quantified by a simple comparison of CO_2/N_2 adsorption isotherms, selectivity data and equilibrium working capacities. Evidently, detailed process modelling, simulation and optimisation, provide the most reliable and robust way to evaluate both qualitatively and quantitatively potential new adsorbents of a single-stage P/VSA process and potential combinations of adsorbents of an integrated two-stage P/VSA process for efficient CO_2 capture. It is clear that, the modelling framework can also help process and material engineers to study, evaluate, design and develop new tailor-made adsorbent materials engineered for enhanced CO_2 separation.

6.2. Main contributions of this work

In summary, the main contributions of this thesis have been:

- A mathematical modelling and optimisation framework of P/VSA processes for post-combustion CO_2 capture from dry flue gas has been developed in the gPROMS™ modelling environment.
- Application of the modelling and optimisation framework on both single-stage and integrated two-stage P/VSA processes. Key operating and design variables have been systematically optimised using recent advances on dynamic process optimisation.
- The developed modelling and optimisation framework has been employed for a comparative study of available potential adsorbents, as well as for the evaluation of a novel adsorbent from the family of metal organic frameworks (MOFs).
- The proposed modelling and optimisation framework has been used to study potential new modified zeolite 13X-based adsorbents for more efficient CO_2 capture and evaluate the effect of new adsorbents on the process performance.

6.3. Recommendations for future directions

A range of issues requiring further investigation have been revealed in the course of this work. In particular,

- The synthesis of the P/VSA processes using process systems engineering approach. Here, it would be interesting to consider the application of advanced mixed-integer dynamic optimisation techniques for the integrated synthesis problems in which the number of beds along with their optimal operating schedule (optimal sequence of operating steps) would be optimally defined. This approach would not require a priory statement of the P/VSA cycle configuration and it will automatically define the optimal flowsheet of the P/VSA process.
- The integrated design and control of the P/VSA process. Here, the application of integrated design and control approaches would offer significant opportunities to explore the synergistic benefits between process design and control in view of designing both operable and economically attractive P/VSA processes under uncertainty, disturbances and tight operating constraints.
- A technoeconomic assessment of the single-stage P/VSA process. It would be valuable to perform a technoeconomic assessment of the P/VSA process and analyze the trade-offs between capital and operating costs and separation quality of the P/VSA process.
- A technoeconomic comparison of the integrated two-stage P/VSA process with the competitive monoethanolamine (MEA) absorption process. Although from the energy consumption point of view the two-stage P/VSA process may compare favorably with the MEA absorption process, the footprint of the two-stage P/VSA process is typically much larger than that of the MEA absorption system and further studies are required before general comparative conclusions are made.
- The description of the impact of the perturbation of the zeolite 13X isotherm on the physicochemical and/or structural characteristics of the modified zeolite 13X-based adsorbent. It would be interesting to perform detailed molecular simulations that would target on getting the perturbated

isotherms and this could be a subject of a future study as it requires a combination of experimental and theoretical work at the molecular level.

REFERENCES

References

Aaron D., Tsouris C., 2005. Separation of CO_2 from flue gas: A review. *Sep. Sci. Techol.* 40, 321-348.

Abanades J. C., Arias B., Lyngfelt A., Mattisson T., Wiley D. E., Li H., Ho M. T., Mangano E., Brandani S., 2015. Emerging CO_2 capture systems. *Int. J. Greenhouse Gas Control*, 40, 126-166.

Agarwal A., 2010. Advanced Strategies for Optimal Design and Operation of Pressure Swing Adsorption Processes. *PhD Thesis, Department of Chemical Engineering Carnegie Mellon Pittsburgh*.

Agarwal A., Biegler L.T., Zitney S.E., 2010. A superstructure-based optimal synthesis of PSA cycles for post-combustion CO_2 capture. *AIChE J.* 56, 1813-1828.

Biegler L.T., Jiang L., Fox V.G., 2004. Recent advances in simulation and optimal design of pressure swing adsorption systems. *Sep. Purif. Rev.* 33, 1-39.

Choi C.T., Wen-Chung H., 1994. Incorporation of a valve equation into the simulation of a pressure swing adsorption process. *Chem. Eng. Sci.* 49, 75-84.

Choi W.K., Kwon T.I., Yeo Y.K., Lee H., Song H.K., Na B.K., 2003. Optimal Operation of the Pressure Swing Adsorption (PSA) Process for CO_2 Recovery. *Korean J. Chem. Eng.* 20, 617-623.

Chou C.T., Chen C.Y., 2004. Carbon dioxide recovery by vacuum swing adsorption. *Sep. Purif. Technol.* 39, 51-65.

Chue K.T., Kim J.N., Yoo Y.J., Cho S.H., Yang R.T., 1995. Comparison of activated carbon and zeolite 13X for CO_2 recovery from flue gas by pressure swing adsorption. *Ind. Eng. Chem. Res.* 34, 591-598.

Cruz P., Magalhães F.D., Mendes A., 2005. On the optimization of cyclic adsorption separation processes. *AIChE J.* 51, 1377-1395.

Cruz P., Santos J.C., Magalhães F.D., Mendes A., 2003. Cyclic adsorption separation processes: analysis strategy and optimization procedure. *Chem. Eng. Sci.* 58, 3143-3158.

D'Alessandro D.M., Smit B., Long J.R., 2010. Carbon dioxide capture: Prospects for new materials. *Angew. Chem.*, Int. Ed. 49, 6058-6082.

DOE/NETL, 2015. Cost and Performance Baseline for Fossil Energy Plants. *National Energy Technology Laboratory*.

Feron P.H.M., Hendriks C.A., 2005. CO_2 capture process principles and costs. *Oil Gas Sci. Technol.* 60, 451-459.

Gomes V.G., Yee K.W.K., 2002. Pressure swing adsorption for carbon dioxide sequestration from exhaust gases. *Sep. Purif. Technol.* 28, 161-171.

Grande C.A., Cavenati S., Rodrigues A.E., 2005. Pressure swing adsorption for carbon dioxide sequestration *presented at ENPROMER, 4th Mercosur Conference on Process Systems Engineering*, Rio de Janeiro, Brasil

Haghpanah R., Majumder A., Nilam R., Rajendran A., Farooq S., Karimi I.A., Amanullah M., 2013a. Multiobjective optimization of a four-step adsorption process for postcombustion CO_2 capture via finite volume simulation. *Ind. Eng. Chem. Res.* 52, 4249-4265.

Haghpanah R., Nilam R., Rajendran A., Farooq S., Karimi I.A., 2013b. Cycle synthesis and optimization of a VSA process for postcombustion CO_2 capture. *AIChE J.* 59, 4735-4748.

Haghpanah R., Rajendran A., Farooq S., Karimi I.A., 2014. Optimization of one- and two-staged kinetically controlled CO_2 capture processes from postcombustion flue gas on a carbon molecular sieve. *Ind. Eng. Chem. Res.* 53, 9186-9198.

Hasan M.M.F., Baliban R.C., Elia J.A., Floudas C.A., 2012. Modeling, simulation, and optimization of postcombustion CO_2 capture for variable feed concentration and flow rate. 2. Pressure swing adsorption and vacuum swing adsorption processes. *Ind. Eng. Chem. Res.* 51, 15665-15682.

Hasan M.M.F., First E.L., Floudas C.A., 2013. Cost-effective CO_2 capture based on in silico screening of zeolites and process optimization. *Phys. Chem. Chem. Phys.* 15, 17601-17618.

Houghton J. T., Ding Y., Griggs D. J., Noguer M., van der Linden P. J., Dai X., Maskel K., Johnson C.A., 2001. Climate Change 2001: The scientific basis, *Cambridge, UK*.

Hu X., Mangano E., Friedrich D., Ahn H., Brandani S., 2014. Diffusion mechanism of CO_2 in 13X zeolite beads. *Adsorption* 20, 121-135.

IEA, 2008. Energy Technology Perspectives 2008, Scenarios & Strategies to 2050. *International Energy Agency*.

IEA/WEO, 2006. World Energy Outlook 2006 *tech. rep. International Energy Agency*, Paris, France.

IPCC, 2005. Special report on carbon dioxide capture and storage Intergovernmental Panel on Climate Change, New York, NY: *Cambridge University Press*.

Jiang L., Biegler L.T., Fox V.G., 2003. Simulation and optimization of pressure-swing adsorption systems for air separation. *AIChE J.* 49, 1140-1157.

Jiang L., Fox V.G., Biegler L.T., 2004. Simulation and optimal design of multiple-bed pressure swing adsorption systems. *AIChE J.* 50, 2904-2917.

Khajuria H., 2011. Model-based Design, Operation and Control of Pressure Swing Adsorption Systems. *PhD Thesis, Department of Chemical Engeeneering Imperial College London*.

Khurana M., Farooq S., 2016. Simulation and optimization of a 6-step dual-reflux VSA cycle for post-combustion CO_2 capture. *Chem. Eng. Sci.* 152, 507-515.

Kikkinides E.S., Nikolic D., Georgiadis M.C., 2011. Modeling of Pressure Swing Adsorption Processes, in: *Dynamic Process Modeling*, (Georgiadis M.C., Banga J.R. and Pistikopoulos E.N. editors), 137-172.

Kikkinides E.S., Yang R.T., Cho S.H., 1993. Concentration and recovery of CO_2 from flue gas by pressure swing adsorption. *Ind. Eng. Chem. Res.* 32, 2714-2720.

Ko D., Siriwardane R., Biegler L.T., 2004. Optimization of pressure swing adsorption and fractionated vacuum pressure swing adsorption processes for CO_2 sequestration. *AIChE Annual Meeting*, 5391-5424.

Ko D., Siriwardane R., Biegler L.T., 2005. Optimization of pressure swing adsorption and fractionated vacuum pressure swing adsorption processes for CO_2 capture. *Ind. Eng. Chem. Res.* 44, 8084-8094.

Krishnamurthy S., Rao V.R., Guntuka S., Sharratt P., Haghpanah R., Rajendran A., Amanullah M., Karimi I.A., Farooq S., 2014. CO_2 capture from dry flue gas by vacuum swing adsorption: A pilot plant study. *AIChE J.* 60, 1830-1842.

Kumar R., Fox V.G., Hartzog D.G., Larson R.E., Chen Y.C., Houghton P.A., Naheiri T., 1994. A versatile process simulator for adsorptive separations. *Chem. Eng. Sci.* 49, 3115-3125.

Lee S.Y., Park S.J., 2015. A review on solid adsorbents for carbon dioxide capture. *J. Ind. Eng. Chem.* 23, 1-11.

Leperi K.T., Snurr R.Q., You F., 2016. Optimization of Two-Stage Pressure/Vacuum Swing Adsorption with Variable Dehydration Level for Postcombustion Carbon Capture. *Ind. Eng. Chem. Res.* 55, 3338-3350.

Ling J., Ntiamoah A., Xiao P., Webley P.A., Zhai Y., 2015. Effects of feed gas concentration, temperature and process parameters on vacuum swing adsorption performance for CO_2 capture. *Chem. Eng. J.* 265, 47-57.

Liu Z., Grande C.A., Li P., Yu J., Rodrigues A.E., 2011. Multi-bed vacuum pressure swing adsorption for carbon dioxide capture from flue gas. *Sep. Purif. Technol.* 81, 307-317.

Liu Z., Wang L., Kong X., Li P., Yu J., Rodrigues A.E., 2012. Onsite CO_2 Capture from Flue Gas by an Adsorption Process in a Coal-Fired Power Plant. *Ind. Eng. Chem. Res.* 51, 7355-7363.

Maring B.J., Webley P.A., 2013. A new simplified pressure/vacuum swing adsorption model for rapid adsorbent screening for CO_2 capture applications. *Int. J. Greenhouse Gas Control* 15, 16-31.

Mason J.A., Sumida K., Herm Z.R., Krishna R., Long J.R., 2011. Evaluating metal-organic frameworks for post-combustion carbon dioxide capture via temperature swing adsorption. *Energy Envir. Sc.* 4, 3030-3040.

Na B.K., Koo K.K., Eum H.M., Lee H., Song H.K., 2001. CO_2 Recovery from Flue Gas by PSA Process using Activated Carbon. *Korean J. Chem.* Eng. 18, 220-227.

Na B.K., Lee H., Koo K.K., Song H.K., 2002. Effect of rinse and recycle methods on the pressure swing adsorption process to recover CO_2 from power plant flue gas using activated carbon. *Ind. Eng. Chem. Res.* 41, 5498-5503.

Nalaparaju A., Khurana M., Farooq S., Karimi I.A., Jiang J.W., 2015. CO_2 capture in cation-exchanged metal-organic frameworks: Holistic modeling from molecular simulation to process optimization. *Chem. Eng. Sci.* 124, 70-78.

NETL, 2012. Quality guidelines for energy system studies: CO_2 impurity design parameters, Technical report. *National Energy Technology Laboratory (NETL), U.S. Department of Energy*.

Nikolaidis G.N., Kikkinides E.S., Georgiadis M.C., 2016. Model-Based Approach for the Evaluation of Materials and Processes for Post-Combustion Carbon Dioxide Capture from Flue Gas by PSA/VSA Processes. *Ind. Eng. Chem. Res.* 55, 635-646.

Nikolic D., Giovanoglou A., Georgiadis M.C., Kikkinides E.S., 2008. Generic modeling framework for gas separations using multibed pressure swing adsorption processes. *Ind. Eng. Chem. Res.* 47, 3156-3169.

Nikolic D., Kikkinides E.S., Georgiadis M.C., 2009. Optimization of multibed pressure swing adsorption processes. *Ind. Eng. Chem. Res.* 48, 5388-5398.

Nilchan S., 1997. The Optimisation of Periodic Adsorption Processes. *PhD Thesis, Department of Chemical Engeeneering and Chemical Technology Imperial College of Science Technology and Medicine London.*

Nilchan S., Pantelides C.C., 1998. On the Optimisation of Periodic Adsorption Processes. *Adsorption* 4, 113-147.

Park J.H., Beum H.T., Kim J.N., Cho S.H., 2002. Numerical analysis on the power consumption of the PSA process for recovering CO_2 from flue gas. *Ind. Eng. Chem. Res.* 41, 4122-4131.

Process Systems Enterprise Ltd., 2011. *gPROMS Model developer guide*. http://www.psenterprise.com

Rajagopalan A.K., Avila A.M., Rajendran A., 2016. Do adsorbent screening metrics predict process performance? A process optimisation based study for post-combustion capture of CO_2. *Int. J. Greenhouse Gas Control* 46, 76-85.

Rao A.B., Rubin E.S., 2002. A technical, economic, and environmental assessment of amine-based CO_2 capture technology for power plant greenhouse gas control. *Environ. Sci. Technol.* 36, 4467-4475.

Reynolds S.P., Ebner A.D., Ritter J.A., 2006. Stripping PSA cycles for CO_2 recovery from flue gas at high temperature using a hydrotalcite-like adsorbent. *Ind. Eng. Chem. Res.* 45, 4278-4294.

Reynolds S.P., Mehrotra A., Ebner A.D., Ritter, J.A., 2008. Heavy reflux PSA cycles for CO_2 recovery from flue gas: Part I. Performance evaluation. *Adsorption* 14, 399-413.

Riboldi L., Bolland O., 2015. Evaluating Pressure Swing Adsorption as a CO_2 separation technique in coal-fired power plants. *Int. J. Greenhouse Gas Control* 39, 1-16.

Ruthven D.M., 1984. Principles of adsorption and adsorption processes. *Wiley, New York*.

Ruthven D.M., Farooq S., Knaebel K.S., 1994. Pressure swing adsorption. *VCH Publishers, New York*.

Sankararao B., Gupta S.K., 2007. Multi-Objective Optimization of Pressure Swing Adsorbers for Air Separation. *Ind. Eng. Chem. Res.* 46, 3751-3765.

Shen C., Liu Z., Li P., Yu J., 2012. Two-Stage VPSA Process for CO_2 Capture from Flue Gas Using Activated Carbon Beads. *Ind. Eng. Chem. Res.* 51, 5011-5021.

Shen C., Yu J., Li P., Grande C.A., Rodrigues A.E., 2011. Capture of CO_2 from flue gas by vacuum pressure swing adsorption using activated carbon beads. *Adsorption* 17, 179-188.

Sircar S., Kratz W.C., 1988. Simultaneous production of hydrogen and carbon dioxide from steam reformer off-gas by pressure swing adsorption. *Sep. Sci. Techol.* 23, 2397-2415.

Smith Iv O.J., Westerberg A.W., 1991. The optimal design of pressure swing adsorption systems. *Chem. Eng. Sci.* 46, 2967-2976.

Takamura Y., Narita S., Aoki J., Hironaka S., Uchida S., 2001. Evaluation of dual-bed pressure swing adsorption for CO_2 recovery from boiler exhaust gas. *Sep. Purif. Technol.* 24, 519-528.

Vassiliadis V.S., Sargent R.W.H., Pantelides C.C., 1994. Solution of a class of multistage dynamic optimization problems. 2. Problems with path constraints. *Ind. Eng. Chem. Res.* 33, 2123-2133.

Wakao N., Funazkri T., 1978. Effect of fluid dispersion coefficients on particle-to-fluid mass transfer coefficients in packed beds. Correlation of sherwood numbers. *Chem. Eng. Sci.* 33, 1375-1384.

Wakao N., Kaguei S., Funazkri T., 1979. Effect of fluid dispersion coefficients on particle-to-fluid heat transfer coefficients in packed beds. Correlation of nusselt numbers. *Chem. Eng. Sci.* 34, 325-336.

Wang L., Liu Z., Li P., Wang J., Yu J., 2012. CO_2 capture from flue gas by two successive VPSA units using 13XAPG. *Adsorption* 18, 445-459.

Wang L., Yang Y., Shen W., Kong X., Li P., Yu J., Rodrigues A.E., 2013a. CO_2 Capture from Flue Gas in an Existing Coal-Fired Power Plant by Two Successive Pilot-Scale VPSA Units. *Ind. Eng. Chem. Res.* 52, 7947-7955.

Wang L., Yang Y., Shen W., Kong X., Li P., Yu J., Rodrigues A.E., 2013b. Experimental evaluation of adsorption technology for CO_2 capture from flue gas in an existing coal-fired power plant. *Chem. Eng. Sci.* 101, 615-619.

Wu H., Zhou W., Yildirim T., 2009. High-Capacity Methane Storage in Metal–Organic Frameworks M2(dhtp): The Important Role of Open Metal Sites. *J. Am. Chem Soc.* 131, 4995-5000.

Xiao P., Zhang J., Webley P., Li G., Singh R., Todd R., 2008. Capture of CO_2 from flue gas streams with zeolite 13X by vacuum-pressure swing adsorption. *Adsorption* 14, 575-582.

Yang R.T., 1987. Gas separation by adsorption processes. *Butterworths, Boston*.

Zaman M., Lee J.H., 2013. Carbon capture from stationary power generation sources: A review of the current status of the technologies. *Korean J. Chem. Eng.* 30, 1497-1526.

Zhang J., Webley P.A., 2008. Cycle development and design for CO_2 capture from flue gas by vacuum swing adsorption. *Environ. Sci. Technol.* 42, 563-569.

Zhang J., Webley P.A., Xiao P., 2008. Effect of process parameters on power requirements of vacuum swing adsorption technology for CO_2 capture from flue gas. *Energy Convers. Manage* 49, 346-356.

THESIS PUBLICATIONS

Thesis publications

A. Journal articles

- Nikolaidis G. N., Kikkinides E. S., Georgiadis M. C., Model-Based Approach for the Evaluation of Materials and Processes for Post-Combustion Carbon Dioxide Capture from Flue Gas by PSA/VSA Processes, *Industrial and Engineering Chemistry Research*, 2016, 55 (3), 635-646. http://pubs.acs.org/doi/10.1021/acs.iecr.5b02845
- Nikolaidis G. N., Kikkinides E. S., Georgiadis M. C., An Integrated Two-stage P/VSA Process for Post-Combustion CO_2 Capture Using Combinations of Adsorbents Zeolite 13X and Mg-MOF-74, *Industrial and Engineering Chemistry Research*, 2017, 56 (4), 974-988. http://pubs.acs.org/doi/abs/10.1021/acs.iecr.6b04270
- Nikolaidis G. N., Kikkinides E. S., Georgiadis M. C., A model-based approach for the evaluation of new zeolite 13X-based adsorbents for the efficient post-combustion CO_2 capture using P/VSA processes, Accepted for publication in *Chemical Engineering Research and Design*, May 2017.

B. Refereed conference proceedings

- Nikolaidis G. N., Kikkinides E. S., Georgiadis M. C., Modelling and Simulation of Pressure Swing Adsorption (PSA) Processes for post-combustion Carbon Dioxide (CO_2) capture from flue gas, *Computer Aided Chemical Engineering*, Elsevier, 2015, 37, 287-292. *25th European Symposium on Computer Aided Process Engineering (ESCAPE)*, Copenhagen, Denmark, 31 May-4 June 2015, (conference proceedings). http://dx.doi.org/10.1016/B978-0-444-63578-5.50043-8

- Nikolaidis G. N., Kikkinides E. S., Georgiadis M. C., Modelling, Simulation and Optimisation of an Integrated Two-Stage P/VSA Process for Post-Combustion CO_2 Capture Using Combinations of Adsorbents, *27th European Symposium on Computer Aided Process Engineering (ESCAPE)*, Barcelona, Spain, 1-5 October 2017, (Accepted for publication in conference proceedings).

C. Other international peer-reviewed conferences

- Nikolaidis G.N., Georgiadis M.C., Kikkinides E.S., Brandani S., Blomb R., Modeling, Simulation and Optimization of Pressure Swing Adsorption (PSA) Processes for Post-Combustion Carbon Dioxide (CO_2) Capture from Flue Gas, *2016 AIChE Annual Meeting*, San Francisco, U.S.A., 13-18 November 2016, (conference proceedings).
  https://aiche.confex.com/aiche/2016/webprogram/Paper453471.html

D. Selected book chapter

- Nikolaidis G. N., Kikkinides E. S., Georgiadis M. C., Modelling and Optimisation of Pressure Swing Adsorption (PSA) Processes for Post-Combustion CO_2 Capture from Flue Gas, in: *Process Systems and Materials for CO_2 Capture: Modelling, Design, Control and Integration,* (Papadopoulos A.I. and Seferlis P., editors), John Wiley & Sons Ltd., 2017, 343-369.
  http://www.wiley-vch.de/en/areas-interest/engineering/energy-10eg/fossil-fuels10eg1/carbon-capture-storage-10eg13/process-systems-and-materials-for-co2-capture-978-1-119-10644-9

E. National conferences

- Nikolaidis G.N., Kikkinides E.S., Georgiadis M.C., Modelling and Simulation of Pressure Swing Adsorption (PSA) Processes for Post-Combustion Carbon Dioxide (CO_2) Capture from Flue Gas (in Greek language), *10th National*

Scientific Congress of Chemical Engineering, Patras, Greece, 4-6 June 2015, (conference proceedings).

- Nikolaidis G.N., Kikkinides E.S., Georgiadis M.C., Modelling, Simulation and Optimisation of Pressure/Vacuum Swing Adsorption (P/VSA) Processes for Post-Combustion Carbon Dioxide (CO_2) Capture from Flue Gas (in Greek language), *22th National Congress of Chemistry*, Thessaloniki, Greece, 2-4 December 2016, (conference proceedings).
- Nikolaidis G.N., Kikkinides E.S., Georgiadis M.C., Comparative Study Employing Different Types of Adsorbents in Carbon Dioxide (CO_2) Capture from Flue Gas by Pressure/Vacuum Swing Adsorption (P/VSA) Process (in Greek language), *11th National Scientific Congress of Chemical Engineering*, Thessaloniki, Greece, 25-27 May 2017, (conference proceedings).

F. Presentations in international conferences

- Nikolaidis G.N., Kikkinides E.S., Georgiadis M.C., Modelling and optimisation of materials and processes for post-combustion CO_2 capture from flue gas by Pressure Swing Adsorption (PSA) and Vacuum Swing Adsorption (VSA), *PSE Advanced Process Modelling Annual Forum 2015*, London, United Kingdom, 21-23 April 2015.
- Nikolaidis G.N., Kikkinides E.S., Georgiadis M.C., Modelling and Simulation of Pressure Swing Adsorption (PSA) Processes for post-combustion Carbon Dioxide (CO_2) capture from flue gas, *12th International Symposium on Process Systems Engineering and 25th European Symposium on Computer Aided Process Engineering (ESCAPE)*, Copenhagen, Denmark, 31 May-4 June 2015.